Project report

TTK4550, Specialization Project, Engineering Cybernetics

Student Tor Arne Tjåland

Design Report NTNU - Drillbotics™ 2020 Phase I

Trondheim, December 17th, 2019

NTNU
Norwegian University of Science and Technology
Department of Engineering Cybernetics

Preface

During the past four months, a team consisting of two cybernetic students and three petroleum students has designed and planned the work ahead to successfully create an autonomous drilling rig. The main purpose of the project is to discover new and innovative techniques for autonomous drilling in the annual Drillbotics© competition. To qualify for the competition, a design report containing the overall design and plan of the drilling rig is handed in. This project thesis is the 2020 NTNU team's design report in its entirety.

Since this is the 4th year the competition is being held, the difficulty of the competition objectives has increased. Compared to the previous years, the need for a robust and accurate position control system is even more significant. Therefore, the electrical instrumentation, communication, and control system parts are handled by the two cybernetic students Tor Arne Tjåland and Mads Sundseth.

As it is difficult to design a mechanical system without control considerations and vice versa, the whole report is based on contributions from all team members. The main contributions by the students from Cybernetics and Robotics are written in sections 5.4 (Theoretical Background: Control Theory), 9 (Electrical System and Instrumentation) and 10 (System Description and Control Design). Although both students are responsible for all these sections in their entirety, they have been divided up by the following points

Sections written by Tor Arne Tjåland

- 5.4.1 - 5.4.5
- 9.1 - 9.2
- 10.1 - 10.3

Sections written by Mads Sundseth

- 5.4.6 - 5.4.7
- 9.3 - 9.5
- 10.4 - 10.7

NTNU
Norwegian University of Science and Technology
Department of Geoscience and Petroleum

Design Report NTNU - Drillbotics™ 2020 Phase I

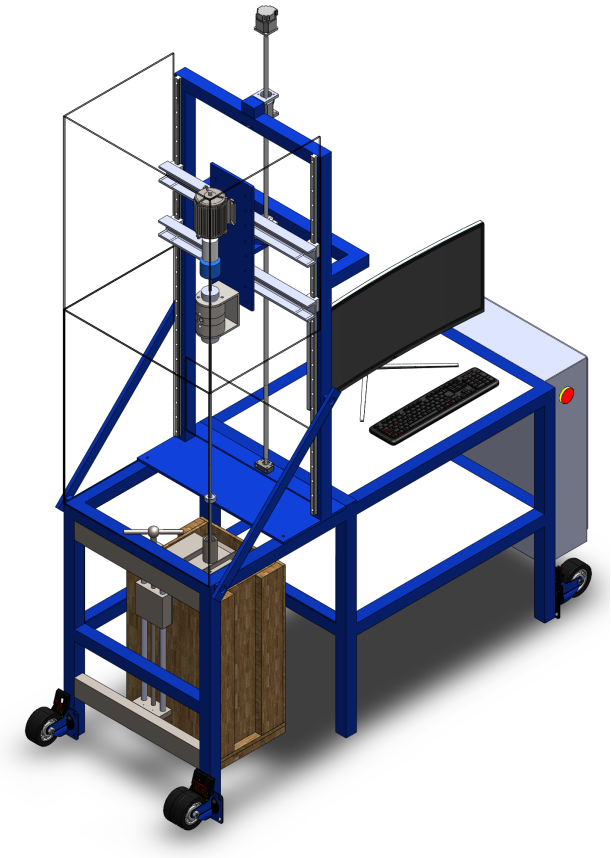

Submitted by:
Jonas Mannsverk
Arman Hiwa
Vilde Romslo Meyer
Mads Sundseth
Tor Arne Tjåland

Date:
June 26, 2020

Executive Summary

This marks the 4th year NTNU is participating in the Drillbotics© competition, with superior results from previous years. This year's competition main goal is to autonomously drill a directional well through a homogeneous rock sample using a miniature drilling rig, while still maintaining well integrity and wellbore quality. In Phase I the teams are to discuss and develop a final design. As NTNU have great success from previous years, this year's team are basing their design on previous findings.

The final mechanical design proposed from this year's team is a Positive Displacement Motor (PDM) with an adjustable bent housing and using aluminum drill pipe. Only making minor modification the rig will be as previous years. The rig consists of a hoisting motor with the ability to move vertical, which makes it able to control Weight on Bit (WOB). Then there is a top drive for rotational power, where an electrical swivel is connected below; merging the electrical cables and equipment. From this the drill string will be connected with the PDM and adjustable bent housing. The team will be using water as the drilling fluid.

The whole drilling operation will be executed autonomously with the use of sensors that gathers data in real-time, to be used in a closed-loop feedback control system. The control system mainly consists of two parts, where the first one regards control of WOB, while the second regards control of drill bit position to achieve a generated well path that goes through the given competition points. The closed-loop feedback part of the control system is achieved through a wired communication scheme between a sensor card located in the Bottom Hole Assembly (BHA) and a top side computer. The control system consists of different phases defined as states in a state machine. These states are used during different parts of the drilling operation and are mainly separated into the vertical and directional drilling phases. If there are any measurements from the sensors exceeding any defined safety thresholds, the system will transition to a safety layer, ensuring safe operation.

Acknowledgement

Firstly, we would like to express our very great appreciation to our professors supervising on this project; Alexey Pavlov, Lars S. Imsland, Tor Berge S. Gjersvik, Sigbjørn Sangesland and Sigve Hovda for their guidance throughout the project, sharing your thoughts, ideas and practical knowledge helping us conclude on a feasible design. Thank you for sharing your time during our bi-weekly meetings and for giving us feedback on our progress.

Secondly, we want to thank the lab engineers helping with day-to-day challenges. Foremost thank you to Noralf Vedvik and Steffen W. Moen assisting with practical problems encountered and answering questions. The team appreciate the contribution and time spent during Phase I.

Thirdly, we would like to show our gratitude to Norwegian University of Science and Technology (NTNU), respectively Department of Geoscience and Petroleum (IGP) and Department of Engineering Cybernetics (ITK), giving us the opportunity to work together as a multidisciplinary team on such a comprehensive project providing valuable hands-on experience prior to our future careers. In addition, the team is grateful to Drilling System Automation Technical Section (DSATS) for providing a platform giving us the opportunity to solve highly relevant engineering challenges and compete on an international basis.

Finally, we would like to thank BRU21 (Better Resource Utilization in the 21^{st} century) for economic support. The team highly appreciated your contribution. By supporting this project, BRU21 together with its partners shows their dedication to developing the drilling automation technology.

Contents

Acronyms

API American Petroleum Institute.
BHA Bottom Hole Assembly.
BUR Build-Up Rate.
CL Course Length.
CO Control output.
DD Directional Drilling.
DH Downhole.
DLS Dogleg Severity.
DP Drill pipe.
DSATS Drilling System Automation Technical Section.
DTM Downhole Turbine Motor.
EMM Electrical Miniature Motor.
ERD Extended Reach Drilling.
HM Hoisting motor.
HP Horsepower.
HSE Health, Safety and Environment.
IGP Department of Geoscience and Petroleum.
IMU Intertial Measurement Unit.
ITK Department of Engineering Cybernetics.
KOP Kick-Off Point.
NTNU Norwegian University of Science and Technology.
OD Outer Diameter.
PDC Polychrystalline-Diamond Compact Bits.
PDM Positive Displacement Motor.
POI Point of Interest.
PPE Personal Protective Equipment.
PV Process variable.
RC Radius of Curvature.
RKB Rotary Kelly Bushing.
ROP Rate of Penetration.
RPM Revolutions per Minute.
RSS Rotary Steerable System.
SP Set point.
SPE Society of Petroleum Engineers.
TD Top Drive.
TVD True Vertical Depth.
WOB Weight on Bit.

List of Figures

List of Tables

1 Introduction

Many industries are gradually advancing from manual labor to automated solutions as the advantages outrank the challenges. Benefits with automation include higher production rates, increased productivity, better product quality, and most significantly improved safety. As the world's petroleum resources are becoming less accessible and more challenging to produce, new innovative technologies and solutions are essential for the industry to still be economically feasible. In 2008, Society of Petroleum Engineers (SPE) established the Drilling System Automation Technical Section (DSATS) to invest more resources into drilling automation. The main objective of the organization is to develop technology that links surface machines with downhole tools and measurements, ultimately increasing the drilling efficiency and safety. The Drillbotics© competition came about in 2014, with the intention of involving university students in the continuous development of automation in the industry.

The outline of the 2020 Drillbotics© competition is for each team to design and build a miniature drilling rig, that is to drill a rock sample autonomously using downhole sensors and control algorithms. The design should be able to drill directional, respectively be able to build inclination angle and change azimuth. To complete such a complex engineering task, a multi-disciplinary team is assembled to design a sustainable solution.

This is the fourth year Norwegian University of Science and Technology (NTNU) participates in the competition, with great results from previous years. Respectively being ranked first in the preliminary round in 2019, taking first place in 2018 and second place in 2017. With the findings from previous years as a good foundation, the team will this year seek to further develop and optimize the design to deliver safer and more efficient solutions. Mechanical adjustments, as well as communication and control algorithms will be in focus to improve sustainability, borehole quality and safety.

The mechanical improvements to be done, both on preexisting rig features and the drill string, will be discussed in this report, as well as optimization of the control system and the electrical system. The report will present possible solutions and emphasize with discussion and calculations why certain assumptions and decisions are made for the final design proposed.

2 Organization

The tasks that are given heavily depend on collaboration and teamwork, which is why the Drillbotics© committee recommends assembling a team of students with multidisciplinary academic background. Students from the petroleum and cybernetics department make up Norwegian University of Science and Technologys (NTNUs) team, with supervisors and lab engineers from these departments supporting and giving guidance to the team. To conquer the problem effectively, a well-structured team dividing the responsibilities between themselves is important, as well as working together to get sustainable and economic feasible design. This section will cover who this year's team is, their responsibilities and the support system, in addition to the team's project management approach.

2.1 Team

The 2020 NTNU Drillbotics© Team consists of five students, respectively three from the Department of Geoscience and Petroleum (IGP) and two from the Department of Engineering Cybernetics (ITK); see Figure 2.1. In addition, the team is supported by four supervisors from IGP and one from ITK on the theoretical aspects, as well as lab engineers on the practical challenges. An organizational chart of the support system is shown in Figure 2.2.

Figure 2.1: 2020 NTNU Drillbotics© Team.

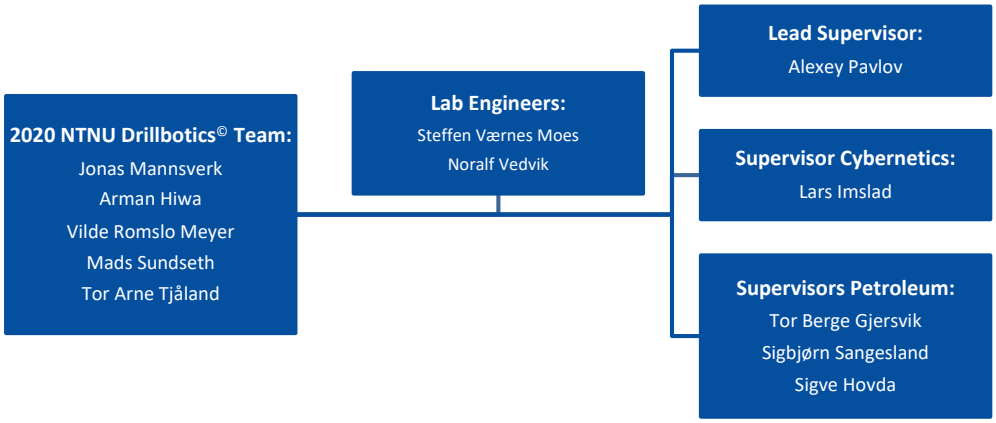

Figure 2.2: Support System for the 2020 NTNU Drillbotics© Team.

An overview of what is required to solve the competition task was made before assigning responsibilities amongst the team. From this, the team showed interest in the different responsibilities based on interest and competence, and divided the topics thereafter to take advantage of each team member's strengths. As the semester progressed new topics were introduced and divided between the team members as best seen fit. Though everyone had their responsibilities, the team collaborated, discussed and consulted with one another, the supervisors and the lab engineers. Bi-weekly meetings were coordinated with the supervisors, where the team gave a progress update, and the supervisors gave guidance and useful input. The lab engineers assisted with the daily work in the lab, as well as challenges the team faces throughout the process.

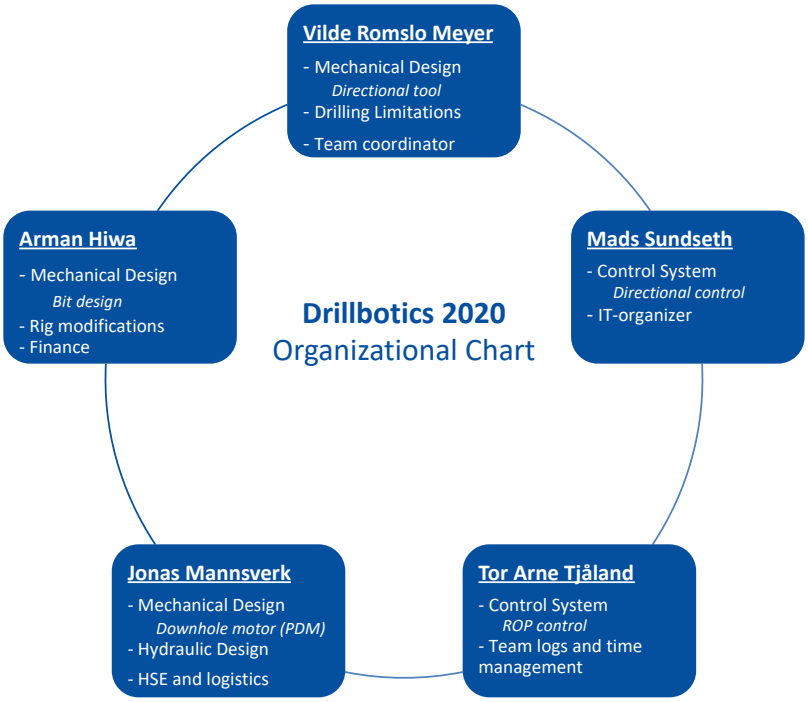

Figure 2.3: Organization chart for the 2020 NTNU Drillbotics© Team.

2.2 Project Management

To avoid time wasted on misunderstandings and miscommunication amongst the team members, expectations were discussed and guidelines formed as the team first got together. Besides, the team had a kick-off meeting with supervisors and lab engineers discussing ground rules for the preparation phase as well as expectations for the collaboration and the competition itself. A common office for the team with immediate proximity to the lab engineers and supervisors was established early, used for day-to-day discussion and collaboration. To maintain a level of structure, Microsoft Teams were used for daily communication as well as storing and sharing documents, such as team logs, logistics, to-do-list, calculations and other relevant documents. GitHub is used to effectively share scripts between the team members.

The team started the semester reading up on relevant literature, familiarize themselves with previous years competition objectives, and brainstorming about possible solutions. As the guidelines for this year's competitions were released the team started discussing concrete final design ideas. From this point the team established a planer and consecutively set deadlines for tasks to be completed, trying to avoid time management issues as the deadline for design submission approaches.

3 Health, Safety and Environment (HSE)

Health, Safety and Environment (HSE) is the number one priority in the petroleum industry, focusing on reducing risks to facilities, the environment and most importantly the people. Though everything is scaled down for the Drillbotics© competition compared to the industry standard, the team seek to maintain the same HSE standards. Every operation and rig component shall therefore be planned and designed to improve the overall safety and not be a limiting factor.

Starting with the working environment, only authorized personnel have access to the workshop, where all are required to use appropriate Personal Protective Equipment (PPE) at all times. At the beginning of the semester every team member completed the required HSE training in accordance with Department of Geoscience and Petroleums (IGPs) safety regulations, consisting of both an e-learning course and safety walk-through in the workshop. Main takeaways from the course include probable hazards, handling of environmental waste, required PPE, procedures in case of unwanted incidents and general behavior in the workshop.

Risk assessment is a key aspect when talking about safety, meaning every component of the rig should be risk assessed to reveal any potential hazards. Risk is defined as:

$$Risk = Probability \cdot Consequence \tag{3.1}$$

The Probability/Consequence relationship presented in Equation 3.1 is more applicable in a risk matrix, and the matrix will, therefore, be used for further risk assessment.

Table 3.1: Risk matrix.

Consequence / Probability	Negligible	Minor	Moderate	Significant	Severe
Very likely	Low medium	Medium	Medium high	High	Ekstremely high
Likely	Low	Low medium	Medium	Medium high	High
Possible	Low	Low medium	Medium	Medium high	Medium high
Unlikely	Low	Low medium	Low medium	Medium	Medium high
Very unlikely	Low	Low	Low medium	Medium	Medium

3.1 Safety Hazards

There are many safety hazards associated with this project, and all team members are obligated to be aware of the hazards present at all times. Before starting any task the team shall identify all hazards present, and taking risk preventive actions. Safety hazards affiliated with the project include [1]:

- **Hazardous Energy.** The team must follow proper operating procedures in the presence of hazardous energies, respectively mechanical, electrical and hydraulic. Also, personnel might be exposed to these uncontrollable sources of energy if the equipment is not designed, installed or maintained properly. Injuries associated with these types of hazards include crushing, cutting and lacerations and electrical shock. Other consequences include permanent damage to equipment and fire.
- **Ergonomic Hazards.** Injuries related to ergonomics - including muscle strains, lower back and shoulder injuries - results from lifting-, pushing- and pulling heavy, working in demanding body postures, or repetitively performing a task.
- **Machine Hazards.** These types of hazards include the moving parts of the rig, and the team is advised to keep their distance unless needed within immediate distance. These types of hazards might get personnel stuck between the moving part, and injuries include pinching, crushing and cutting.

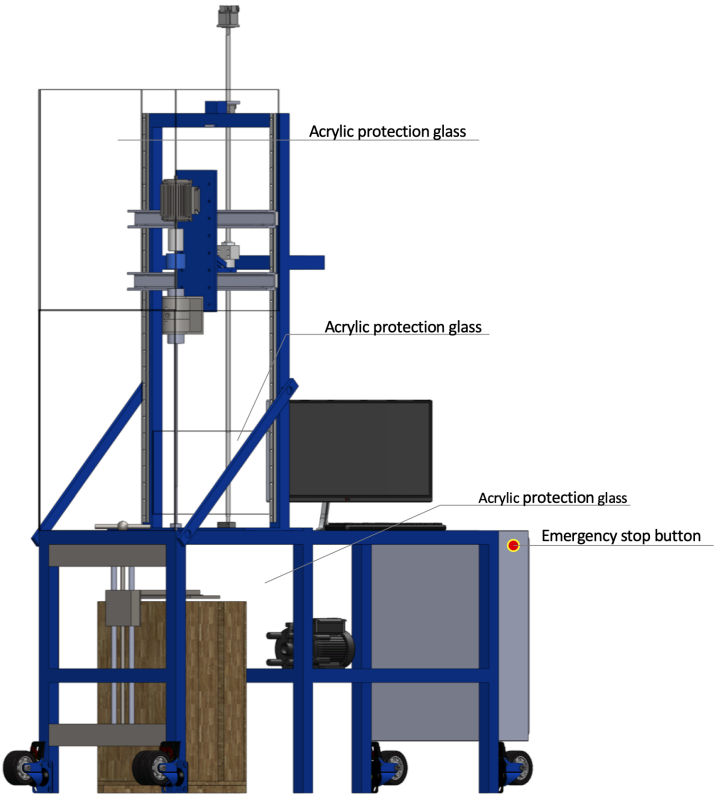

Figure 3.1: Rig in operational mode, labeled with its safety barriers.

3.2 Prevention and Mitigation

The safety of the personnel, environment and equipment is of utmost importance, and the team seeks to take distinctive measures preventing and mitigating potential hazards. Starting with the most basic, all team members should use proper PPE at all times. Safety glasses are always required in the workshop, beyond

that personnel present are required to inform if additional PPE is needed on the PPE board. Loose clothes and hair should be avoided at all times, especially in proximity of moving components to prevent getting stuck or caught.

The preventive measures taken on the rig are illustrated in Figure 3.1. The acrylic protective glass, both above and below the rig floor, works as a safety barrier for moving components, dust, the unwanted splashing of drilling fluid and flung debris from material damaged caused by high internal pressures. To mitigate material failures the internal pressure should be kept below the bursting limit, together with pipe stresses and vibrations kept low to prevent buckling and twist-off of the Drill pipe (DP). The other mitigating action taken is the emergency stop bottom, located outside of the electrical cabinet. In case of any unwanted activity, push the stop bottom and power to all rig components will immediately be shut down. As a safety measure, at least one person will be close by the emergency stop bottom. Permanent preventive measures taken are smaller modifications on the rig to improve its overall safety, this is described to detail in section 11.1.

Handling of rock samples must be done right to avoid permanent back- and pinching injuries. Preventive measures taken are wearing the appropriate PPE, respectively gloves and proper footwear. Most importantly the right lifting technique should be practiced, and the team seek to correct each other if not done right.

Electrical equipment generates fire hazards, and to mitigate this the team has familiarized themselves with the different types of fire extinguishers, where they are located and procedures in case of fire. Modifications of electrical equipment shall only be done by qualified personnel, all power should be turned off in this case. Fluid should be kept separate from electrical components.

Stop Work Authority

Stop work authority entails the operation to be stopped if a worker perceives a situation as unsafe or hazardous. It shall be practiced by all personnel, if a hazard arises or the team member sees a situation as unsuitable to continue work will be stopped immediately. Personnel is obligated to not start working again until the hazard has been corrected.

4 Competition Objectives

The international Drillbotics© competition was first arranged in 2014, making this the sixth competition. Norwegian University of Science and Technology (NTNU) is participating for the fourth time, with a stellar record to show from previous years, and this year's team seeks to continue this excellence. The main objective of the competition has been to autonomously drill a rock sample provided by the Drilling System Automation Technical Section (DSATS) committee since the competition was introduced, with gradually expanding the scope. When the NTNU Drillbotics© Team in 2018 drilled through the 35 cm rock sample in 3 minutes and 15 seconds [2], the vertical challenge was presumed accomplished. The scope was therefore extended in last year's competition, including directional drilling as the main objective. This year changing azimuth is a requirement in addition to building an inclination angle.

The main objectives presented in the 2020 Guidelines for the Drillbotics© Group A competition includes[3]:

- Hit one or more targets, given X/Y coordinates and vertical depth(s).
- Drill 4" in vertical direction before kicking-off. Targets given will not exceed 30° inclination from vertical, 15° azimuth change or 10" displacement.

The mechanical design has been the main objective in the competition thus far, this year though the committee encourages the teams to shift the focus moreover to the autonomous aspect. A closed-loop control system is, therefore, a requirement, with control algorithms and downhole sensors. Requirements regarding the control system, to make the system autonomous include [3]:

- Drilling/survey mode switching should be automated. This entails a built-in survey interval and drill string movement.
- Calculations concerning steering, such as slide face and tool face direction, must be performed autonomously.
- Directional surveying should be made entirely autonomous.
- Rig floor display must show dogleg severity required in order to hit the target(s). The distance and direction respectively must be calculated autonomously.

Though the committee emphasizes making the system autonomous this year, the mechanical design is still significant in order to maintain borehole quality, well integrity and avoid drilling dysfunctions. Mechanical requirements include [3]:

- 1.5" bit diameter.
- Stainless steel or aluminum drill pipe with diameter 3/8" and wall thickness 0.049".

5 Theoretical Background

This section will cover theory in compliance with the objectives of this year's competition and will be a foundation for further discussion, as well as assumptions and decisions made as a basis for the final design proposed.

5.1 Directional Drilling

Directional Drilling (DD) was first introduced as an objective in last year's competition. This years, in addition to inclination, it goes a step further by implementing change in azimuth. In this section main applications of DD as well as theory regarding the well path will be covered.

5.1.1 Why Directional Drilling?

DD is applied if the reservoir is hard to access or in cases of limitations at the surface. Some applications of DD include [4]:

- Drilling a secondary well from an existing wellbore, usually referred to as sidetracking.
- Drilling multiple wells from the same offshore platform.
- Avoiding challenging formations or geological structures, such as salt domes.
- Geo-Steering.
- Increases the drainage area, as the reservoir lateral length is usually significantly greater than the vertical length.

5.1.2 Well Path

Competing teams will be given a set of X/Y coordinates and vertical depths during the competition, where each team will be scored based on hitting accuracy. The control system must, therefore, be able to understand and handle azimuth, inclination change. Briefly defining these two [4]:

- Azimuth is the compass direction of a directional survey, more specifically the angle between the well path and North axis measured clockwise from North in the plane view.
- Inclination is irrespective of the compass direction and is the deviation from the vertical at a certain point. More specifically it is the angle between a vertical line and a tangent to the well path.

A known fixed point is the reference for measurements and well location during drilling. The coordinates {X, Y, Z} of the reference point is set to {0, 0, 0}, which is equivalent to {0° North, 0° East, 0 m TVD}. All well paths are developed from the reference point to the desired target(s), beginning with drilling vertical until reaching a formation that can withstand the extra strain applied from a deviated section. Kick-Off Point (KOP) is the measured depth where the drill string starts building angle if a change in compass

direction is desired. This is referred to as turn rate. A 3D curved well path is created, however this curve cannot separately be composed into azimuth or inclination due to the turning and building. To avoid getting inaccurate coordinates it should be presented as dogleg angle (ϕ) or Dogleg Severity (DLS). $DLS[^\circ/m]$ is predicted using the following equation:

$$DLS = \frac{\phi}{CL} \tag{5.1}$$

Where $\phi[^\circ]$ is the dogleg angle and $CL[m]$ is the course length. Figure 5.1a illustrates where dogleg angle (ϕ) is found and Figure 5.1b gives the parameters for calculating the Course Length (CL).

$$CL = \frac{RC\pi(I_2 - I_1)}{180} \tag{5.2}$$

$RC[m]$ is the radius of curvature and can be calculated for inclination and azimuth angle separately.

$$\begin{aligned} RC_I &= \frac{(180)(30)}{\pi\, B}, \\ RC_A &= \frac{(180)(30)}{\pi\, T} \end{aligned} \tag{5.3}$$

Here B is build-up rate and T is turn rate. Figure 5.1 illustrates important parameters when developing a well path, including inclination, azimuth and dogleg angle (ϕ).

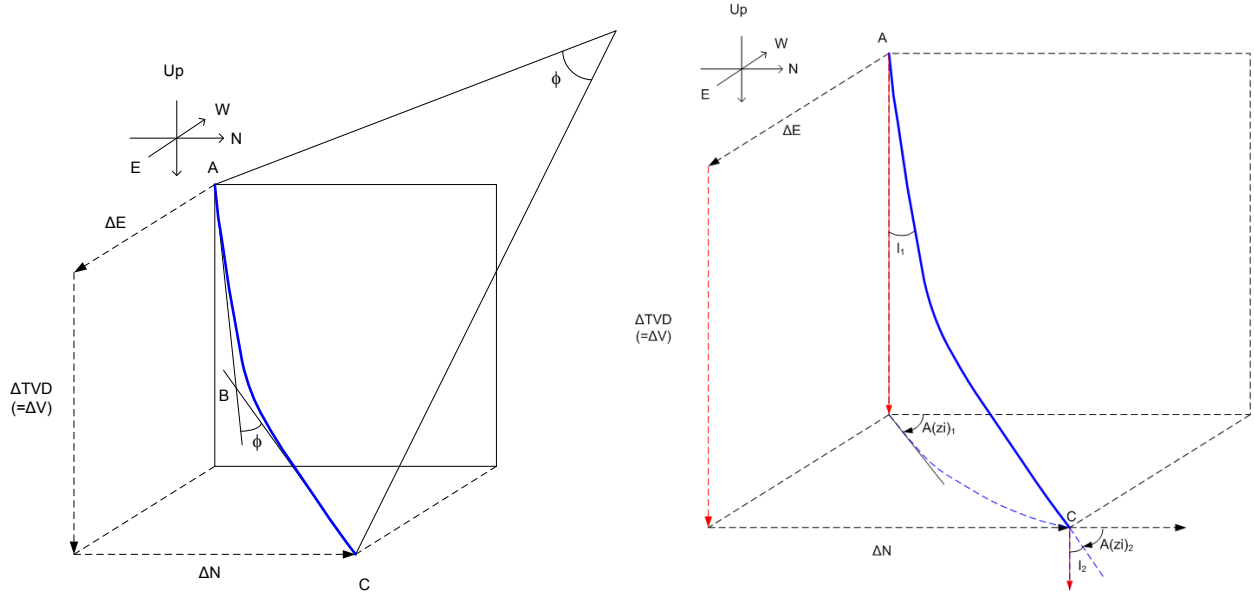

(a) Dogleg Angle (ϕ)

(b) Inclination (I) and Azimuth (A)

Figure 5.1: Relevant parameters when developing a well path [4].

5.2 Bottom Hole Assembly (BHA)

The Bottom Hole Assembly (BHA) design is one of the most decisive factor whether the solution proposed is mechanically sustainable. The basis for further discussion and final proposed design in regards to the BHA is presented in this section.

5.2.1 Directional Steering

The trajectory of the wellbore is affected by the BHA, therefore the intention when designing the BHA is to obtain directional control to foremost match the trajectory planned. To acquire direction the most commonly used BHAs include [4]:

- Traditional assemblies
- Steerable motor assemblies
- Rotary Steerable System (RSS)

Traditional assemblies are usually a straight motor in combination with a bent sub. This solution carries out some restrictions though, as the bit depends on a mud motor to cut the formation because the drill string itself cannot rotate, ultimately limiting its ability to create curvature. For these reasons, the traditional assemblies are only applicable in cases with larger hole sizes [5].

Directional control evolved significantly with steerable motor assemblies, which consists of a mud motor together with a bent sub or bent housing. Compared to the traditional assemblies this solution is much more sustainable and versatile emphasized with its ability to kick off and build angle, providing accurate directional control and its ability to drilling tangent sections. This technology is often utilized with vigorous parameters to increase drilling performance in challenging drilling environments.

The primary solution amongst many operators for directional control is RSS - as it can rotate and steer at the same time. However, with the technology being relatively new, complex and expensive, this solution is not always economically feasible. There are two concepts identified with this solution, respectively push the bit and point the bit. The difference between the two will be described to more detail in section 5.2.2.1.

5.2.1.1 Dogleg Severity Based on BHA Configuration

Equation 5.1 is one way to predict DLS, there is however an alternative based on the BHA configuration [4]:

$$DLS = \frac{2\,\theta}{L_1 + L_2} \tag{5.4}$$

Where $\theta[^\circ]$ is the bit tilt, $L_1[m]$ is the distance from the motor stabilizer to the bend and $L_2[m]$ is the distance from the bend to the bit; all parameters are illustrated in Figure 5.2.

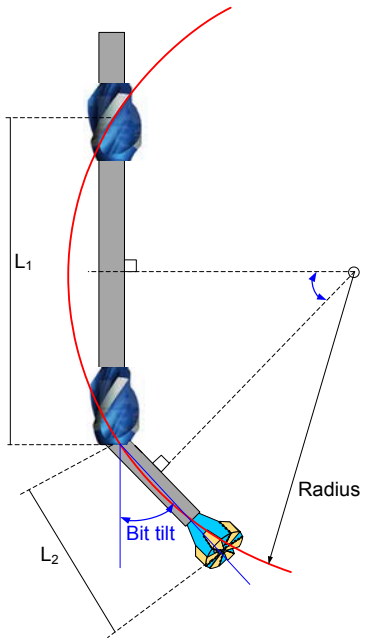

Figure 5.2: Dogleg Severity parameters based on BHA configurations [4].

5.2.2 Positive Displacement Motor (PDM)

As mentioned, a steerable motor assembly is made up of a mud motor and a bent housing or bent sub. There are two types of downhole mud motors, respectively Positive Displacement Motor (PDM) and Downhole Turbine Motor (DTM), of them PDM is by far most common. PDM was first introduced in the late 1950s, and has since improved directional drilling applications greatly. A steerable drilling system is required to manage both inclination and azimuth change, which is the main objective of this year's competition. Components making up a standard PDM are respectively a power section, an adjustable bend, and a bearing section. These components are illustrated in Figure 5.3, their function, and applicability will be discussed below.

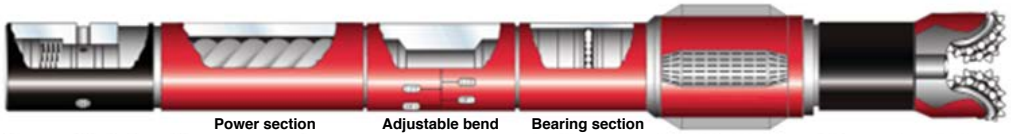

Figure 5.3: PDM Components [4].

Power Section

The power section is based on the Moineau principle and generates mechanical energy from hydraulic energy making the driveshaft rotate. The bit is connected to the driveshaft, therefore the bit Revolutions per Minute (RPM) will depend on motor speed and drill string rotation. The main components, rotor and stator, have similar profilesexcept for the rotor having one less lobe; shown in Figure 5.5. Moineau principle states that a helical rotor will rotate eccentrically if the stator has more lobes than the rotor, illustrated in Figure 5.4.

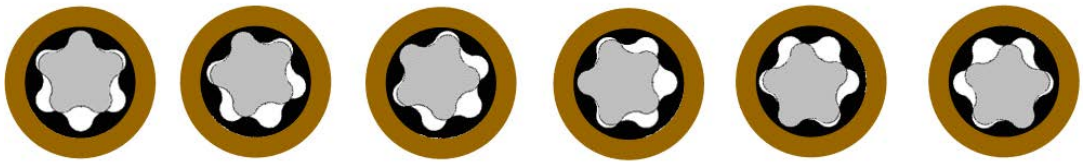

Figure 5.4: Cross section of power section at different depths [4].

The drilling fluid circulating through the motor shall have high velocity, therefore the rotor should be manufactured using a corrosion-resistant stainless-steel to reduce abrasion and friction. Material of the stator should preferably be of steel in combination with an elastomer or rubber lining. A total number of lobes affects torque and RPM, with the general idea being that torque is increasing with the number of lobes present, while RPM decreases as shown in Figure 5.5.

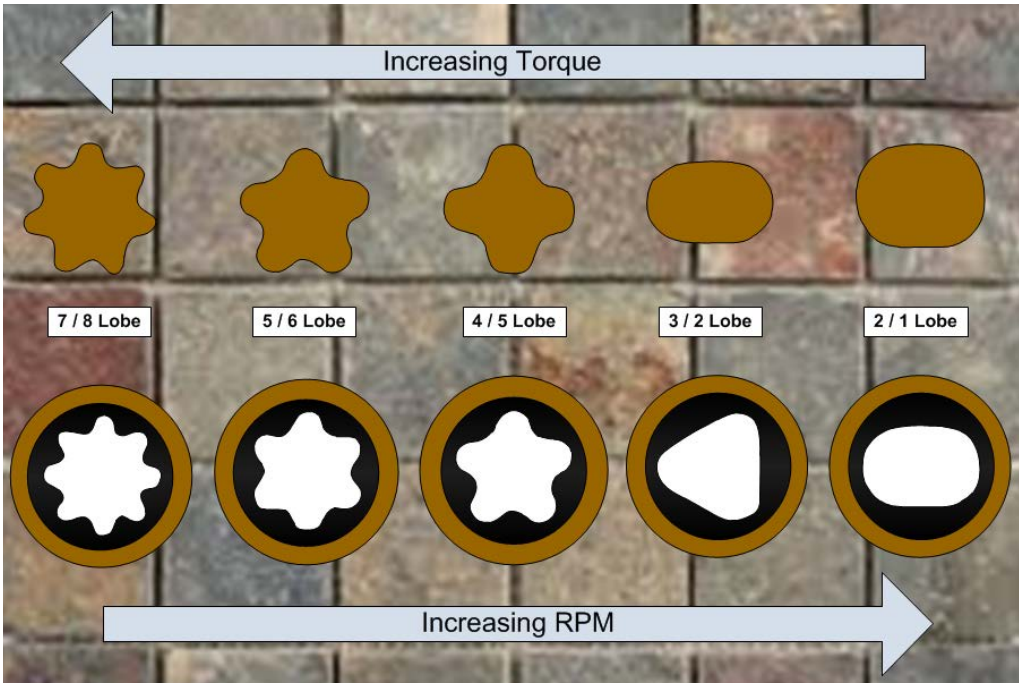

Figure 5.5: Number of lobes affect on Torque and RPM [4].

To best utilize the PDM, an estimate of its performance is vital. Pressures lost through the PDM will affect the hydraulic system, which again will change the RPM and torque it can deliver. In the event of the required torque to rotate ends up being too high, the PDM will begin to stall, and possibly lose its functionality. This is due to no pressure increase in the cavities, resulting in no RPM and torque as there will not be any rotor rotation. Knowing the motor producing capacity is therefore of the utmost importance, as the control system has to keep the PDM within its continuous operating range while still optimizing the drilling parameters to obtain the highest possible Rate of Penetration (ROP).

In practice, power sources of this sort are associated with a performance chart showing the performance ability of a given model for different scenarios. The team will develop their own PDM design, and with that,

some rough calculations are needed. Equation 5.5 estimates fluid displacement, $q_0[gal/min]$, of the motor looking at the PDM geometry, respectively number of lobes, i, the major stator diameter, $D_h[in]$, and length of stator, $L_{PDM}[in]$ [6].

$$q_0 = 0.00433 \cdot 0.79 \frac{i(i+1)}{(2-i)^2} D_h^2 L_{PDM} \tag{5.5}$$

Estimating ideal PDM torque, $T[Nm]$, and RPM are done using Equation 5.6 and 5.7; input variables include fluid displacement predicted with Equation 5.5, flow rate, $q[gal/min]$, and PDM pressure drop, $\Delta P_{PDM}[psi]$ [7].

$$RPM = \frac{q}{q_0} \tag{5.6}$$

$$T = 1.256 \cdot 3.066 q_o \Delta P_{PDM} \tag{5.7}$$

Parameters such as frictional loss and slip flow are neglected.

Bent Housing

Bit tilt is accomplished using a bent housing, which respectively is divided into two possible solutions; fixed angle or adjustable angle. A fixed angle bent sub, illustrated in Figure 5.6, is made of steel in a fixed bit tilt.

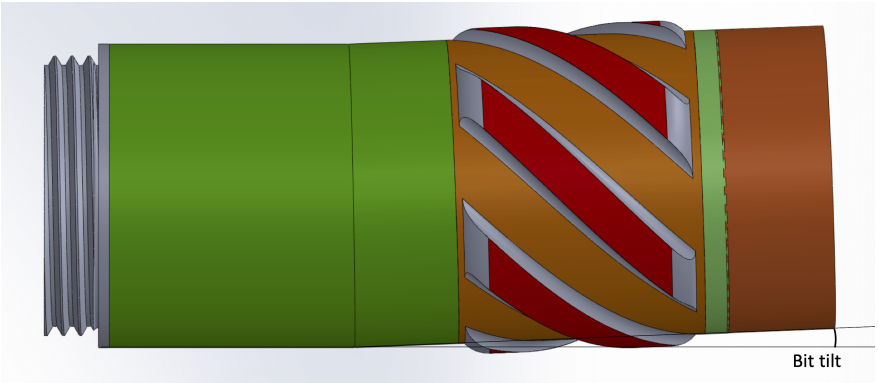

Figure 5.6: Bent sub with fixed angle.

Surface adjustable bent subs consist of a double pin, lock housing, adjusting sleeve and offset housing. Figure 5.7 shows the angle adjusting sequence, which is performed as follows:

1. Unscrew the lock housing and disengage the sleeve from its gear teeth.
2. Adjust to the preferred angle.
3. Tighten the lock housing to detain the wanted angle.

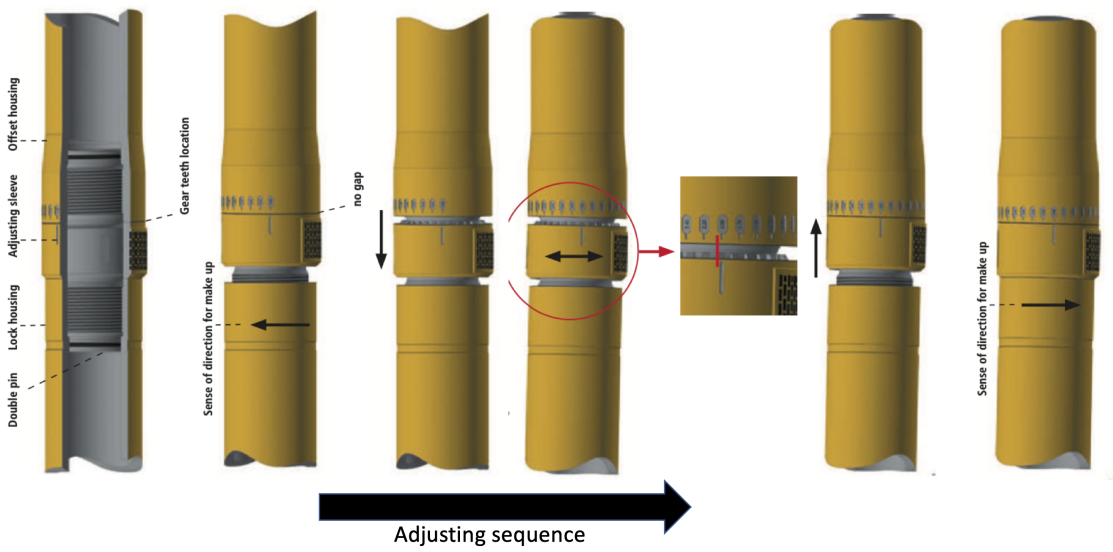

Figure 5.7: Adjustable bend in bent sub [8].

Transmission Section

The transmission section generates concentric rotation from eccentric rotation using the power section. Figure 5.8 shows the two possible transmission joints, respectively a flexible rod and a sequence of u-joints [4]. Flexible rods are preferred in the industry due to low maintenance cost and no lubrication requirement, be aware though lateral bending is limited [9].

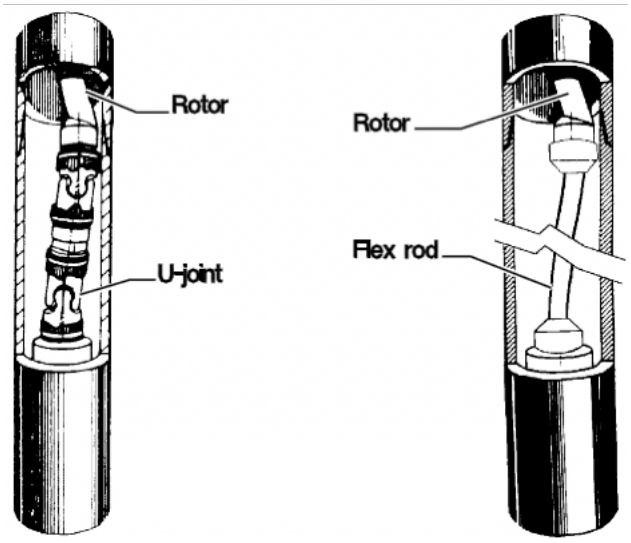

Figure 5.8: U-joint type on left side and flexible joint on right side [4].

Bearing Section

The bearing section transmits torque and RPM to the drill bit, and acts as axial and radial support. It usually consists of three sets of bearing, two radial - and one axial bearing which supports on- and off bottom load and hydraulic thrust. Most of the fluid flows through the driveshaft, however, a small percentage will divert

into the bearings, helping to cool and lubricate them as shown in Figure 5.9. Fluid flow through the bearings generates hydraulic downwards thrust, which needs to balance with the upward thrust from Weight on Bit (WOB) to increase the bearing lifetime [10].

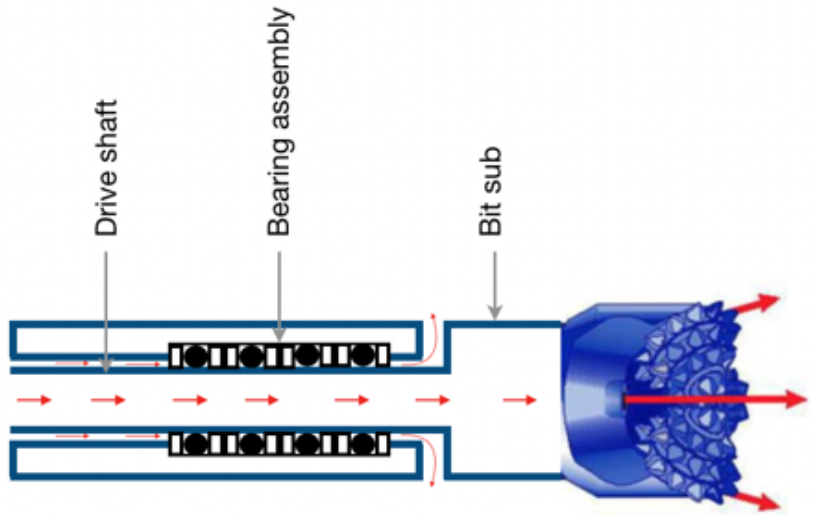

Figure 5.9: Bearing section with flow paths in red.

5.2.2.1 Rotary Steerable System (RSS)

RSS conquers the drawbacks associated with steerable motors and conventional rotary assemblies and is a significant development in directional-drilling technology. This technology allows for continuous drill string rotation while steering the bit, as a result, penetration rate is improved. Other benefits with RSS include improved hole quality, lower torque and drag, and better hole cleaning as rotation of the drill string in deviated wells generates disturbance in the annular flow pattern. To provide directional control, this solution utilizes the three points of contact principle, respectively the bit, near-bit stabilizer and upper stabilizer. As briefly mentioned, the two methods related to RSS are:

- **Push the bit.** Motorized pads are applied on the outer part of the tool, respectively at the middle geometric contact. Direction is built as a result of force created by the pads being pressed against the borehole wall.
- **Point the bit.** This solution is rather flexible adjusting the direction of the bit using a motorized mechanism when pointing the bit, separating it from a mud motor that manually has to orient the drill string. The general idea, however, is the same with the bit having an offset from the center axis.

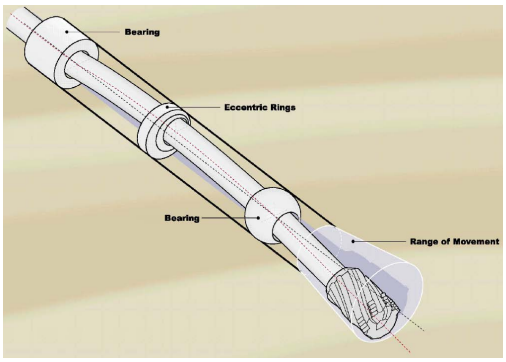

(a) Push the bit

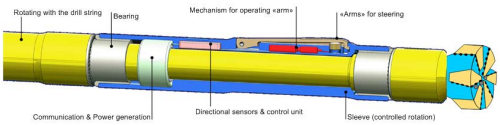

(b) Point the bit

Figure 5.10: The two methods of RSS [4].

RSS provides constant drilling parameters, making the weight transfer and vibration issues to the bit more efficiently controlled and manageable. The well path is typically smoother, as a result of less tortuosity. Even though there are obvious advantages with RSS, one should emphasize the complexity of this technology both mechanically and electronically, limiting the usage of it as a result of economic feasibility. Typically this solution is used for complex profiles applicable for designer wells or extreme Extended Reach Drilling (ERD).

5.3 Drill String Mechanics

Being aware of mechanical limits while drilling is essential, as exceeding them might result in drill string failure. This section covers probable challenges encountered during a drilling operation, and formulas associated to calculate mechanical limits.

5.3.1 Buckling

Avoiding drill string failure is essential. Drill string buckling appears in two stages, sinusoidal and helical [11]. The first stage occurs with increasing compressive loads and is know as sinusoidal buckling, which in short means the drill string will resemble a sinus wave, in other words, a two-dimensional waveform. In practice, this means the drill string will wind back and forth against the wellbore. If further compressive load is applied, the second stage will be entered which is referred to as helical buckling. The drill string will then go up and down the side of the wellbore in a helix shape. Maintaining the same WOB requires more axial load as the increased contact area between drill string and wellbore increases drag.

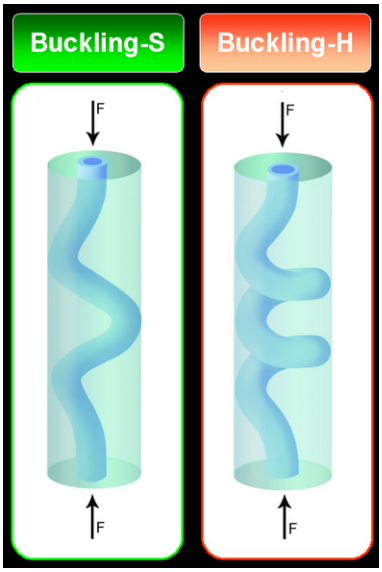

Figure 5.11: Illustrates how the drill string might act as a result of overload [12].

As described, in the event of excessive axial compressive force exceeding its critical value the drill pipe will buckle. Critical buckling limit is predicted using Euler's column formula for long columns [13]:

$$\sigma_{cr} = \frac{F_{cr}}{A} = \frac{\pi^2 E}{\left(K\frac{L}{r_g}\right)^2} \tag{5.8}$$

Where $\sigma_{cr}[Pa]$ is the critical load, $E[Pa]$ is the modulus of elasticity, the unsupported pipe length is given by $L[m]$, and radius of gyration is $r_g[m]$. The effective length factor is given by K and is determined by the end condition of the column; the different scenarios are presented in Table 5.1.

Radius of gyration is a function of the second moment of area for a pipe, $I[m^4]$, and the cross-sectional area of the pipe, $A[m^2]$.

$$r_g = \sqrt{\frac{I}{A}} \tag{5.9}$$

$$I = \frac{\pi}{64}\left(OD^4 - ID^4\right) \tag{5.10}$$

Table 5.1: Effective Length Factor, K, which depends on the end conditions of the column [13].

End condition	**Pinned-pinned**	**Fixed-fixed**	**Fixed-pinned**	**Fixed-free**
Illustrations				
Theoretical K	1	0.5	$1/\sqrt{2}$	2
Recommended K	1	0.9	0.9	2.1

Whether a column is susceptible to buckling is indicated by its slenderness ratio. "Long" columns have a high slenderness ratio and are therefore more susceptible to buckling. The slenderness ratio, referred to as R_s, is observed in Equation 5.8 as L/r_g.

$$R_s = \frac{L}{r_g} \tag{5.11}$$

As mentioned the Euler formula (Equation 5.8) is used for long columns, while Johnson formula is used for intermediate columns[13]. Johnson's formula is presented in Equation 5.12, where $\sigma_{ys}[Pa]$ is the material yield strength.

$$\sigma_{cr} = \sigma_{ys} - \left(\frac{\sigma_{ys} K L}{2\pi r}\right)^2 \left(\frac{1}{E}\right), \qquad \frac{L}{r_g} \leqslant \left(\frac{L}{r_g}\right)_{cr} \tag{5.12}$$

The critical slenderness ratio decides whether Euler's or Johnson's formula is used to predicting the buckling limit for a given column, with certain end conditions. Equation 5.13 is used to predict the critical slenderness ratio.

$$\left(\frac{L}{r_g}\right)_{cr} = \sqrt{\frac{2\pi^2 E}{K^2 \sigma_{ys}}} \tag{5.13}$$

Maximum allowable WOB to avoid buckling can easily be estimated from the critical compression, predicted from the Euler formula (Equation 5.8) or the Johnson formula (Equation 5.12) depending on the critical

slenderness ratio.

$$F_{max\ WOB} = \sigma_{cr} A \tag{5.14}$$

5.3.2 Burst

Pipe burst occurs as a result of the internal pressure exceeding what the pipe can withstand. Barlow's equation has, for a long time, been used as a standard equation for calculating burst in the industry, however, the equation has shown to be over-conservative for thick-walled pipe [14]. The American Petroleum Institute (API) burst-pressure equation (Equation 5.15) is based on Barlow's equation, but takes into account the uncertainties concerning wall thickness by adding a reduction factor of 0.875 [15].

$$P_{burst} = 2\frac{0.875\sigma_{ys}t}{OD\ SF} \tag{5.15}$$

Where $t[m]$ is the material thickness and SF a safety factor, here $SF = 3$ when drilling and $SF = 2$ when tripping [12].

5.3.3 Twist-off

Twist-off is a result of induced shear stress, caused by high torque, exceeding shear strength of the pipe. This will then be a limiting factor for torque allowance on the Drill pipe (DP). Using the thin wall assumption, $\tau(r)$ is constant, and mean radius the maximum allowable torque is defined by [12]:

$$T_{max} = \tau_{max}\frac{\pi}{16}(OD^2 - ID^2)(OD + ID) \tag{5.16}$$

The Von-Mises criterion is then used to find τ_{max}, assuming $\sigma_{23} = \sigma_{31} = 0$ and $\sigma_{12} = \tau_{max}$:

$$\tau_{max} = \sqrt{\frac{2\sigma_{ys}^2 - [(\sigma_z - \sigma_\theta)^2 + (\sigma_\theta - \sigma_r)^2 + (\sigma_r - \sigma_z)^2]}{6}} \tag{5.17}$$

The radial and angular stresses is only caused by internal pressure and can be found by using Equation 5.18 and 5.19 [16]. Total axial stress on the drill string is a sum of axial stress from pressure, bending and WOB, which is calculated using Equation 5.20, 5.21 and 5.22.

$$\sigma_r = \frac{(\frac{ID}{OD})^2 - (\frac{ID}{2r})^2}{1 - (\frac{ID}{OD})^2}p \tag{5.18}$$

$$\sigma_\theta = \frac{(\frac{ID}{OD})^2 + (\frac{ID}{2r})^2}{1 - (\frac{ID}{OD})^2}p \tag{5.19}$$

$$\sigma_z^p = \frac{(\frac{ID}{OD})^2}{1-(\frac{ID}{OD})^2}p \tag{5.20}$$

Where $r[m]$ is the distance from center of pipe to Point of Interest (POI).

$$\sigma_z^{WOB} = \frac{WOB}{A_{cs}} \tag{5.21}$$

5.3.4 Pipe Bending

Bending stress is the axial stress induced by DP bending. Bending stress for a beam is given by Equation 5.22. Assuming the cross-sections perpendicular to the neutral axis of the beam remains constant [16]. A pipe becomes temporarily thinner on the stretch side when bent and thicker where it is compressed [17].

$$\sigma_z^b = \frac{E}{RC}r \tag{5.22}$$

5.3.5 Fatigue

The most common and costly consequential failure when drilling is drill string fatigue. Fatigue is a dynamic phenomenon resulting from stresses applied repeatedly initiating microcracks in the drill pipe which with time can propagate into macrocracks. In combination with corrosion, the cyclic stress shortens the expected lifetime of a drill string significantly.

Fatigue, in principle, only occurs if the drill string rotates while it is axially curved, this curved section respectively experiences one stress cycle per revolution[11]. The cyclic stress is affiliated with bending stress generated from the curvature, as the stress amplitude is directly proportional to the degree of curvature. Bending stress, which is calculated using Equation 5.22, represents the cyclic stress, and relationship illustrated in this equation shows that the bending stress increases with increasing Outer Diameter (OD). In wells with high DLS a smaller size drill string might therefore be desirable to minimize fatigue damage.

The fatigue limit of a material is expressed by its correlating S-N curve. The bending stress should not exceed the endurance stress limit given by the fatigue (S-N) curve, as the drill string is not limited to number of rotations. In cases where the material reaches its plastic limit due to high enough appliance of stress, fewer stress cycles is needed to break the material.

5.4 Control Theory

To be able to create an autonomous drilling rig, control theory has to be utilized. In this section, relevant theory and how these may be utilized will be presented.

5.4.1 PID Controller

When controlling the drill bit to follow the reference path, the team will use a proportional-integral-derivative controller, or PID for short. Both linear-quadratic regulator and model predictive control has been considered, but will not be used due to sub-par state knowledge. A PID controller is shown in Figure 5.12. A reference signal of our desired states is calculated and then compared with the estimated states of the drill bit. Once the error is calculated, the PID controller multiplies the proportional, integral and derivative of the error by parameters K_p, K_d and K_i respectively, which produces an input for the actuators [18]. The calculated input is therefore expressed by Equation 5.23.

$$u(t) = K_p e(t) + K_i \int_0^t e(\tau)d\tau + K_d \frac{de(t)}{dt}. \tag{5.23}$$

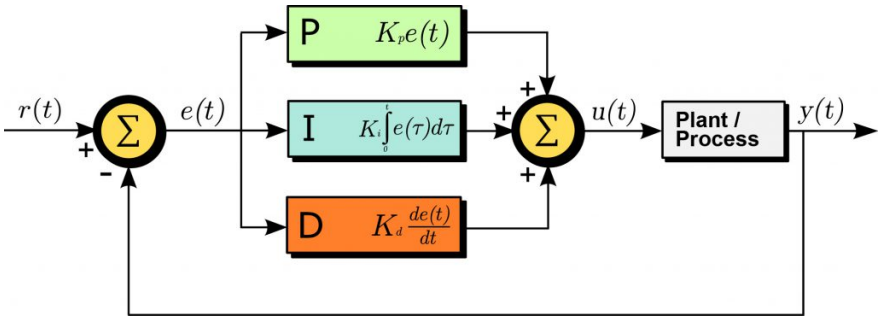

Figure 5.12: A typical PID controller scheme [19].

To better understand the different parts of the PID controller and how these affect the response of the states in the system, the different parts will be explained below together with Figure 5.13 [20].

- P - Proportional
  The parameter K_p is used to change the impact of the proportional part of the PID controller. By changing K_p, we can determine how fast we want the states of the system to reach a certain reference. The rise time is the time it takes for the state to reach a certain percentage of the reference, and is what will be controlled by changing K_p.

- I - Integral
  The parameter K_i is used to increase or decrease the integral part of the PID controller, and is used to remove the steady-state error. Usually, the proportional part of a PID controller is not enough for the state to reach the desired reference as the error decreases. The integral part is therefore used to make sure the deviation gets canceled.

- D - Derivative
  The parameter K_d is used to control the relevance of the derivative part of the PID controller. This part is often also referenced to as the dampening effect, as it dampens out the response. The percent of overshoot and settling time can thus be controlled by this part

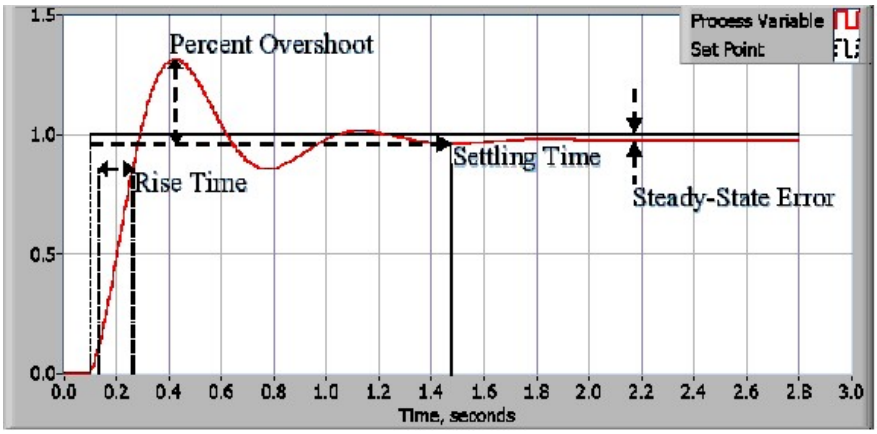

Figure 5.13: A typical response from a PID controller showing the different parameters [20].

5.4.2 Coordinate Frames

When working with points and vectors given in different frames, it is needed to translate them into the same frame. An example of such a situation is given in Figure 5.14, where there is an inertial frame, and a UAV with measurements given in its coordinate frame. The dynamics of controlling a drilling rig has many similarities with this situation, as there are downhole measurements that need to be used to control the drillbit in a path defined in the inertial frame.

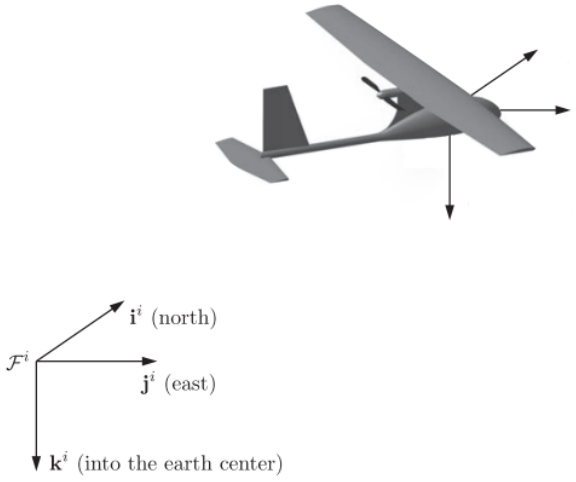

Figure 5.14: A UAV relative to an inertial frame [21].

In order to transform vectors given in one coordinate frame to another, the team will use both translation and rotation matrices. Translation matrices are used to linearly move vectors from one frame to another, while rotation matrices are used to get the correct direction of the vector in the new coordinate frame. The team will base all transformation from the desired inertial frame to the drill bit using linear translation matrices, and the three rotational matrices given in Equation 5.24, 5.25 and 5.26.

$$\mathbf{R}_z(\psi) = \begin{bmatrix} \cos\psi & -\sin\psi & 0 \\ \sin\psi & \cos\psi & 0 \\ 0 & 0 & 1 \end{bmatrix} \tag{5.24}$$

$$\mathbf{R}_y(\theta) = \begin{bmatrix} \cos\theta & 0 & \sin\theta \\ 0 & 1 & 0 \\ -\sin\theta & 0 & \cos\theta \end{bmatrix} \tag{5.25}$$

$$\mathbf{R}_x(\phi) = \begin{bmatrix} 1 & 0 & 0 \\ 0 & \cos\phi & -\sin\phi \\ 0 & \sin\phi & \cos\phi \end{bmatrix} \tag{5.26}$$

These are the essential rotation matrices in the often used ROLL-PITCH-YAW system. To get from the inertial frame to the body frame, a translation transformation is done, followed by a YAW-PITCH-ROLL rotation. Yaw is given by ψ, pitch by θ and roll by ϕ. Rotations as these, where the rotation is described as a rotation around axis by axis is called simple rotation [22]. An important observation is that these matrices are a more general class of orthonormal rotation matrices, which gives the properties given by Equation 5.27, 5.28 and 5.29,

$$(\mathbf{R}_a^b)^{-1} = (\mathbf{R}_a^b)^T = R_b^a \tag{5.27}$$

$$\mathbf{R}_b^c\mathbf{R}_a^b = \mathbf{R}_a^c \tag{5.28}$$

$$det(\mathbf{R_a^b}) = 1, \tag{5.29}$$

where the subscript variable of the matrices represent the original coordinate frame, and the superscript variable is the destination coordinate frame. By using these properties, it is possible to transform vectors from inertial to body frame, as well as from body to inertial frame [22]. The full rotation around each of the axis to get from coordinate frame a to b is given by Equation 5.30,

$$\mathbf{R}_b^a = \mathbf{R}_z(\psi)\mathbf{R}_y(\theta)\mathbf{R}_x(\phi), \tag{5.30}$$

where the coordinate frame a is first rotated ϕ around the x-axis and then θ and ψ around the already rotated coordinate frames. A coordinate point $\mathbf{p}^b$ given in frame $\{b\}$, can be translated to the point $\mathbf{p}^a$ in $\{a\}$ as seen in Equation 5.31.

$$\mathbf{p}^a = \mathbf{R}_b^a\mathbf{p}^b \tag{5.31}$$

Angular velocity transformation is given by

$$\boldsymbol{\omega}_{ab}^{a} = \boldsymbol{\omega}(\dot{\psi}) + \mathbf{R}_z(\psi)\boldsymbol{\omega}_y(\dot{\theta}) + \mathbf{R}_z(\psi)\mathbf{R}_y(\theta)\boldsymbol{\omega}_x(\dot{\phi}) \tag{5.32}$$

5.4.3 Inertial Measurement Unit

Intertial Measurement Unit (IMU) consists of three different measurement units. Angular rate is measured by a gyroscope, acceleration by an accelerometer, and heading by using a magnetometer. The measurements obtained can be used to calculate position, velocity and orientation. These calculations might be inaccurate due to the fact that computations are done by integrating measurements containing bias, which can cause drift. If the IMU is mounted at the center of the body frame, $\{b\}$, the measurements can be expressed as [23]

$$\mathbf{a}_{imu}^{b} = \mathbf{R}_n^b(\boldsymbol{\Theta})(\dot{\mathbf{v}}_{nb}^{b} - \mathbf{g}^n) + \mathbf{b}_{acc}^{b} + \mathbf{w}_{acc}^{b} \tag{5.33}$$

$$\boldsymbol{\omega}_{imu}^{b} = \boldsymbol{\omega}_{nb}^{b} + \mathbf{b}_{gyro}^{b} + \mathbf{w}_{gyro}^{b} \tag{5.34}$$

$$\mathbf{m}_{imu}^{b} = \mathbf{R}_n^b(\boldsymbol{\Theta})\mathbf{m}^n + \mathbf{b}_{mag}^{b} + \mathbf{w}_{mag}^{b} \tag{5.35}$$

where $\boldsymbol{\Theta} = [\phi, \theta, \psi]$ is a vector of Euler angles and $\mathbf{R}_n^b(\Theta)$ is the rotation matrix between the inertial frame and body frame shown in section 10.5.1. The accelerometer and gyro bias are denoted as b_{acc}^{b} and b_{gyro}^{b}, while b_{mag}^{b} is the local magnetic disturbance. w_{acc}^{b}, w_{gyro}^{b} and w_{mag}^{b} are Gaussian measurement noise. This IMU measurement model is only valid for low speed operations.

Calculating Yaw Angle Using Magnetometer

When ϕ and θ are non-zero, the angle ψ_m can be calculated by using Equation 5.36 and 5.37. First, the magnetometer measurements gets converted to the horizontal plane by using Equation 5.36.

$$\begin{bmatrix} h_x \\ h_y \\ h_z \end{bmatrix} = \mathbf{R}_{y,\theta}\mathbf{R}_{x,\psi} \begin{bmatrix} m_x \\ m_y \\ m_z \end{bmatrix} \tag{5.36}$$

The sign of h_x and h_y must be taken into account when computing the heading ψ. This can be done by using Equation 5.37.

$$\psi_m \begin{cases} 180^\circ - \frac{180^\circ}{\pi}\arctan\frac{h_y}{h_x} & \text{if } h_x < 0 \\ -\frac{180^\circ}{\pi}\arctan\frac{h_y}{h_x} & \text{if } h_x > 0, h_y < 0 \\ 360^\circ - \frac{180^\circ}{\pi}\arctan\frac{h_y}{h_x} & \text{if } h_x > 0, h_y > 0 \\ 90^\circ & \text{if } h_x = 0, h_y < 0 \\ 270^\circ & \text{if } h_x = 0, h_y > 0 \end{cases} \tag{5.37}$$

Calculating Roll and Pitch Using Accelerometer

To calculate the pitch angle θ and roll angle ϕ, it must be assumed that $\dot{\mathbf{v}}_n^b = 0$. There is also an assumption

that the biases $\mathbf{b}_{acc}^{b}$ is removed by calibration, and the measurement noise $\mathbf{w}_{acc}^{b}$ is removed by filtering the signal. Equation 5.33 can be simplified to

$$\mathbf{a}_{imu}^{b} \approx -\mathbf{R}_{n}^{b}(\boldsymbol{\Theta})\mathbf{g}^{n} \tag{5.38}$$

Using Equation 5.38, it is possible to express roll and pitch as [23]

$$\phi \approx \arctan\left(\frac{a_y}{a_z}\right) \tag{5.39}$$

$$\theta \approx -\arctan\left(\frac{a_x}{\sqrt{a_y^2 + a_x^2}}\right) \tag{5.40}$$

5.4.4 State Estimation with Kalman Filter

A Kalman filter is an optimal state estimator that estimates states of a linear or a nonlinear system based on measurements and a physical model of the system. It is used in combination with sensors since it can estimate unmeasured states as well as remove noise from the measurements. In the case where we have temporary loss of measurements, the Kalman filter can also work as a state predictor, often also called dead reckoning [23]. In the case of using a Kalman filter in autonomous drilling, it is well suited to both estimate the position of the drill bit based on other measurements, as well as removing measurement noise and noise from the high amount of vibrations.

Understanding the Kalman Filter

The working principles of a Kalman filter can be illustrated by an example of vehicle position estimation. The initial estimate is given in Figure 5.15, and is denoted as $\hat{\mathbf{x}}_{\mathbf{k-1}}$. The car can be anywhere inside this curve, but it is expected that the car will be at the mean of the curve with the highest probability. To estimate the next position of the car, a prediction is done to get a prior estimate $\hat{\mathbf{x}}_{\mathbf{k}}^{-}$. In Figure 5.15, it can be seen that the prior estimate is not very accurate. The error covariance matrix $\mathbf{P}_{k}^{-}$, translates to uncertainty in predicting new states solely based on the state space model. By combining the uncertain prior estimate with the system measurements y_k, a better estimate can be found. This is called the posterior estimate $\hat{\mathbf{x}}_{\mathbf{k}}$ and is found by first calculating the Kalman gain $\mathbf{K}_k$, which then is used to minimize the error covariance for the posterior estimate $\hat{\mathbf{x}}_{\mathbf{k}}$.

When driving a car, one would be able to estimate the position of the car by integrating the angular velocity and size of the wheels. Once the car drives in holes, or if it is slippery, the wheels might slip or spin, which would be interpreted as positional movement by the model $\hat{\mathbf{x}}_{\mathbf{k}}^{-}$. By now combining this estimation with the measured position of the car with for example a GPS, which also has measurement noise, one would be able to better estimate the real position of the car, $\hat{\mathbf{x}}_{\mathbf{k}}$.

If there are no disturbances in the measurement, and there is only one state that can be measured perfectly,

$C = 1$, which gives a Kalman gain of $\mathbf{K_k} = 1$. In this case, the posterior estimate will be equal to the measurement $\hat{\mathbf{x}}_\mathbf{k} = \mathbf{y_k}$. On the other side, if we have a perfect model of the system, the prediction is perfect, which gives a prior error covariance of $\mathbf{P}^- = 0$, which gives a Kalman gain of $\mathbf{K_k} = 0$. This will, in turn, produce a posterior estimate which is only dependent on the prediction $\hat{\mathbf{x}}_\mathbf{k} = \hat{\mathbf{x}}_\mathbf{k}^-$. This illustrates how the Kalman filter is able to combine the certainties of the predictions and measurements to output the optimal estimate for the system.

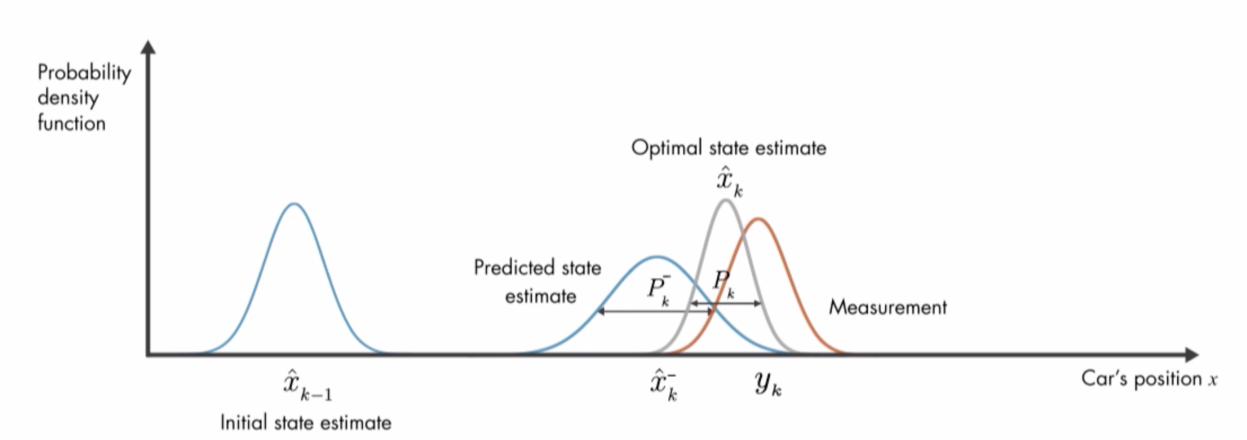

Figure 5.15: The working principle of the Kalman filter is described with the different probability distributions [24].

The discrete Kalman filter algorithm consists of the following steps. The general state dynamics can be described as follows

$$\mathbf{x}\left[k+1\right] = \mathbf{A}_d\mathbf{x}\left[k\right] + \mathbf{B}_d\mathbf{u} + \mathbf{w}[k] \tag{5.41}$$

$$\mathbf{y} = \mathbf{C}\mathbf{x} + \mathbf{v}[k], \tag{5.42}$$

where the algorithm gets initialized as follows

$$\hat{\mathbf{x}}^-(0) = \mathbf{x}_0 \tag{5.43}$$

$$\mathbf{P}^-(0) = E\left[(\mathbf{x}(0) - \hat{\mathbf{x}}(0))(\mathbf{x}(0) - \hat{\mathbf{x}}(0))^T\right] \tag{5.44}$$

$$\mathbf{Q} = E\left[\mathbf{w}\mathbf{w}^\mathbf{T}\right] \text{ , } \mathbf{R} = E\left[\mathbf{v}\mathbf{v}^\mathbf{T}\right] \tag{5.45}$$

The estimation is then done by the following steps

$$\mathbf{K}[k] = \mathbf{P}^-[k]\mathbf{C}^T\left(\mathbf{C}\mathbf{P}^-[k]\mathbf{C}^T + \mathbf{R}\right)^{-1} \tag{5.46}$$

$$\hat{\mathbf{x}}[k] = \hat{\mathbf{x}}^-[k] + \mathbf{K}[k]\left(\mathbf{y}[k] - \mathbf{C}\hat{\mathbf{x}}^-[k]\right) \tag{5.47}$$

$$\mathbf{P}[k] = \left(\mathbf{I} - \mathbf{K}[k]\mathbf{C}\right)\mathbf{P}^-[k]\left(\mathbf{I} - \mathbf{K}[k]\mathbf{C}\right)^T + \mathbf{K}[k]\mathbf{R}k[k]^T \tag{5.48}$$

$$\hat{\mathbf{x}}^-[k+1] = \mathbf{A}_d\hat{\mathbf{x}}[k] + \mathbf{B}_d u[k] \tag{5.49}$$

$$\mathbf{P}^-[k+1] = \mathbf{P}[k]\mathbf{A}_d\mathbf{P}^T[k] + \mathbf{Q}. \tag{5.50}$$

At each iteration, the Kalman filter algorithm uses the prior estimate $\hat{\mathbf{x}}^-[k]$ and the prior error covariance matrix $\mathbf{P}^-[k]$ to calculate the new Kalman gain $\mathbf{K}[k]$. The new Kalman gain is then used to estimate the new states and the new error covariances, $\hat{\mathbf{x}}[k]$ and $\mathbf{P}[k]$. The final two steps are to calculate the next prior estimate of the state and the prior error covariance, $\hat{\mathbf{x}}^-[k+1]$ and $\mathbf{P}^-[k+1]$. $\mathbf{R}$ is the covariance matrix of the measurement noise, and can be found experimentally by testing different $\mathbf{R}$ matrices and checking the result. $\mathbf{Q}$ is the covariance matrix of the process noise, and is not that easily found. It can be used to tune how much the Kalman filter should rely on the state space model and the measurements. With high values in $\mathbf{Q}$, the uncertainty of the prediction is increased, extending the range of where the true state vector lies. This means that with low $\mathbf{Q}$ values, there is more computation needed which renders a slower system, while the measurement noise gets better filtering. Both the process noise and measurement noise is assumed to be zero-mean Gaussian [25][23].

5.4.5 State Calculation with Euler's Method

When calculating state variables based on their derivatives, Euler's method is often used. The state variables evolve according to Equation 5.51,

$$y_{n+1} = y_n + hf(y_n, t_n), \tag{5.51}$$

where y_{n+1} is the new calculated state, y_n is the previous state, h is a defined step length, and $f(y_n, t_n)$ is the time-derivative of the function $y(t)$. By using Euler's method, the team will be able to integrate the time derivative states measured by the bottom hole sensors, which in turn gives the positional states.

An important consideration to make when using Euler's method is the step length. It is important to choose this variable so that the system is stable. The stability function for Euler's method is given by,

$$R(h\lambda) = 1 + h\lambda \tag{5.52}$$

where λ is the eigenvalues of the system. Stability of Euler's method is then achieved as long as,

$$|R(h\lambda)| \leq 1, \tag{5.53}$$

which gives stability when the following criteria is met

$$h \leq -\frac{2}{\lambda}. \tag{5.54}$$

The stability region is therefore given by a circle of radius $r = 1$, with center in $Re = -1$, and $Im = 0$, as seen in Figure 5.16. This theory is based on [22].

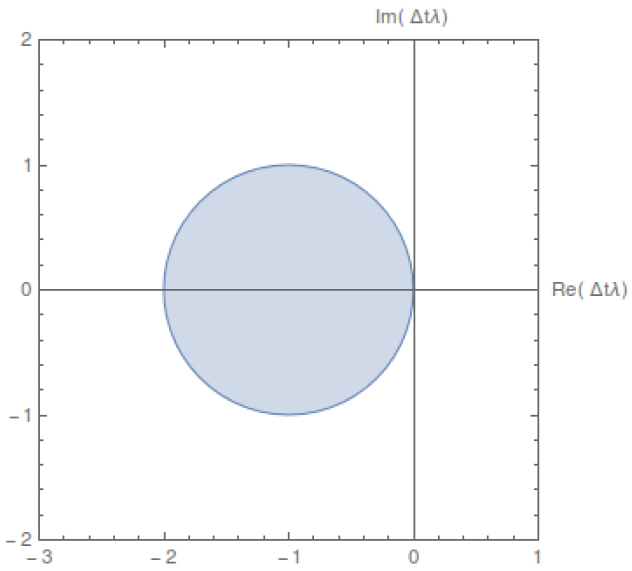

Figure 5.16: Stability region of Euler's method [26].

5.4.6 Cohen-Coon for PID Tuning

In order to tune the parameters of the PID controllers, Ziegler-Nichols method and the Cohen-Coon method have been evaluated. The former works well on processes that do not require fast adjustments [27], which is not the case with an autonomous drilling rig. The Cohen-Coon method has also been used in the earlier years with success, which is why this year's team also will use this method to find initial parameters.

The steps of finding the PID parameters can be split up into the following steps [28]:

- Give a constant Control output (CO) for the controller and wait for the Process variable (PV) to settle around this new point.
- Give a step response to the CO and wait for PV to settle around this new reference. Measure the total percentage change in PV, as well as CO, and calculate the process gain g_p with Equation 5.55. An example of such a response can be seen in Figure 5.17.

$$g_p = \frac{\Delta PV\%}{\Delta CO\%} \tag{5.55}$$

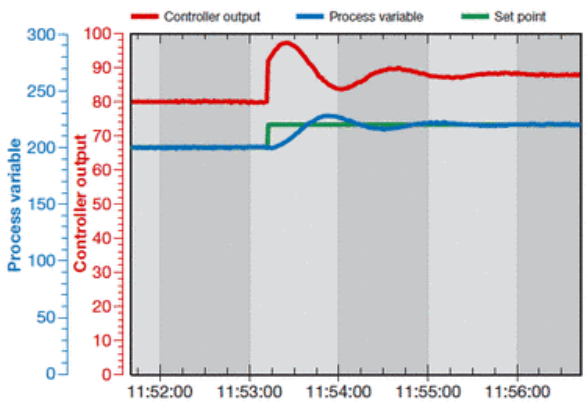

Figure 5.17: Finding the process gain based on the PID response [28].

- Examine the PV response to find the dead time t_d. This is found by drawing a line through the maximum slope of the response, as well as a line through the PV before the CO change. Measure the distance from the initial step response of the CO to the intersection between the two drawn lines. This gives the dead time t_d, and is shown in more detail in Figure 5.18.
- Examine the PV response to find the time constant τ. First calculate what 63% of the total PV change is, and locate this point on the response plot as shown in Figure 5.18. Measure the distance from this point to the intersection point found in the previous step. This is then the time constant τ.

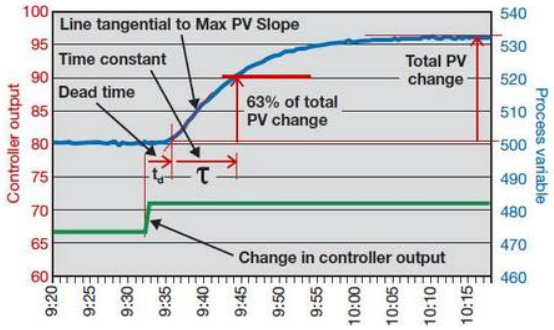

Figure 5.18: Finding the dead time and time constant in Cohen-Coon tuning method [28].

- Do the previous steps until a stable average value for the three parameters g_p, t_d and τ is found.
- Use the average value for the three parameters in the equations given in Table 5.2 to find the controller gain, integral time and derivative time.

Note that this method is done with open loop tuning. There is no feedback to the controller, and we are only changing the CO and measuring the response of the PV. After the initial tuning, we may test and change K_c or T_I to get an optimal response.

Table 5.2: Equations to find controller gain, integral time and derivative time [27].

	Controller gain (K_c)	Integral time (T_I)	Derivative time (T_D)
P	$K_c = \frac{1.03}{g_p}(\frac{\tau}{t_d} + 0.34)$		
PI	$K_c = \frac{0.9}{g_p}(\frac{\tau}{t_d} + 0.092)$	$T_I = 3.33t_d\frac{\tau+0.092t_d}{\tau+2.22t_d}$	
PD	$K_c = \frac{1.24}{g_p}(\frac{\tau}{t_d} + 0.129)$		$T_D = 0.27t_d\frac{\tau+0.324t_d}{\tau+0.129t_d}$
PID	$K_c = \frac{1.35}{g_p}(\frac{\tau}{t_d} + 0.185)$	$T_I = 2.5t_d\frac{\tau+0.185t_d}{\tau+0.611t_d}$	$T_D = 0.37t_d\frac{\tau}{\tau+0.185t_d}$

5.4.7 Cubic Spline Interpolation for Path Generation

Cubic spline interpolation is a method used to create a smooth function between given some coordinate points. By using cubic spline interpolation, it is possible to avoid oscillations that may occur when trying high polynomial methods. This is also called Runge's phenomenon. The method is based on solving a set of equations, based on the number of points given. Given $N + 1$ points, the algorithm uses N equations given by the general form shown in Equation 5.56. The equations created are valid for two following points, i.e. The first equation C_1 is valid for p_0 and p_2, and C_2 is valid for p_1 and p_2 [29].

$$C_i(x) = a_i + b_i x + c_i x^2 + d_i x^3 \tag{5.56}$$

Given three points $[x_0, y_0]$, $[x_1, y_1]$ and $[x_2, y_2]$, the method starts by creating two equations based on Equation 5.56. This gives the following two equations.

$$C_1(x) = a_1 + b_1 x + c_1 x^2 + d_1 x^3 \tag{5.57}$$

$$C_2(x) = a_2 + b_2 x + c_2 x^2 + d_2 x^3 \tag{5.58}$$

The first equation is valid for the left two points, and the second is valid for the right two points. The equation will join each other in x_1, which means that the equations are equal to each other in that point. This also holds for their derivatives and double derivatives. For a natural cubic spline, the endpoints of the second derivative is set to be zero. The coefficients can be found be solving the following system of equations.

$$C_1(x_0) = y_0 \tag{5.59}$$

$$C_1(x_1) = y_1 \tag{5.60}$$

$$C_2(x_1) = y_1 \tag{5.61}$$

$$C_2(x_2) = y_2 \tag{5.62}$$

$$C_1'(x_1) = C_2'(x_1) \tag{5.63}$$

$$C_1''(x_1) = C_2''(x_1) \tag{5.64}$$

$$C_1''(x_0) = 0 \tag{5.65}$$

$$C_2''(x_3) = 0 \tag{5.66}$$

After solving for the coefficients, the functions between the points will be given by Equation 5.67.

$$S(x) = \begin{cases} C_1(x) & \text{for } x_0 \leq x \leq x_1 \\ C_2(x) & \text{for } x_1 \leq x \leq x_2 \end{cases} \tag{5.67}$$

5.5 Drilling Hydraulics

The hydraulic system in the oil and gas industry is one of the most important factors to achieve sufficient drilling performance, as it has great impact on hole cleaning and then the ROP. The main responsibility of the drilling fluid is to remove cuttings from under the bit. To achieve sufficient hole cleaning the drilling fluid has several other functions and tasks that are listed below [4]:

- Removal of cuttings from under the bit.
- Transportation of cuttings from bottom to surface.
- Wellbore stability, keep the well in overbalance.
- Cooling and lubrication of the bit and drill string
- Creation of mud cake, to prevent fluid loss to natural of induced cracks.
- Data transfer, by mud pulse technology

5.5.1 Hole Cleaning

In general, the ROP is what the drilling operation will be evaluated upon as a high ROP will decrease time to drill a well and then save money. When drilling, there will constantly be generated cuttings. To achieve desired ROP, there is a need to transport the cuttings away from the bit and out of the well.

The transportation of cuttings out of the well can be divided into three different flow regimes, based on the hole inclination:

- Vertical section - $[0° - 30°]$
- Tangent section - [30° ~ 65°]
- Horizontal section - [~ $65° - 90°$]

The Drillbotics© competition will not require wellbore inclination in excess of $30°$, therefore it will only be focused on hole cleaning theory in a vertical section flow regime. The derivation of cuttings transport formulas can be found in the appendix section B and only the needed formulas will be presented in this section.

The slip velocity of cutting particles in a laminar flow regime is given as:

$$v_{sl} = \frac{d_s^2 g(\rho_s - \rho_f)}{18\mu_f} \tag{5.68}$$

where $d_s[m]$ is cutting diameter, $\rho_s[kg/m^3]$ is cutting density, $\rho_f[kg/m^3]$ fluid density and $mu_f[Pas]$ is fluid viscocity. As not all the fluid flow can be described by the laminar flow regime, there is need to express the slip velocity for all flow regimes:

$$v_{sl} = \sqrt{\frac{4(\rho_s - \rho_f)gd_s^2}{3f\rho_f}} \tag{5.69}$$

f is an empirical friction factor determined from Figure 5.19. The final slip velocity is found by estimating slip velocity with Equation 5.68, calculating the Reynolds number, estimating friction factor and then calculating slip velocity with Equation 5.69.

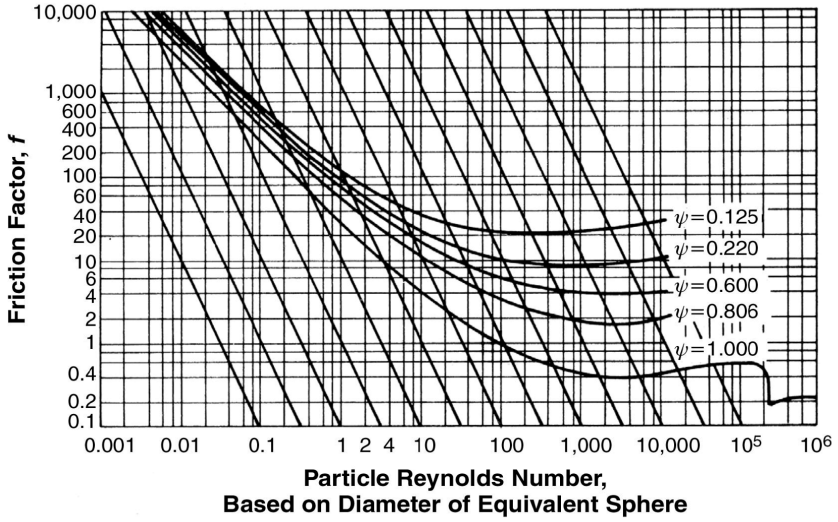

Figure 5.19: Relationship between f and Re for settling particles in Newtonian fluids [15].

When the slip velocity is determined, the required flow rate is found by using Equation 5.70:

$$q = A_{cs}\frac{v_{sl}}{1 - R_t} \tag{5.70}$$

where $R_{transport}$ is the desired transport ratio and $A_{cs}[m^2]$ is cross section area to the section of interest.

5.5.2 Pressure Losses

Hydraulic energy in the drilling system is created by the mud pumps, the pumps take the drilling fluid at the inlet and transfer it to the hose while increasing its pressure to the desired value. The fluid enters the DP by passing through a swivel and then down to the bit. The transportation of fluid through each component

decreases the pressure, also known as pressure loss. By dividing the whole hydraulic system into different components, the pump pressure can be expressed as a sum of the different component's pressure loss:

$$P_{pump} = \Delta P_{hose} + \Delta P_{swivel} + \Delta P_{DP} + \Delta P_{BHA} + \Delta P_{nozzle} + \Delta P_{ann}$$

where only the major pressure losses is taken into account, the minor pressure losses is neglected and compensated by adding a safety factor to the required pump pressure.

5.5.2.1 Pipe Pressure Losses

The pipe pressure loss can be estimated by using Equation 5.71 [30], this is valid for flow inside pipe by using Equation B.9 as d_h and Equation B.8 as d_h for annular flow.

$$\Delta P_i = f_i \frac{L_i}{d_{h,i}} \frac{\rho_f v_i^2}{2} \tag{5.71}$$

Here $\Delta P[Pa]$ is the pressure loss, $L_i[m]$ is the length of component, $v_i[m/s]$ is the fluids velocity and f is the friction factor, based on flow regime. Flow regime is estimated from the Reynolds number in Equation B.7, for laminar flow $Re < 2300$ and turbulent flow $Re > 4000$ [31]. Further the friction factor can be estimated using the Colebrook equation [30]:

$$\frac{1}{\sqrt{f}} = -2.0 \log_{10}(\frac{\epsilon/ID}{3.7} + \frac{2.51}{Re\sqrt{f}}) \tag{5.72}$$

Colebrook equation is a implicit equation, so the friction factor needs to be iterative estimated. Equation 5.73 is a simpler estimate of the friction factor, only applicable for laminar flow and independent on pipe roughness as long as its not extreme [30].

$$f = \frac{64}{Re} \tag{5.73}$$

5.5.2.2 Bit Pressure Losses

In order to aid cuttings removal from the bottom, high-velocity fluid needs to exit the bit nozzles. The needed velocity increase is done by having a relatively small cross-sectional area of the bit nozzles, which will induce a pressure drop to the system. The pressure drop can be found by using the estimation of fluid velocity v_n in the nozzles, given by Equation 5.74.

$$v_n = C_d \sqrt{\frac{2\Delta P_{nozzle}}{\rho_f}} \tag{5.74}$$

Experimental measurements have found this value to be a overestimate, therefore the discharge coefficient C_d is used and equal to 0.95 [32]. Rearranging of Equation 5.74 and writing velocity as a function of flow

rate and total nozzle area, the pressure loss across the bit nozzles is calculated by Equation 5.75:

$$\Delta P_{nozzle} = \frac{\rho_f q^2}{2A_n^2 C_d^2} \tag{5.75}$$

where $q[m^3/s]$ is the flow rate and $A_n[m^2]$ is the total flow area of the nozzle(s).

6 Design Limits and Uncertainties

Table 6.1 gives an overview of the parameters used as a basis for all further calculations. The diameter of the Bottom Hole Assembly (BHA) is scaled up to meet this year's bit size compared to last year's. These parameters will be used in this section to estimate the limits and uncertainties of the design.

Table 6.1: Relevant parameters.

Named Variable	Symbols	Value	Unit
OD DP	OD_{DP}	3/8	in
Wall thickness	t_{DP}	0.049	in
Length DP	L_{DP}	36	in
Elasticity Modulus[3] [33]	E	200	GPa
Elasticity Modulus[2] [34]	E	68.9	GPa
Material Yield Strength[3] [33]	σ_{ys}	196	MPa
Material Yield Strength[2] [34]	σ_{ys}	276	MPa
Fatigue Strength [1] [2] [33]	σ_{ys}	96.5	MPa
OD BHA	OD_{BHA}	1.42	in
ID BHA	ID_{BHA}	1.04	in
Length BHA	L_{BHA}	3.35	in
ID Swivel + Hose	$ID_{Swivel+Hose}$	0.47	in
Length Swivel + Hose	$L_{Swivel+Hose}$	98.4	in
Fluid Density	ρ_f	1000	kg/m^3
Solid Density	ρ_s	2650	kg/m^3
Fluid Viscosity	μ_f	1	cP

[1] 500,000,000 cycles completely reserved stress
[2] Aluminium 6061-T6
[3] Stainless Steel, AISI316

6.1 Well Path

This year's directional objectives is given as following in the guidelines appendix [3]:

- *Hit one or more targets at one or more vertical depth(s) and X/Y coordinates*
- *The starting directional plan to hit the targets will not require wellbore inclination in excess of 30° from vertical, 15° change in azimuth, or 10" displacement(departure from the vertical axis at well center)*

As it emerges from the objectives either a 30° from vertical or a 10" displacement is maximum requirement of displacement, this needs to be investigated further to find the limiting factors. The competition rock dimensions will be 12"x 24"x 24", where the well path will start to be drilled at least 4" in the vertical direction.

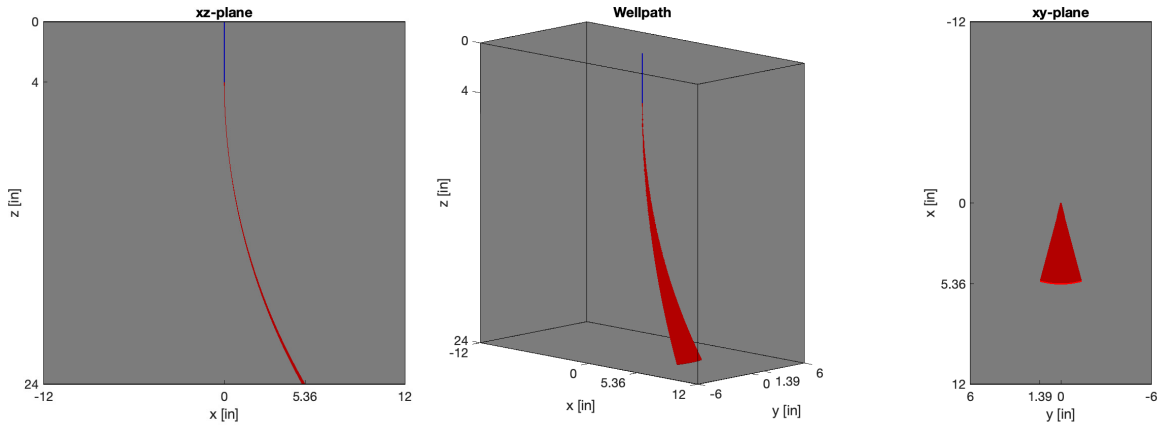

(a) Well path in xz-plane. **(b)** Well path in 3D-view. **(c)** Well path in xy-plane.

Figure 6.1: Theoretical possible well path inside given rock dimensions.

The theoretical well path is shown in Figure 6.1, assuming constant build rate. Figure 6.1a shows the maximum vertical displacement is $5.36\ in$ from well center, using an exit-angle of $30°$.

6.2 Drill Pipe

This year's competition opens up for use of stainless steel as Drill pipe (DP) material, but still having aluminium as an option. The decision regarding choice of DP material needs several calculations and considerations to ensure that it will withstand the forces applied due to rotation, bending and pressure.

6.2.1 Pipe Bending

As this year's objective is to hit multiple targets at varying True Vertical Depths (TVDs), it is critical that the pipe is operating within its elastic limits. The pipe is safe within its elastic zone when the total axial stress is below the material's yield strength.

Equation 5.20, 5.21 and 5.22 is used to calculate the total axial stress, with the result plotted in Figure 6.2 for both aluminium and stainless steel material. Input parameters used are stated in Table 6.1.

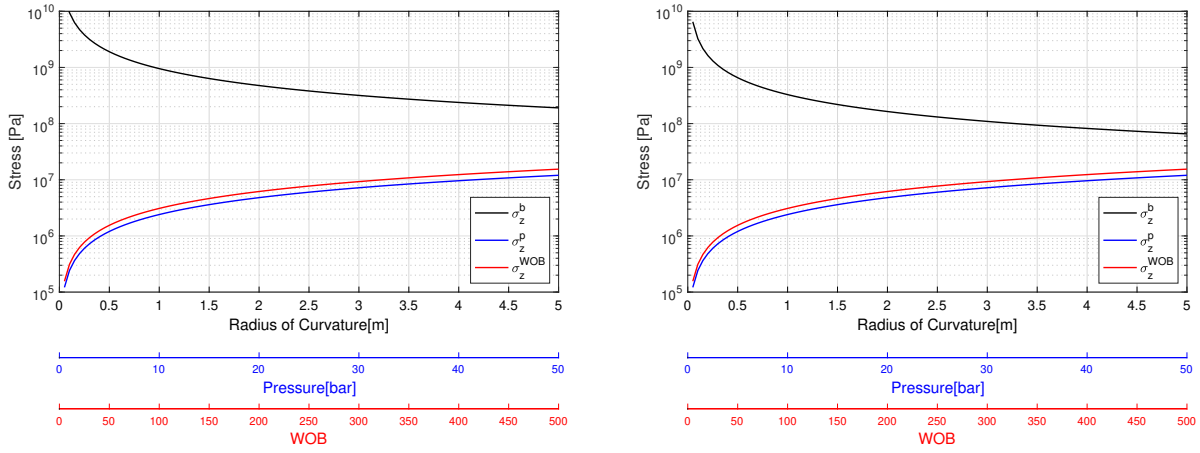

(a) Stainless steel grade 316. **(b)** Aluminium 6061-T6.

Figure 6.2: Axial stresses for different values of RC, P and WOB.

Figure 6.2 shows that for both materials, the axial stress from pressure and applied Weight on Bit (WOB) is negligible compared to axial stress from bending. To find the minimum Radius of Curvature (RC) the pipe can do in its elastic zone, the axial stress from bending will be compared to the material's yield strength.

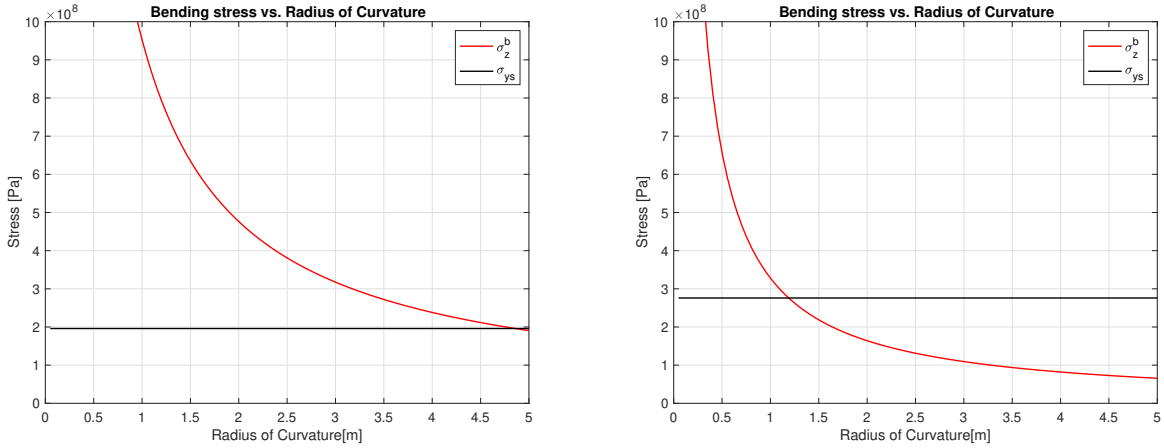

(a) Stainless steel grade 316. **(b)** Aluminium 6061-T6.

Figure 6.3: Axial stress from bending for different values of RC, compared with material yield strength.

Figure 6.3a illustrates that if the DP should be of stainless steel, the minimum RC is $4.86m$ which corresponds to a horizontal displacement of 1.05". Figure 6.3b presents the estimated axial stress from bending for aluminium DP. The minimum RC for this material to be within its elastic zone is $1.19m$, which corresponds to a horizontal displacement of 4.48".

Based on the results shown in Figure 6.3 a stainless steel DP will not be able to obtain sufficient horizontal displacement without exceeding its elastic limit. Aluminium on the other hand will not obtain the maximum RC shown in Figure 6.1a, but as this is the maximum value, the RC should be well within expected limits. As a precaution, safety limits for the minimum RC will be applied. For further calculations, the minimum RC used is 1.32, which is equivalent to a horizontal displacement of 4". Aluminium is used as the material for DP.

6.2.2 Buckling

Equation 5.8 and 5.12 are used to estimate the critical buckling limit of the DP, with diameter $3/8$" and wall thickness 0.049"; as instructed in the guidelines [3]. Table 5.1 presents the possible end conditions a column can have and the effective length factor (K) associated with it. The upper sections of the drill string resemble a fixed-fixed column, as the top drive and stabilizers will work as fixed points and avoid radial movement. While the lower section is similar to the fixed-pinned scenario, as the stabilizer will work as a fixed point and the borehole wall will give some support as a pinned point would. Figure 6.4 shows the maximum allowable WOB to the length, considering the relevant K values; both recommended and theoretical K values.

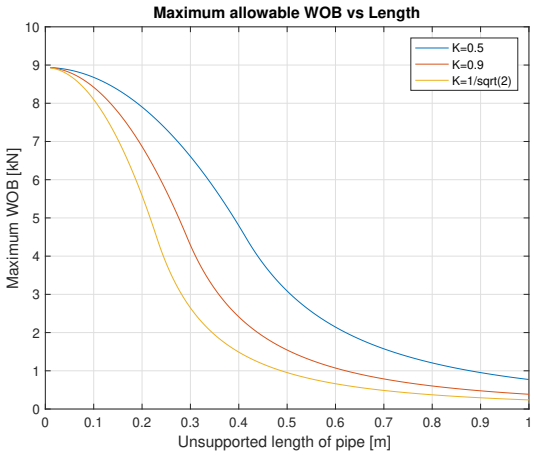

Figure 6.4: Buckling limit calculations for Aluminium DP.

Table 6.2 presents the applicable maximum values for WOB to avoid DP buckling. As presented in Table 5.1, the recommended K value for both fixed-fixed and fixed-pinned end conditions is the same, which of course means the maximum WOB for the different lengths with this condition is the same. The critical WOB is $0.83kN$ for both the fixed-fixed and fixed-pinned scenarios with recommended effective length factor, $K = 0.9$.

Table 6.2: Buckling calculations.

		Fixed-Fixed		Fixed-Pinned	
	K	0.5	0.9	$\frac{1}{\sqrt{2}} = 0.71$	0.9
	L [m]	**Maximum WOB [kN]**			
Drillpipe length (36 in)	0.91	2.68	0.83	1.34	0.83
Rock height (24 in)	0.61	4.68	1.86	3.01	1.86
Curved section (20 in)	0.51	5.19	2.68	4.03	2.68
Length of pipe left (8 in)	0.3	6.16	5.74	5.97	5.74

6.2.3 Burst

Equation 5.15 calculates the burst pressure for a thin-walled pipe. The resulting burst pressure, during drilling, of our chosen DP is found by using the material yield strength of aluminum and dimensions of the DP, found in Table 6.1. A safety factor of 3 is used as we calculate burst pressure for drilling operation:

$$P_{burst} = 2\frac{0.875 \cdot 276MPa \cdot 0.049in}{\frac{3}{8}in \cdot 3} = 210 \cdot 10^5 Pa$$

6.2.4 Twist-off

Twist-off calculations estimates the limit for applied torque on the DP while drilling. Twist-off torque is calculated using Equation 5.16 and 5.17 with σ_r (Equation 5.18), σ_θ (Equation 5.19) and σ_z as input variables. The axial stress, σ_z, is the sum of axial stresses from internal pressure (Equation 5.20), pipe bending (Equation 5.22) and WOB (Equation 5.21).

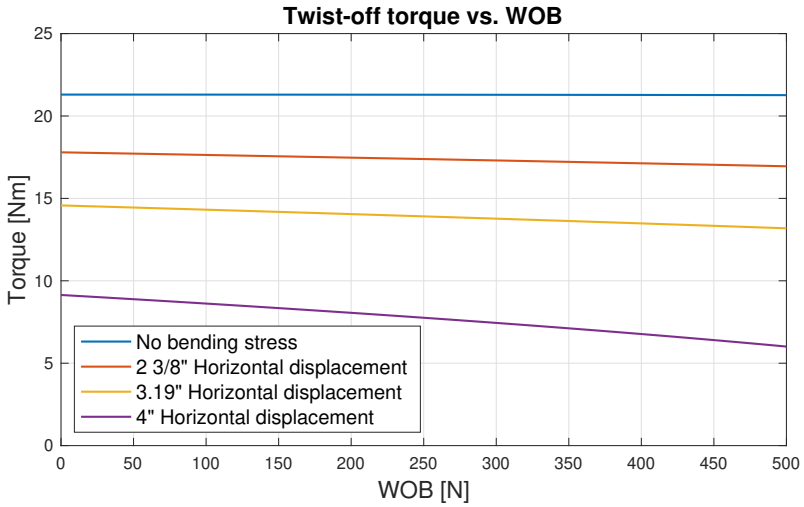

Figure 6.5: Calculated twist-off torques for different trajectories and WOB.

Figure 6.5 shows the result from the twist-off calculations from four different bending cases and for different WOBs, all stresses are calculated outside of the pipe wall. The pipe's internal pressure had a negligible effect on the torque and therefore it is calculated with $P = 100\ bar$ in Figure 6.5. The twist-off torque limits for different pressures are presented in Table 6.3, it shows that the difference in pressure is negligible for twist-off torque and further set the lowest as the limiting value.

Table 6.3: Twist-off torque ranges for different bending cases and WOB.

Pressure	**Horizontal Displacement**			
	0"	**2 3/8"**	**3.19"**	**4"**
10 bar	21.3 - 21.4 Nm	17.0 - 17.9 Nm	13.3 - 14.7 Nm	6.2 - 9.3 Nm
100 bar	21.3 - 21.3 Nm	17.0 - 17.8 Nm	13.2 - 14.6 Nm	6.0 - 9.1 Nm
Twist-off limit	***21.3 Nm***	***17.0 Nm***	***13.2 Nm***	***6.0 Nm***

Last year's team performed test drilling of the 4" vertical hole, where they observed a maximum torque of $3.34\ Nm$ [35]. These observations are well with in the limits estimated.

6.3 Drilling Requirements

To be able to choose components for the design, it is important to be aware of drilling requirements. Especially in the decision regarding downhole power section.

6.3.1 Required Drilling Rate

The required drilling rate can be found by assuming the worst possible path, which respectively is the path with the maximum horizontal displacement. In section 6.2.1 the maximum horizontal displacement is calculated and found to be 4", which equals to a RC of $1.32m$ with an exit angle of $22.6°$.

Using Equation 5.2, where I_1 is set to $0°$, and the desired I_2 = $22.6°$ and the $RC = 1.32m$, the resulting course length of the well is set to be $52.1cm$. The time limit for drilling in the competition is 3 hours, aiming for 2 hours drilling time therefore gives a sufficient safety factor to estimate the Rate of Penetration (ROP). Assuming an operation with $52.1cm$ to drill in 2 hours gives an average ROP of $0.434cm/min$ to be able to complete the task.

6.3.2 Torque & RPM

As this year's development will further progress on last year's rig, the team will use data acquired during last year's testing. Shown in Table 6.4 the results from a test drilling is presented, with a required ROP of $0.434cm/min$ achieved with $147N$ WOB and $68RPM$.

Table 6.4: Showing test data from drilling. A constant top drive velocity is set with increasing WOB.

Run	Time [min]	RPM	WOB [N]	Torque diff. [Nm]	Avg. ROP [cm/min]	Sufficient ROP
1	0,35	68	98	0,22	0,23	No
2	0,36	68	108	0,21	0,29	No
3	0,30	68	118	0,20	0,26	No
4	0,33	68	127	0,21	0,37	No
5	0,64	68	137	0,21	0,31	No
6	0,64	68	147	0,21	0,67	Yes

As it is important to have a BHA that can handle the requirements of around $0.21Nm$ torque and a drilling rate of $0.434cm/min$, a reasonable minimum requirement of $0.7Nm$ and $70RPM$ when taking into account the bit increase from last year's testing.

6.3.3 Pressure on ROP and Torque

During one of the test runs, the pump speed was changed to see the effect of pressure on the drilling test. During this part of the test, the weight on bit and top drive speed parameters were kept constant at $98N$ and

50 RPM. No effect on ROP could be observed, in part due to the ROP not being perfectly constant at constant parameters. The torque appeared to increase with increased pump speed [35].

6.3.4 Bit Tilt

To achieve directional drilling it is necessary for the bit to have tilted angle. This angle will be created by the bent housing and therefore needed to be determined before manufacturing it.

With the use of Equation 5.1, where $\phi = 22.6°$, and $CL = 52.1cm$ acquired from section 6.2.1, the Dogleg Severity (DLS) is equal to $43.4°/m$. With the knowledge of required DLS , the bit tilt ϕ can be calculated with the use of Equation 5.4.

With the use of estimated lengths in the BHA, the section length above the bent sub will be $L_1 = 15cm$ and the section length below bent sub $L_2 = 8.5cm$. This results in a maximum required bit tilt angle of:

$$\phi = \frac{DLS(L_1 + L_2)}{2} = 5.1°$$

6.4 Drilling Hydraulics

The drilling hydraulic calculations determines the minimum required outputs from the hydraulic components. By drilling with parameters below the minimum requirements, the risk of insufficient drilling is highly possible.

6.4.1 Hole Cleaning

All calculations regarding cuttings transport is done with the use of water as drilling fluid, as this is the planned fluid selection. The assumption is that the cuttings generated from drilling are spherical. Based on previous years data, the cutting sizes were set to 2 mm (2018) and 2.2 mm (2019) [35]. Due to the increase in bit diameter this year, the team could assume an increase in cutting size. Based on a trending line, an increase in $0.2mm$ is a sensible assumption. Which will make the maximum cutting size assumed to be set to $d_s = 2.4mm$, but will in Phase II be more precisely measured. Further on, the rock sample is known to be a homogeneous sandstone and the assumption is that the cuttings will have a density of 2650 kg/m^3. All the parameters used are listed in Table 6.1.

Table 6.5: Hole cleaning calculations and result.

Calculations	Equations	BHA	DP
v_{sl}	Equation 5.68	5.18	5.18
Re	Equation B.7	10530 (Turbulent)	148000 (Turbulent)
f	Figure 5.19	0.44	0.55
v_{sl}	Equation 5.69	0.017	0.015
q	Equation 5.70	0.24	1.93

Table 6.5 shows the results from the calculations to obtain required flow rate for sufficient hole cleaning. One thing to notice is that the velocity is calculated with an efficiency of transport of 50% in mind, which is the desired value to acquire. The required flow rate to achieve sufficient hole cleaning is below $3lpm$.

6.4.2 Pressure Losses

As directional drilling is one of the main parts of accomplishing the challenge, it is increasingly important to have control of pressure and flow rate. The use of a Positive Displacement Motor (PDM) as power section increases the importance of keeping pressure control in the hydraulic system, as the PDM's performance is highly dependent on available pressure.

The system pressure drop is calculated using Equation 5.71 and Equation 5.75, using Table 6.1 as input converted to SI-units. In the estimation of friction factor, a pipe roughness factor of $\epsilon = 1.3e - 6$ is used. The results for different flow rates is presented in Table 6.6.

Table 6.6: Pressure drops given in bars for different parts of the system and for different flow rates.

$Q[lpm]$	$\Delta P_{hose+swivel}$	ΔP_{dp}	ΔP_{bha}	ΔP_{nozzle}	$\Delta P_{annulus}$	ΔP_{tot}
6	0.025	0.115	2.033e-5	0.351	0.002	**0.494**
8	0.041	0.192	3.332e-5	0.624	0.004	**0.861**
10	0.061	0.285	4.897e-5	0.975	0.006	**1.326**
12	0.084	0.395	6.717e-5	1.403	0.008	**1.890**
14	0.110	0.520	8.781e-5	1.910	0.010	**2.551**
16	0.140	0.661	1.108e-4	2.495	0.013	**3.309**
18	0.172	0.818	1.361e-4	3.158	0.016	**4.163**
20	0.207	0.989	1.637e-4	3.898	0.019	**5.113**

Table 6.6 shows that the biggest expected pressure drop is to be slightly above 5 bar. The calculation does not take into account the pressure loss over the PDM, so the remaining pressure will be available to the PDM. The pressure drop is dominated by pressure drop through bit nozzles which is at this point estimated from last year's bit design, with a nozzle diameter of 2 mm and four nozzles. The final bit design will be decided in Phase II, but there is not expected severe changes to the system pressure loss.

7 Mechanical Design

The mechanical design of the drilling rig is an important and critical part of the optimization regarding drilling efficiency. For a miniature drilling rig to be as efficient as possible, an elegant combination of software and hardware is essential. This section will cover the mechanical hardware part which will be a base for the final design in Phase II.

7.1 NTNU Miniature Drilling Rig

Figure 7.1 shows last year's rig with its main mechanical components. Given that this year's competition has some minor changes regarding the physical parts of the rig, several alternatives the team has discussed will also be presented, in addition to also explain the reason behind some of the design choices made. The rig's mechanical components can be divided into four different "systems": the Hoisting system, Rotary system, Hydraulic system and Drilling system. Each system with its components will be thoroughly explained in this chapter.

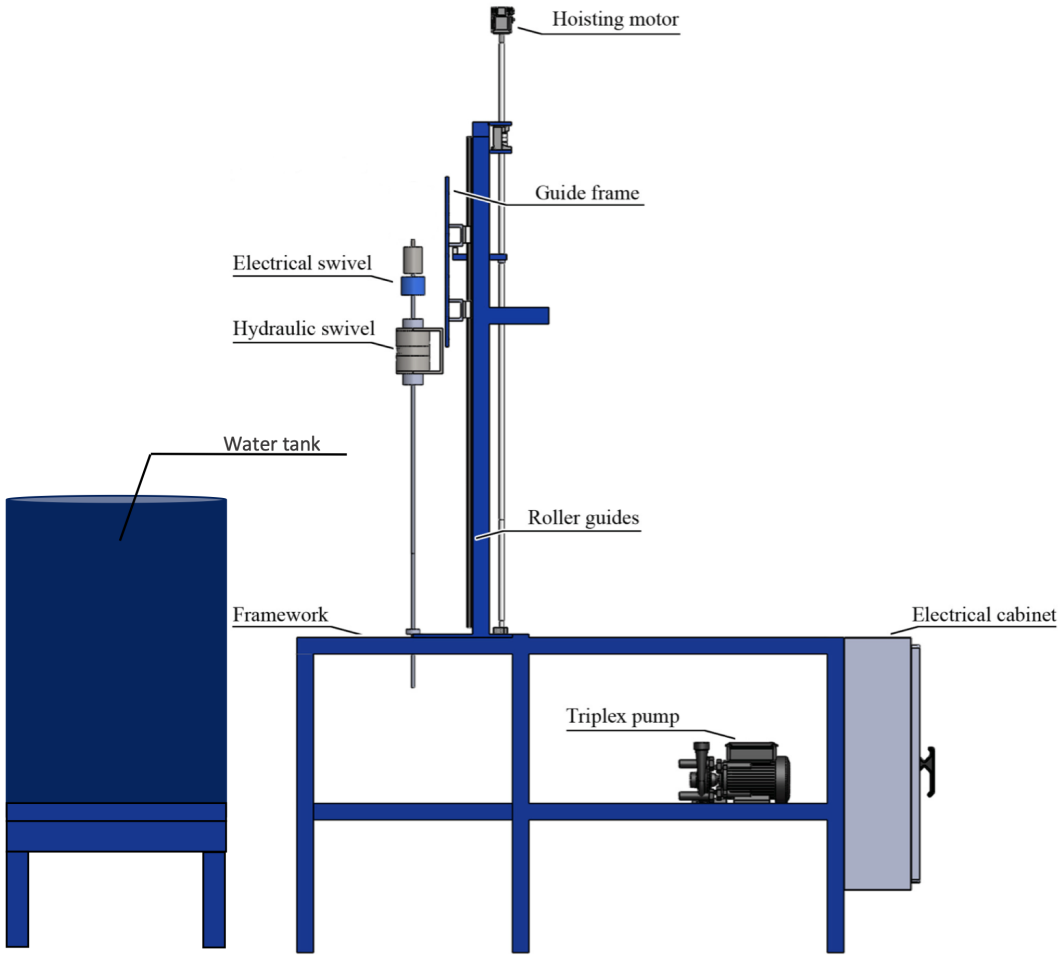

Figure 7.1: The miniature rig and its components from last year.

The rig framework is made of 50 $\times$ 50 mm hollow steel beams which make a total vertical height of 2849 mm, length of 1980 mm and 765 mm wide. As the protection glass is lifted up during rig up/down, the rig's maximum vertical height is 3995 mm. The rig is designed in such a way that it can accommodate several components needed to drill the given well path. The rig's dimensions are also shown in Figure 7.2.

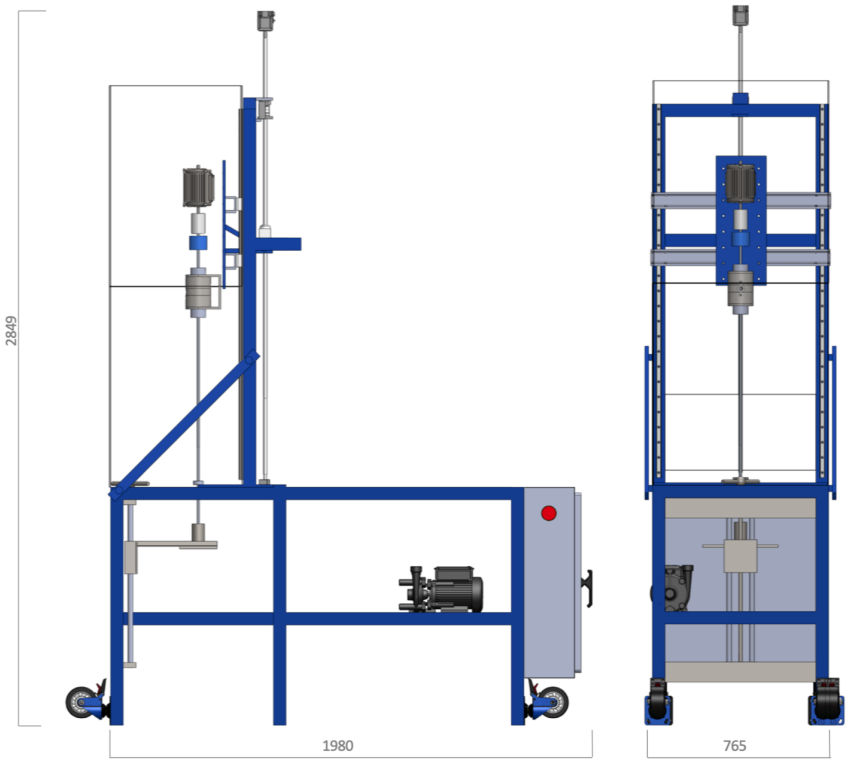

Figure 7.2: Rig dimensions in operational position

To ease transportation of the rig, there is a possibility to lie down the derrick. This gives a total vertical height of 1685 mm and a length of 2540 mm. The rig's dimensions add up a chargeable weight of 546 kg [3]. The rig in transport position is shown in Figure 7.3.

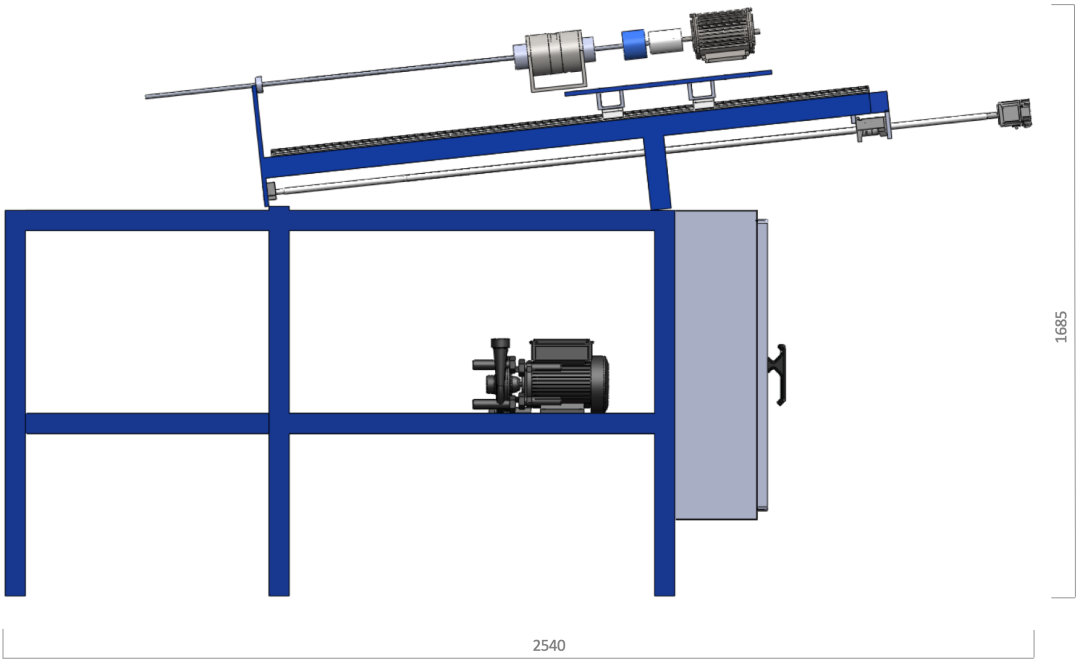

Figure 7.3: Rig dimensions in transport position

7.1.1 Hoisting System

The hoisting system consist of the components that contribute to and controls the vertical movement of the guide frame named in Figure 7.1. The hoisting system components are hoisting motor, load cell and roller guides. The complete hoisting system is shown in Figure 7.4.

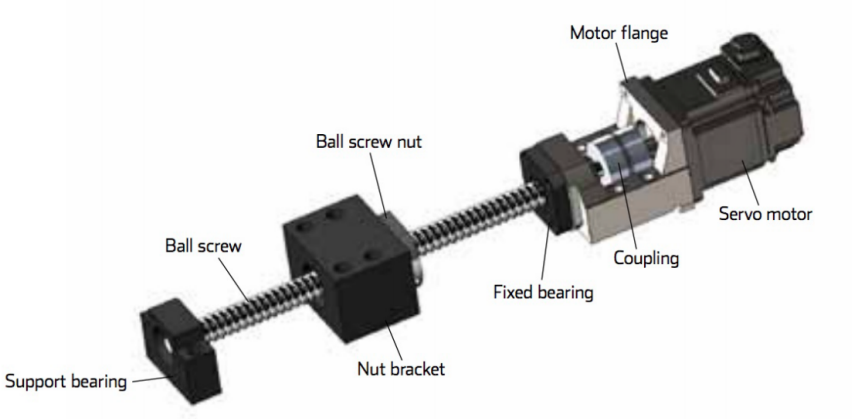

Figure 7.4: Hoisting system with different components labeled.

7.1.1.1 Hoisting Motor

In full-scale drilling, Weight on Bit (WOB) is achieved by adding heavy weighted drill pipes and collars in the drill string. This is challenging in the miniature drilling rig format, as the pipes do not have enough weight to add the required WOB necessary. So what the previous year's teams have done, is to come up with an elegant solution where a hoisting system is used. Through the use of a hoisting motor, an upward and downward motion of the drill string is achieved, which will provide the WOB necessary. As the automated part of the drilling requires continuous monitoring and changes to the WOB, it is important that the hoisting system is accurate. This is achieved with the use of a ball screw. The motor provides rotational motion to the ball screw, which further converts this motion into the vertical movement of a guide frame where the rotating system is mounted. The ball screw is chosen as the solution due to its precision, accurate data gathering function and efficiency.

7.1.1.2 Load Cell

The load cell is located in the middle of the ball screw. As mentioned, the hoisting system's purpose is to apply WOB, which is measured with the use of the load cell. This part is connected to a ball screw nut bracket and is shaped like a hollow cylindrical cell. The load cell is welded onto the guide frame, this is to get a high enough precision on the WOB readings. More details on the load cell sensors are explained in section 9.1.2. The Figure 7.5 shows the placement of the load cell on the rig with a ball screw going through it.

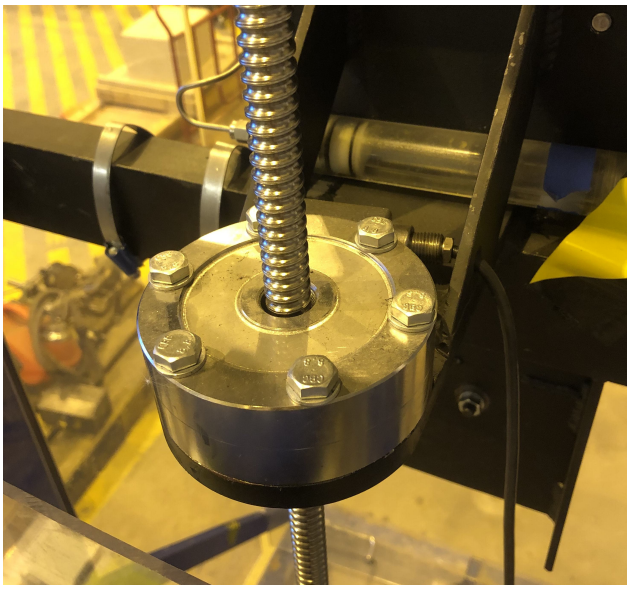

Figure 7.5: Load cell.

7.1.1.3 Roller Guides

The guide frame movement is locked to travel only vertical by roller guides on each side of the derrick. To prevent the movement to go either too high or too low, there are installed stop buttons as shown in Figure 7.6. When the guide frame triggers the stop buttons, the circuit is broken and power to the hoisting motor stopped.

Figure 7.6: Safety mechanism to prevent the rig from hoisting too high or too low.

7.1.2 Rotary System

The rotary system is the components that contribute to drill string rotation, stabilization and transition of an electrical signal to the rotating string. The Bottom Hole Assembly (BHA) and bit is also a part of the rotary system, but as this is one of the key components in the design it will be thoroughly described in section 7.3.

7.1.2.1 Top Drive

On top of the derrick, the top drive is found. This is used to rotate the drill string in addition to provide torque, the top drive delivers around 3 Horsepower (HP) - compared to top drives used in the industry, which can push roughly 1,000 HP. The top drive sits above the electrical swivel and is directly connected to the drill pipes, and can be moved vertically up and down as it is attached to the guide frame.

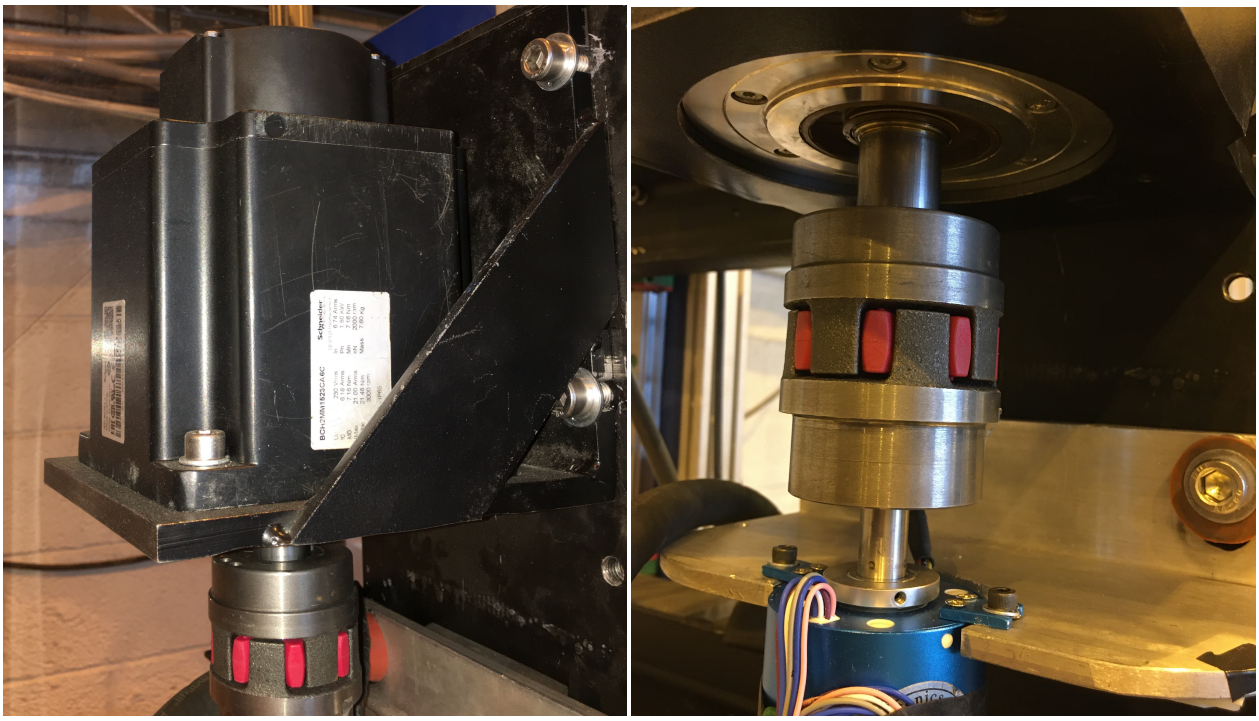

(a) Top Drive. **(b)** Universal Coupling between top drive and el. swivel.

Figure 7.7: Rotary system components.

For the team to be able to control the deviation and position of the drilled hole, it is required to know the exact orientation of the drill string. This is obtained by the servo drive of the motor. With the motor's servo function, which consists of a controller, motor and feedback device, the control system will be able to receive and send signals. With the use of the top drive, the team will be able to acquire data for RPM, torque and position, in addition to adjust the voltage and current applied to the servo motor accordingly to the required closed-loop feedback. More details about the servo motor are to be found in section 9.2.1.

Universal Coupling

Between the top drive and electrical swivel, one can find the universal coupling. This is a solution to reduce misalignment problems of the components below this coupling caused by the top drive motor. The universal coupling is shown in Figure 7.7b

7.1.2.2 Electrical Swivel

Below the top drive and the hydraulic swivel, the electrical swivel is located. This is a bridge for all the electrical wires and connections to be transferred from the rotating drill string over to static conditions.

Figure 7.8: Electrical swivel

7.1.2.3 Drill Pipe

This year, the guidelines have allowed the use of stainless steel as Drill pipe (DP) material, with the same dimensions as last year. The selection of stainless steel is a solution the team highly has taken into consideration. With the use of stainless steel, the wear and tear on the DPs will have a much higher limitation and will allow for more bending and stress. As the calculation and discussion in section 6.2.1 states, the use of stainless steel DP will not be within its elastic zone with the required Radius of Curvature (RC). As the stainless steel possibility is ruled out, the choice of DP material this year will be aluminum of the alloy 6061-T6.

7.1.2.4 Tool Joint

The DP will be connected with a Vertex tool joint shown in Figure 7.9, both in the upper connection to the hydraulic swivel shaft and the lower connection to the BHA. This connection is chosen as it has been reliable over the last two years.

Figure 7.9: Tooljoint to be used.

7.1.2.5 Stabilizers

Stabilizers along the drill string are used to reduce the unsupported lengths of the drill string, this will reduce the risk of the DP to buckle, minimize vibrations and help the alignment of the drill string. The locations of the stabilizers are shown in Figure 7.10

Along the length of the drill string, two stabilizers are located. One of them is located on the drill floor, approximately 95 cm above the floor surface, while the other one is placed inside of the riser. Both stabilizers are roller bearings, with inner diameter to 9.52 mm, which is equivalent to the OD of the drill pipe. The reason for the two stabilizers are so that they both - at a certain distance from each other, are able to give the drill string stability during drilling

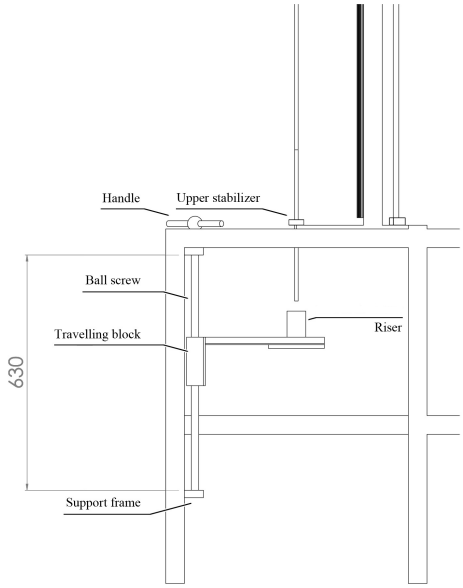

Figure 7.10: Location of stabilizers.

7.1.2.6 Riser Element and Bell Nipple

The riser located below the drill floor has the purpose of guiding the drill string and BHA down in the direction to the rock sample. In addition to the stabilizing feature as mentioned in section 7.1.2.5, the riser prevents and stops drilling fluid from coming out of the hole through the top of the riser with the use of a so-called bell nipple. This is the golden nipple shown in Figure 7.11, and works as a pipe that is supposed to redirect the water coming up from the well.

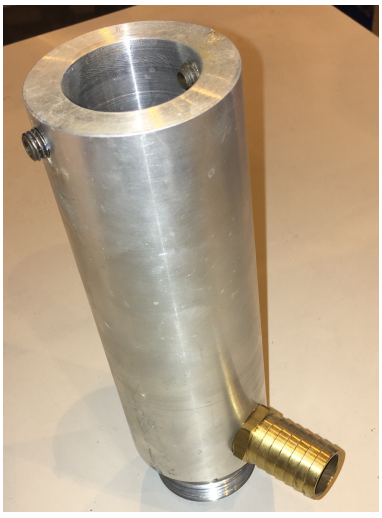

Figure 7.11: Riser element with the bell nipple on the right part of the hollow cylinder.

7.1.3 Hydraulic System

The hydraulic system includes a hydraulic pump, water tank, water hoses and the swivel. The systems fluid circulation will be described in section 8. Components contributing to the circulation system will be described in this section.

7.1.3.1 Hydraulic Swivel

The hydraulic swivel, which sits below the electrical swivel and have direct contact to the DP as shown in Figure 7.12. The function of the swivel is to receive the pressurized water, from the hose connected on side of the swivel and send it downwards into the drill string.

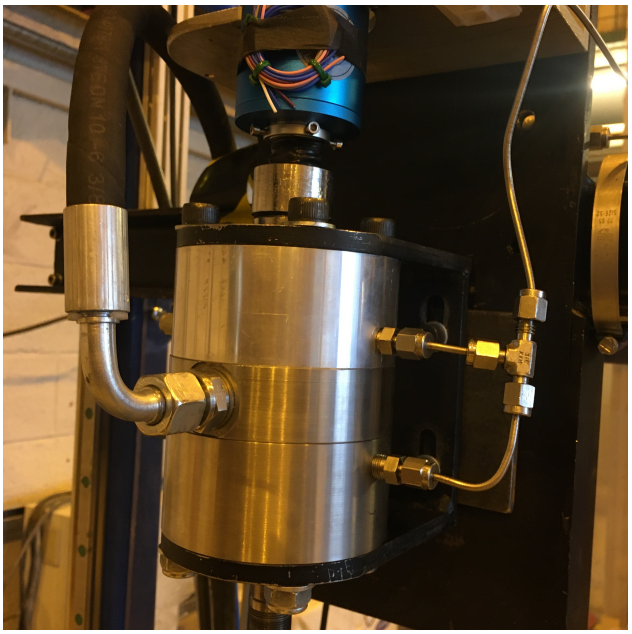

Figure 7.12: Hydraulic Swivel

7.1.3.2 Hydraulic pump

The hydraulic pump is located on the side of the derrick, below the computer table, shown in Figure 7.1. The pump takes in water from the tank and sending out pressurized water downstream. More about the pump performance can be found in section 8.2.1.

7.1.3.3 Water Tank

The water tank is located separately from the drilling rig. It is placed upon the rack to minimize the heat loss from the tank to pump as shown in Figure 7.13.

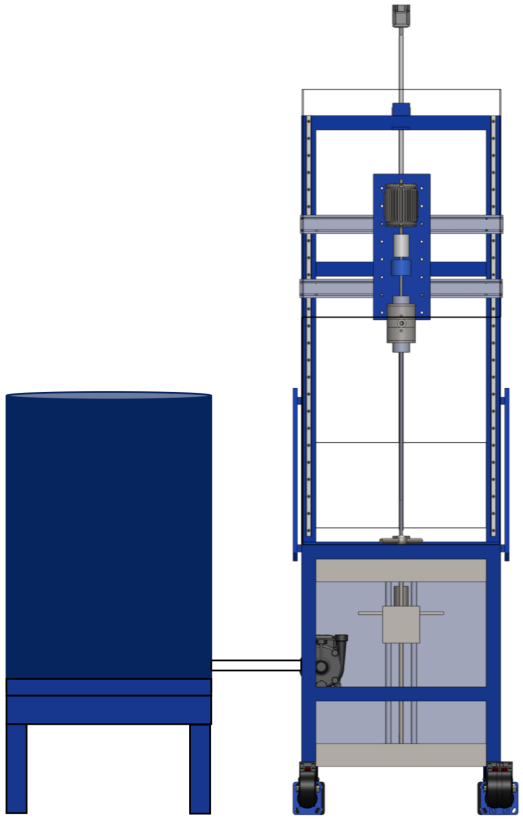

Figure 7.13: Tank system setup.

7.2 Rig Modifications

Each year Norwegian University of Science and Technology (NTNU) has participated in the Drillbotics© competition the starting point has been the respectively last year's rig design. As the design has been improved constantly throughout the three years of competition now, this year's design changes will consist of minor changes in relation to component reliability and safety.

7.2.1 Electrical Swivel

The connections between the lower side of electrical swivel and hydraulic swivels drive shaft has been a weak part of the system, as these connections are easily damaged. This was a problem the first time the rig was installed this year and is something that needs to be improved. The location of the problem is shown in Figure 7.14.

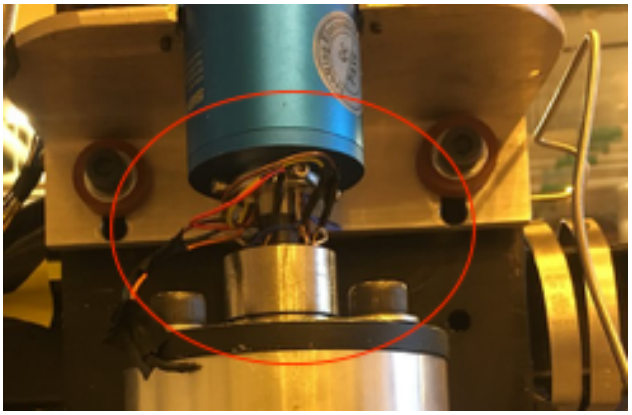

Figure 7.14: Connections between electric and hydraulic swivel.

The plan to make a robust design for the connections is to use a new type of connection pins and a non-conductive protection layer.

7.2.2 Gas Shocks on Protection Glass

The risk analysis in section 11.1 resulted in a low medium risk of an accident where the protection glass will be in free fall downwards. As a consequence of this, there has to be made some risk-mitigating measures. The planned modification is to install a gas shock on each protection glass rail. The final design of this solution is not yet finalized, but the result of this will dampen the glass's downward traveling speed and make it easier handling when hoisting the protection glass.

7.3 Drill String Design/Bottom Hole Assembly and Drill Bit Design

The BHA design is the rotary system's key part to achieve an efficient drilling operation, especially when directional drilling is one of this year's objectives. The BHA consist of stabilizers, power section and bent housing. The plan forward for bit design solution will also be presented in this section.

7.3.1 Stabilizers and Sensor Sub

Last year's BHA design consists of two stabilizers, one near-bit stabilizer and one at the top of the BHA. A stabilizers function is to stabilize drill string and bit, reduce vibrations, and ensure directional control [4].

The upper stabilizer is referred to as a sensor sub, as it has a socket for the sensor card to be placed in as shown in Figure 7.15. The lower stabilizer is located below the bent sub, this stabilizer is ensuring that the BHA follows the bits drilled path. Both stabilizers consist of thick walls and are therefore unlikely to obtain any damage during normal drilling. If such an incident should occur it will most likely be with the sensor sub stabilizer, as it is weakened by the sensor socket.

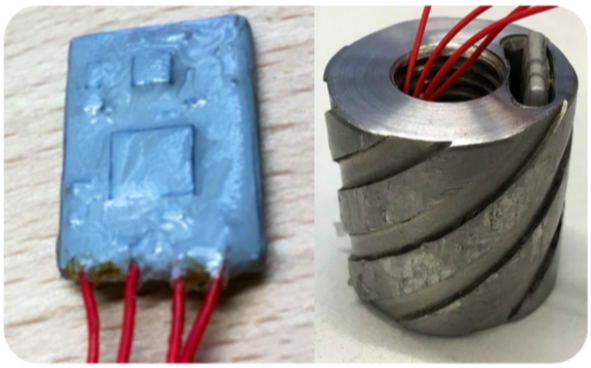

Figure 7.15: Stabilizer with sensor sub

The stabilizer design from last year was proven out to work as expected. This year's design will be based upon last year's, but new solutions will be considered to be implemented. One difficulty with the solution was that the cables had to be pulled through the spacing for cables on the lower end of the sub, this makes the removal and installation of the sensor card tricky. A solution to this that has been discussed is to make a socket with only one opening at the lower side. This solution might be ease to keep the sensor card water-tight, and will be designed and further investigated in Phase II.

7.3.2 Power Section

The need for a power section inside the BHA is introduced as the chosen directional drilling solution requires no rotation on the DP during slide drilling. This makes the power section one of the most critical parts in the BHA design, as the slide drilling is fully dependent on the torque and Revolutions per Minute (RPM) delivered. After a study of different possibilities the choice of power section landed on a Positive Displacement Motor (PDM), the results from the study are presented in section 7.4. As the power section is such a critical part of the design there is chosen to plan for two power section designs, with an Electrical Miniature Motor (EMM) as the secondary choice.

PDM - Primary power section

A PDM will be the primary selection for the power section, as this appeals the most to real size solutions. The PDM will consist of a rotor and stator, which will be placed inside of a protective housing and attached to the rest of the BHA. Through an elegant mechanical design of the PDM, the hydraulic power from the drilling fluid will be converted into mechanical power to supply torque and RPM to spin the drill bit independently from the rest of the drill strings rotation.

Figure 7.16: 3D-printed plastic version of stator and rotor

Last year, the team developed its own design with the use of a 3D-printer. The plan this year is to continue the development of the PDM where it was left off and continue improving it especially in regards to material selection. A 3D-printer has been acquired for the design of a plastic one, and testing will commence as soon as the 3D-printer is up and running. There is not decided on lobe configuration, as there is planned to do testing on different configurations and decide at a later stage. The estimated power output from PDMs with different lobe configurations is calculated in section 7.5.1

EMM - Secondary power section

The secondary selection of power section will be an EMM. As shown in section 7.5.2 the EMM should deliver both torque and RPM within expected range. The plan is to use an 26 mm Outer Diameter (OD) EMM, it will also have a gear that will decrease the RPM and increase torque output.

As the electrical motor is vulnerable against water, the EMM has to be placed inside a special designed housing. Figure 7.17 shows last year's type of housing to redirect the fluid away from the motor [35]. The design will have two weak spots, in the upper part of the motor there will be created a perfect seal to direct the flow as shown in Figure 7.17. The solution to seal off the motor in the lower part has to be tested several by methods, this will be investigated in-depth in Phase II.

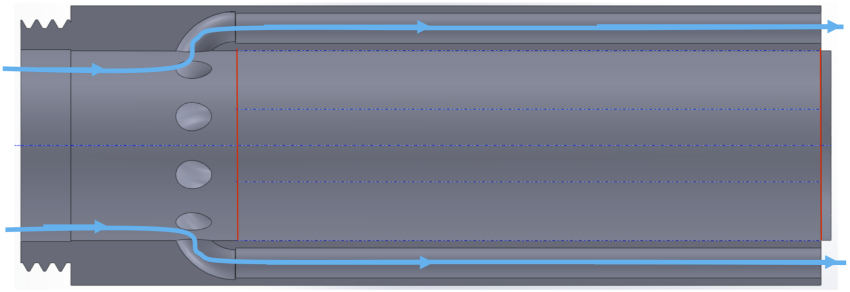

Figure 7.17: Flowpaths in EMM housing. Weak points marked with red lines, left is top of housing.

7.3.3 Bent Housing

Below the power section, the bent housing is located. As there are no specified requirements to determine the required dogleg angle, there is a need to use an adjustable bent housing. The adjustable bend will require a max dogleg angle of $4.63°$, as calculated in section 6.3.4.

Inside of the bent housing the transmission section will be placed, which will transmit the torque and RPM from the power section and towards the bit. The planned transmission type to use is a flexible shaft, this is chosen instead of universal joints to limit the needed length and less moving parts than universal joints.

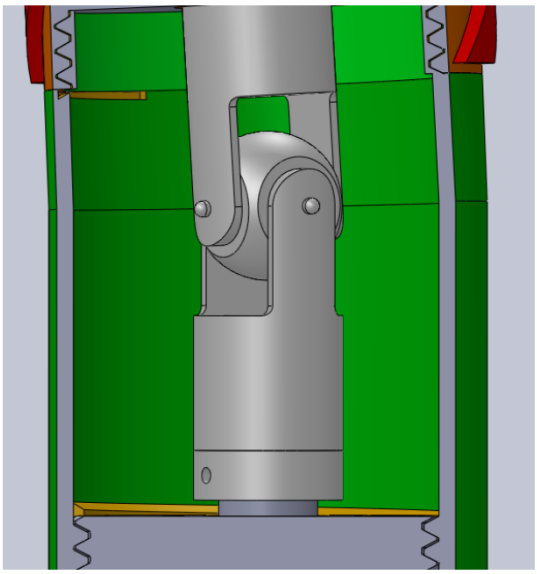

Figure 7.18: Bent housing

7.3.4 Bearing Section

The radial bearing section will be placed inside the lower stabilizer. This will then act as a protection for the radial bearings. The axial bearing's lifetime will depend force balance between the upwards WOB force

and downwards hydraulic force which will be done tests on in Phase II, the axial bearing will be placed in between the driveshaft and the bit sub as shown in Figure 7.19.

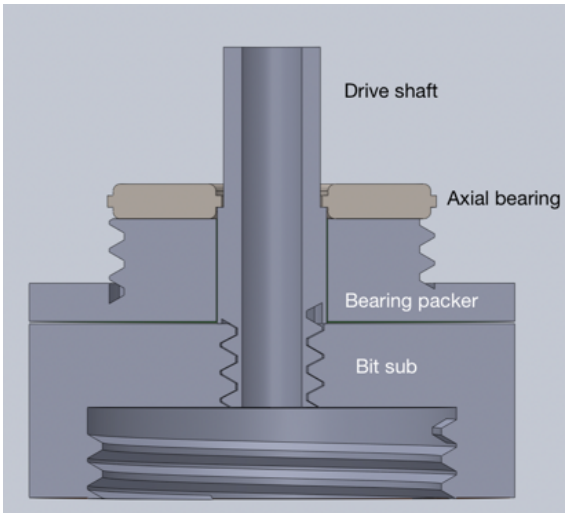

Figure 7.19: Bit sub with location of axial bearing

7.3.5 Drill Bit

Last year, the team decided to design and produce their own drill bits. In collaboration with Lyng Drilling, the team gained valuable knowledge, sketched a bit and ended up 3D-printing an optimal 1.25" diameter and 2" long drill bit with 4 blades, 12 PDC cutters and 4 nozzles.

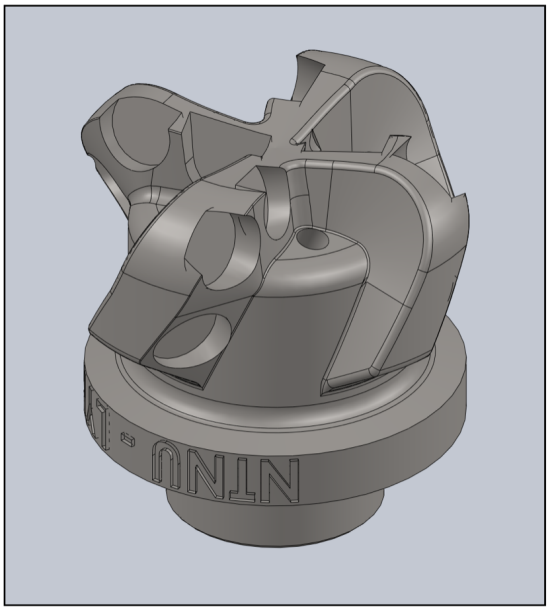

Figure 7.20: Customized drill bit from last year

This year's team has also decided to do the same thing and will also design their own bit. One important

change to last year is that the diameter of the bit has increased from 1.25" to 1.5". This will result in some significant changes regarding the design and optimization of the whole BHA.

7.4 Bottom Hole Power Design Alternatives

The BHA power section design is of the utmost importance when it comes to providing the bit power to drill the deviated well. The team spent quite some time discussing different possibilities for bottom hole power, with the decision of using adjustable bent housing in the BHA to build angle in mind.

Alternative 1: Flexible cable
The flexible cable solution is a kind of improvised solution the team discovered when researching the different solutions for transferring power to the bit, the idea is taken from the string trimmer concept. The concept behind the flexible cable solution is to have a motor, from now referred to as cable motor, rotating a flexible cable, running inside the small diameter drill string. The cables lower end will be connected to the drill bit, which will rotate when the cable motor rotates.

By analyzing the rig and its components the team concluded that this solution would have needed to have a new motor installed, based on experience from last year's team the communication to a new component could end up as a very time-consuming process. A rotating cable inside the DP could have given challenges regarding keeping a robust and stable design of wired downhole communication. The thorough analysis regarding the flexible solution concluded that this solution needed to be the primary solution, not considered as a back-up solution because of the heavy workload in designing such a solution. The decision of using PDM as the primary solution then quickly ruled out the alternative of using the flexible cable solution.

Alternative 2: Positive Displacement Motor
The team from last year tried to make a small scale PDM, which led the current team to discuss the possibility of using it as the downhole power source. With the use of a 3D-printed model, they were able to do some successful test runs, with varying results. This proved that the PDM design is actually possible.

The design of the PDM is stated as a high-risk factor in the project. The possibility of ending up with an non-functioning PDM is rated as high, due to its complicated design with the need of high precision. The reward of drilling with a PDM is what makes the alternative remarkably interesting, as the BHA will be a miniature version of what is used in full-scale drilling. Figure 7.21 shows a concept of the BHA with PDM power section.

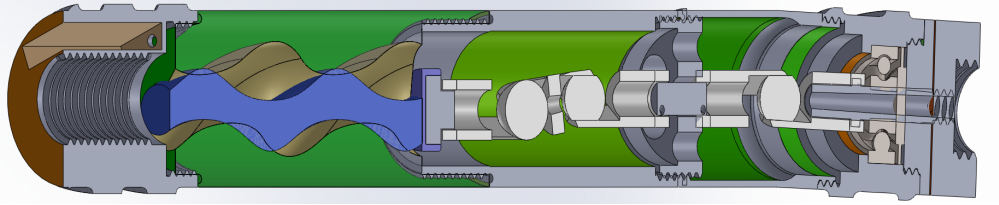

Figure 7.21: Concept design of BHA with PDM as power section.

Alternative 3: Electrical Miniature Motor (EMM)

The use of an EMM as power source is a possibility that seems doable. The positive sides of using an EMM are that the maximum output power can be estimated from data sheets. Negative sides of this alternative are the EMMs vulnerability to water and therefore need of an elegant seal design. If the EMM stalls out, it has peaked its performance and may not deliver as expected. This makes it an untrusty power section, as it is hard to predict its lifetime. Figure 7.22 shows concept of the BHA with EMM power section.

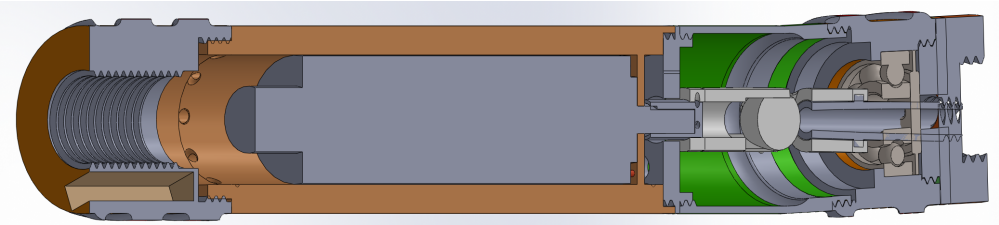

Figure 7.22: Concept of BHA with EMM as power section.

Alternative 4: Turbine Motor

The last idea for the bottom hole power section that was discussed was a miniature Downhole Turbine Motor (DTM). This is similar to the PDM as it uses moving mechanical parts to convert the hydraulic energy into rotational mechanical force. The DTM uses a bladed rotor instead of a helix-shaped part as shown in Figure 7.23. This is rotated at a rate that is proportional to the speed of the fluid. The rotation of the blade itself is often detected with the use of a sensor, which is important for the control of the volumetric flow rate. What separates the turbine from the curve is that it runs on high velocity, but low torque. The DTM has the need of a gear and is therefore seen as a complex solution.

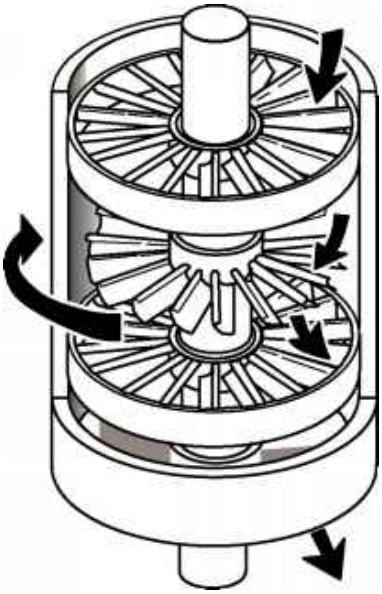

Figure 7.23: Concept of the turbine [4].

Reasons for discarding this concept were due to continued research and development of PDM, as last year's team already had set a lot of groundwork that the current team could improve upon. Further on, designing a turbine using a 3D-printer would be way more difficult and challenging, whereas the gain would most likely be less compared to the PDM. The PDM is a lot more common in real life-sized drilling, as research has confirmed that a well designed displacement motor would be much more energy-efficient and beneficial compared to a turbine motor for drilling [4].

7.5 Downhole Power Output

In this section, the estimations of maximum power output from the two selected power sections will be calculated and presented.

7.5.1 PDM Performance

An estimation of expected output from the PDM can be estimated by use of Equation 5.6 and 5.7.

The geometric values of the PDM is estimated based on last year's design, and scaled up as a consequence of this year's bit diameter increase. The stator outer diameter is set as $D_h = 0.59in$ and stator length as $L_h = 2in$. The use of different lobe configurations will then calculate volume displacement over the PDM with Equation 5.5. By use of Equation 5.6 and 5.7 the ideal RPM and torque, $T[Nm]$, is estimated and shown in Figure 7.24.

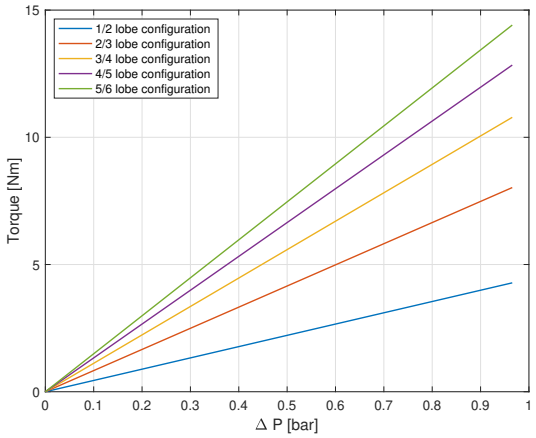

(a) Estimated torque given by PDM.

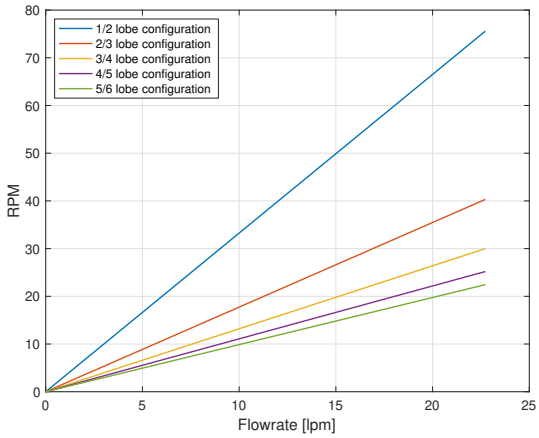

(b) Estimated RPM given by PDM.

Figure 7.24: Estiamted PDM performance.

The results show that the PDM solution should deliver enough power required. As the PDM design and test phase will begin, the test results will be compared with the theoretical knowledge of this will be used further in the design process.

7.5.2 EMM Performance and Specifications

Even though the PDM will be the team's priority and main component, an EMM has been chosen as a backup solution as power source in the BHA as mentioned in section 7.3.2. Calculations for the optimal design of the PDM has been done in the section above, while this section will cover what type of model of a small electrical motor will be used for drilling. It is important to know the size and specifications that are allowed due to the limited space when it comes to width in the BHA. Below are rough estimates for the temporary design of the motor, as well as its specification. It should be notated that changes may apply as the development progresses.

As the bit diameter is 1.5", which equals $38.1mm$, the PDMs OD need to be smaller than the bit to prevent the BHA from getting stuck. Below are all size reduction required listed - and the end result will represent the allowed diameter size of the electric motor that can be used.

The major OD of the stabilizers will have **2 mm** smaller diameter than the bit, and the difference between major and minor OD of the stabilizers will be **2 mm**. The inner diameter of the EMM housing ends up being **8 mm** smaller than the outer diameter which equals the minor stabilizer OD. Below is an overview of the resulting space left for the EMM to fit:

$$D_{EMM} = D_{bit} - D_{stabilizer,major} - D_{stabilizer,minor} - D_{OD,housing} - D_{ID,housing}$$

$$D_{EMM} = 38.1 - 2 - 2 - 1 - 7 = 26.1\ mm$$

The conservative estimation of space remaining for the EMM is **26.1 mm**. The model **DCX 26 L Graphite**

Brushes, DC motor Ø26 mm has been chosen. The data sheet with all the important information can be found under the appendix in section E. The motor has a choice with A voltage delivery of 48 V, which allows it a nominal RPM of 9370. The choice of this motor, combined with a gear that has a reduction ratio of 1:138 is what this calculation will be based upon.

Using the gear, it will decrease the nominal RPM from 9730, to $\frac{9730}{138} = 70\ RPM$. But on the other hand, increase the nominal torque from 59.1 mNm to $59.1 \cdot 10^{-3} \cdot 138 = 8.2\ Nm$. The data sheet states an efficiency of $\eta_{emm} = 91\ \%$ for the motor, while an efficiency for the gear is assumed to roughly be $\eta_{gear} = 60\ \%$.

The final Torque the motor will be able to deliver is $8.2 \cdot 0.91 \cdot 0.6 = 4.5\ Nm$. Which according to the required calculations in section 6.3.2, it meets the necessary demand when it comes to both torque and RPM.

8 Hydraulic Design

A drilling system is highly dependent on the hydraulic system to obtain desired drilling parameters. In this section, the previous year's design will be presented, as well as the proposed changes given by this year's team. With regards to the decision on continuing on last year's Positive Displacement Motor (PDM) design, hydraulic design and especially drilling fluid could have a great impact on the PDM performance. Figure 7.1 shows the drilling rig where the hydraulic system components named. Last year's team introduced the water tank as a new component to the system and had to change to a new water pump as the old one failed.

8.1 Fluid selection

The previous year's team has used water at their circulation fluid. Regarding cuttings transport, hole cleaning and bit cooling the water has performed to a sufficient level as drilling fluid. The primary advantage of water is the environmental advantage, the fluid does not have to be taken care of after use. This simplifies the circulation system as it can be an open system, the fluid and cuttings out the well is transported directly to the drainage system through a water hose.

The team's preferred solution as of now is to continue using water as drilling fluid, but during the PDM's design and testing phase more lubricating fluids effect will be investigated.

8.2 Fluid System

The fluid system is an open system, and consists of the hydraulic triplex pump, water hoses, water tank and swivels. The fluid starts in the water tank and is transferred to the pump by a water hose, the water tank level is measured by a tank level sensor. When the fluid level in the tank is too low, a solenoid valve will open and fill the tank directly from the on-site water supply. Pressurized water exits the pump and flows to the hydraulic swivel, which consists of a roller bearing and the rotating pressure seal. The roller bearing supports the drill strings rotational load and the pressure seal allows fluid circulation towards the lower part of the drill string. When the water has entered the drill string it flows down to the bit and then exits the bit nozzles. The fluid flow from bottom to top will transport the drilled cuttings out of the hole, into the riser and out into a water hose via the flow diverter.

8.2.1 Hydraulic Pump

The pump to be used is a 5CP6120 pump from Cat Pumps, which can deliver up to 23 liters per minute and a maximum outlet pressure of 110 bar [36]. Pump specifications is shown in Figure 8.1.

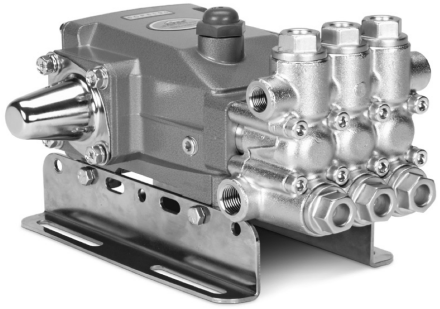

SPECIFICATIONS	U.S. Measure	Metric Measure
5CP6120		
Flow	6.0 gpm	23 lpm
Pressure Range	100 to 1600 psi	6.9 to 110 bar
Pump RPM*	1400 rpm	1400 rpm
Bore	0.787"	20 mm
Stroke	0.709"	18 mm
Weight	19.9 lbs.	9 kg

Figure 8.1: Pump specifications [36].

8.3 Modifications on Fluid System

This year the change of drilling fluid has been discussed. The steel on steel PDM design of last year had tests performed while monitoring Revolutions per Minute (RPM), the result of this test was that the PDM delivered more than 200 RPM with 28 lpm [35] (another pump was used). The problem of the PDM occurred with time, as the steel on steel configuration wore out too fast and the interference fit became too low to deliver the desired RPM. The team has discussed several different solutions that will counteract the material wear, one solution is to change the drilling fluid with a more lubricating fluid than water.

Change of drilling fluid would primarily be to reduce the material wear, but this is something that will need to be tested further in Phase II of the project. Use of a lubricating drilling fluid will most likely cost to get produced, and therefore the available volume will be limited. With limited available drilling fluid, the circulations system will need to be closed so the needed fluid can be reused. A solution with closed-loop circulation needs to have screens or shakers to remove cuttings particles while drilling.

9 Electrical System and Instrumentation

When designing an autonomous drilling rig, the electrical system used and communication between hardware and software is important. In this section, the previous year's design choice regarding this will be presented, as well as the proposed changes given by this year's team. With regard to the changes in competition guidelines, the need for a new electrical system or communication is not necessarily needed, as the previous downhole sensor is adequate. More efficient communication schemes, as for example change in wiring, will be proposed.

9.1 Hoisting System

The main function behind the hoisting system is to hoist the rotary part of the rig up or down. This will in turn provide Weight on Bit (WOB) and Rate of Penetration (ROP) to the drill bit. An AC motor is connected to the ball screw that hoists the rotary system up or down. At the bottom part of the ball screw, a load cell is connected. This is used to measure the WOB which travels through the rotary system, and into the ball screw. An overview of the system can be seen in figure Figure 9.1. The hoisting system has two important parts; the hoisting motor and the load cell. These will each be presented in the two following sections.

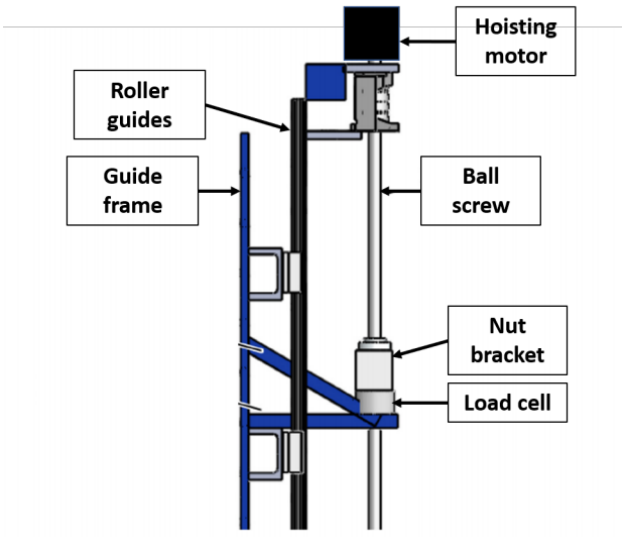

Figure 9.1: The Hoisting motor, ball screw and load cell locations [37].

9.1.1 Hoisting Motor

The hoisting motor used for this year's competition is fully capable of achieving the end goal of this year, and will therefore be used for this years competition as well. As presented in the mechanical design section, the motor model is "Lenze GST03-2M VBR 063C42", and is used to hoist the whole rotary system up or down. The maximum output power is 0.75 kW, and the motor works at a frequency of 120 Hz, with a rotary speed of 3400 RPM. The maximum torque of the motor is 45 Nm, and it has a power factor of 69%, with a

maximum efficiency of 79%. The gear ratio between the connection of the hoisting motor RPM and the ball screw RPM is roughly 1:9.

The hoisting motor has an encoder, which makes it possible to measure position, RPM and torque with high precision. This makes it possible to find the well depth of how far the drill bit has drilled. It is important to note that even if the encoder shows an increasing count, this does not necessarily mean that the well depth is increasing. This is due to a possible bend in the drill string. To better estimate the length, the hoisting motor also has a load cell which will be presented in the next section. A more detailed description of the presented numbers can be found in [38][39][40].

9.1.2 Load Cell

The load cell tthe hat is used is the same as the load cell used in the competition of year 2018 and 2019. The model is TC4-AMP transducer by APE Transducer [41], and is presented in Figure 9.2. As mentioned, the load cell is mounted between the rig frame and the ball screw shown in figure Figure 9.1. When there is a normal force acting on the drill bit, i.e after the drill bit tags the rock, there will be a normal force acting through the rotary system and through the ball screw to the load cell. The output of the measured force can both be represented in voltage or current. In this case, the travel distance for the signal to be read is quite small, which is why the voltage will be used. The outputted voltage is between $[-10V, 10V]$, which translates to a maximum and minimum force measurements of $[-2500N, 2500N]$. This gets translated to WOB [kg] by Equation 9.1.

$$WOB = V\frac{F_2 - F_1}{g(V_2 - V_1)} - m_{offset} \tag{9.1}$$

V is the measured voltage, F_2 and F_1 are the maximum and minimum forces ($2500N$ and $-2500N$ respectively), V_2 and V_1 are the maximum and minimum voltages possible ($10V$ and $-10V$ respectively), and m_{offset} is a constant to cancel the weight of the rotary system. Together with the measurement of the WOB and the measurement from the hoisting motor, the position of the drill bit can be estimated with the use of a Kalman filter and the orientational measurements gotten from the IMU.

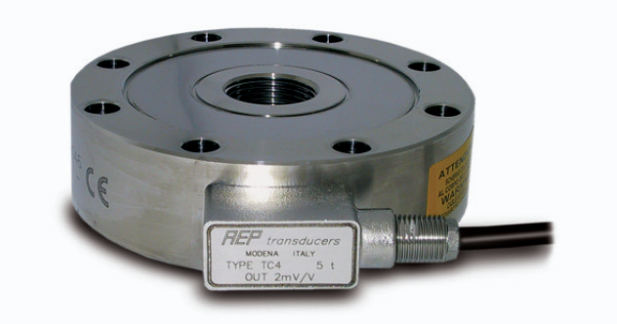

Figure 9.2: Load cell: TC4-AMP transducer by APE Transducer [41].

9.2 Rotary System

The main function behind the rotary system is to provide torque and RPM to the drill string and the directional tool, as well as making it possible to pull wires down to the Bottom Hole Assembly (BHA) for the sensor card. Since the previous year used an electrical downhole motor, while this year's team has decided to use a Positive Displacement Motor (PDM), the need for electrical wires downhole might be redundant. The rotary system can be seen in Figure 9.3.

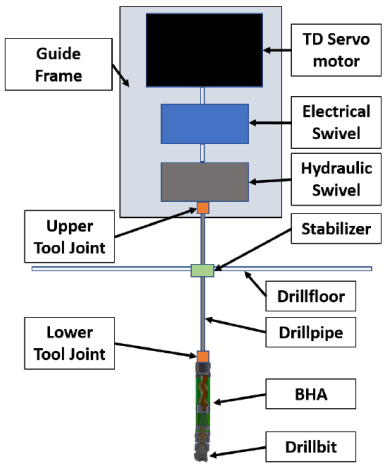

Figure 9.3: The rotary system of the drilling rig with its different components [37].

9.2.1 Top Drive Motor

The top drive motor is used to directly give RPM and torque to the drill pipe for initial drilling of the vertical hole, while it will be used for positional orientation of the directional tool when doing position control of the drill bit. This will be used to control the drill bit to follow the reference path. The servo motor used is Schneider Electric BCH2MM1523CA6C [42], which can provide an RPM to the drill pipe of 2902, which is more than enough for this drilling operation. The twist-off torque of the drill pipe is calculated to be around 6 Nm, which can be seen in Table 6.3, while the top drive motor can give a stall torque of 7.24 Nm, and peak torque of 19.7 Nm. The nominal speed of the top drive is 2000 RPM, and with the calculations given in section 6.3.2, which states a needed RPM of 70, this should be well inside the Top Drive (TD) limits.

Since this year's competition guidelines set more focus on the directional part of the drilling, accurate measurements of the top drive position and drill bit orientation are even more important this year. Therefore, the team is using Schneider Electric LXM28AU15M3X [43] as a servo drive. The accuracy of the internal position controller of the top drive servo drive is stated to be 0.1%, which translates to 0.36^o. This should be sufficient enough to control the drill bit to follow the reference path. The servo motor and servo drive used in the top drive is shown in Figure 9.4.

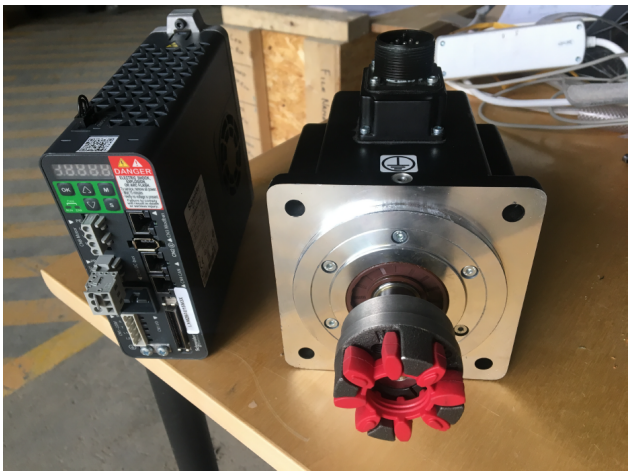

Figure 9.4: The Schneider Electric servo motor and servo drive [37].

9.2.2 Electrical Swivel

In the previous years, there was a need to pull wires down to the BHA as an electrical motor was used. This year, the team has decided to use a PDM, which in turn reduced the number of wires needed downhole. If the team is able to use wireless communication with the sensor card without too much interference, the need for down hole wires will disappear, and therefore also the need for an electrical swivel. With wires, the team must use an electrical swivel to transmit signals from a set of rotary wires in the drill string to static wires above the swivel. The team is using an SNG012-12 [44] series slip ring by Senring as the electrical swivel. The electrical swivel can support up to 5000 RPM, which should be enough as this only considers the maximum RPM of the whole rotary system, and therefore not including the PDM RPM. The electrical swivel may have up to 12 circuit 5A signals that can be pulled through. The swivel can be seen in Figure 9.5.

Figure 9.5: The electrical swivel SNG012-12 to provide rotation to the signal wires down hole [44].

9.2.3 Sensor Card and Communication

Sensor Sub

This year, the team has decided to continue with the PDM, which means that there is no electrical power

needed beneath the sensor card. In Figure 9.6, the sensor sub is presented, which is where the sensor card will be placed. The sensor sub is placed on the top of the BHA, presented in Figure 7.21.

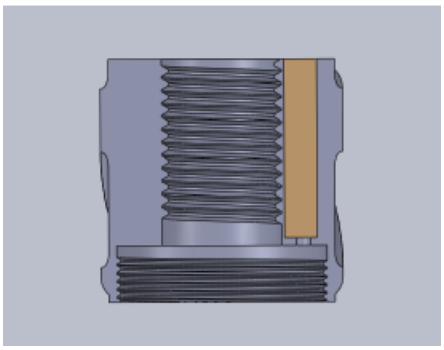

Figure 9.6: The downhole sensor sub on the top of the BHA.

The current design of the sensor sub takes in account the wires that are needed for downhole communication. If the communication method is changed to wireless, the design of the sensor sub will go through significant changes. First, there will no longer be a need for wires into the sensor sub, which removes the leakage problem. On the other hand, the card will need power from a battery, and the amount of space needed is therefore increased.

Wired communication

The current communication solution is shown in Figure 9.7.

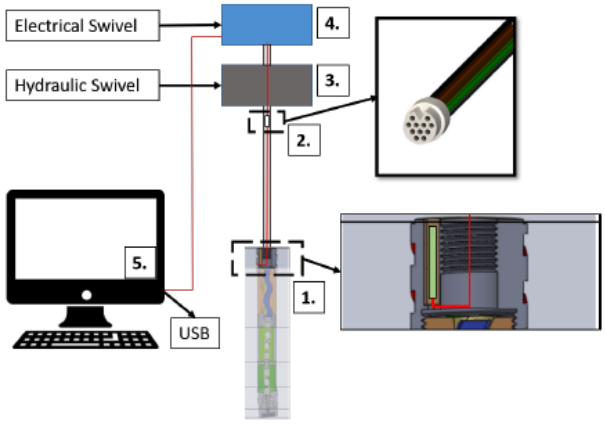

Figure 9.7: The wired downhole communication scheme [37].

As can be seen in the figure, the wires are pulled through the electrical swivel that transforms the signals such that they can be used in the rotary system. The wires are then pulled into the bottom entrance of the sensor sub. With the change from an electrical downhole motor to the PDM, the number of wires downhole needed this year is only 4 compared to last year's 10. If wireless communication works well after testing with regards to the quality of the data passing through the different material in the stone, the wires will be removed completely, and also the electrical swivel.

In the case of using wires, the team will reduce the last year's size of the connectors, as there is no longer a need for 10 downhole wires. This year, the team will use a 6 pin circular plastic shell connector compared to last year's 11 pin connector. The new sizes compared to the two last years are presented in Table 9.1. To better understand the specifications presented in the table, Figure 9.8 shows the different dimensions of the connectors.

Table 9.1: Change in dimensions for the wire connectos [45].

Year	Dimension A	Dimension B	Number of pins
2018	5,6	1,0	6
2019	3,89	0,64	11
2020	3,10	0,64	6

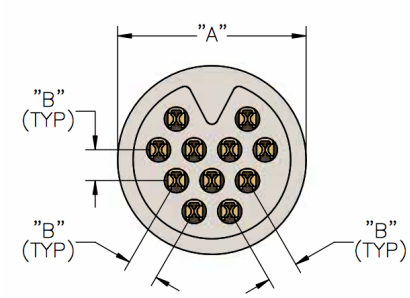

Figure 9.8: The measureable dimensions of the Omnetics Nano connectors [45].

The wires that go into the sensor sub is the most vulnerable part of this communication scheme, as the problem with leakage is hard to prevent when there is used high pressured water for the PDM that passes the sensor sub. However, the team will use epoxy to seal the sub from the water.

Sensor card

The sensor card is the same as in the previous year, which has an Intertial Measurement Unit (IMU) that collects data for further use in the control system. The IMU is of type ICM-20948 [46] 9-axis motion tracking from TDK InvenSense, and is shown in Figure 9.9, and has a gyroscope, accelerometer and magnetometer which can be summarized as follows:

1. **Gyroscope**
    - Digital x-,y- and z-axis angular rate sensors
    - Configurable output range of ± 250, ± 500, ± 1000 or ± 2000 degrees per second (dps)

- User-selectable low pass filters

2. **Accelerometer**
    - Digital-output x-, y-, and z-axis accelerometer
    - Configurable output range of $\pm 2g$, $\pm 4g$, $\pm 8g$ or $\pm 16g$
    - Integrated 16-bit analog-to-digital converter (ADC)
    - User-selectable low pass filters
    - Wake-on-motion interrupt for low power operation of applications processor
3. **Magnetometer**
    - 3-axis Hall-effect magnetic sensors
    - Output data resolution of 16-bits
    - Maximum output range of $\pm 4900 \mu T$

Figure 9.9: The ICM-20948 IMU used in the sensor card [46].

With the measurements from the IMU, the team will be able to control the drill path based on the orientation of the IMU.

The sensor card also includes an EFM32 Gecko microcontroller (EFM32G210F128-QFN32) [47] that the team will program and configure in Simplicity Studio. This will mostly revolve around reading and writing to the different registers. A PCB 2D model of last year's sensor card with all the different component placements is shown in Figure 9.10.

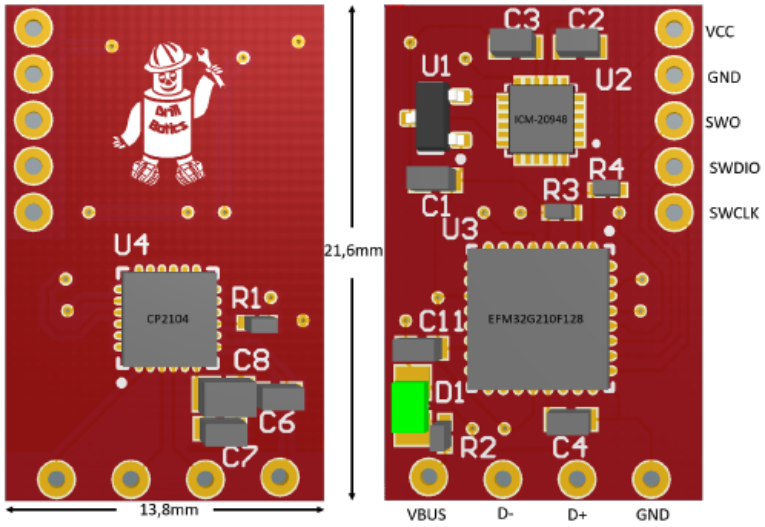

Figure 9.10: PCB 2D model of the sensor card with component placement, input/output pins and dimensions [37].

The product name, details and supplier can be found in Table 9.2.

Table 9.2: PCB components, specification and supplier [37].

Name	Product Name	Details	Supplier
U1	EF3318AIDBZT	3,3V-1,8V DC/DC converter	Texas Instruments
U2	ICM-20948	9-axis Motion Tracking device	TDK Invensense
U3	EFM32G210F128	microcontroller	Silicon Labs
U4	CP2104	USB-to-UART-bridge	Silicon Labs
R1-2	1kΩ	Resistor	RS components
R3-4	1kΩ	Resistor	RS components
D1	X	LED diode	RS components
C1+C4-7+C9-12	C0603C105K9RACAUTO	$1.0\mu F$ Capacitor	RS components
C2-3	C0603C105K9RACAUTO	$0.1\mu F$ Capacitor	RS components
C8	C0603C105K9RACAUTO	$100pF$ Capacitor	RS components

The communication flow of the components in the sensor card is presented in Figure 9.11. As seen, the data from the IMU is sent to the EFM32 microcontroller over I2C communication, which is programmed to

receive the data from the IMU. The data from the microcontroller is sent to the PC via a USB-cable. CP2104 is therefore between the microcontroller and the USB as a USB-to-UART-bridge.

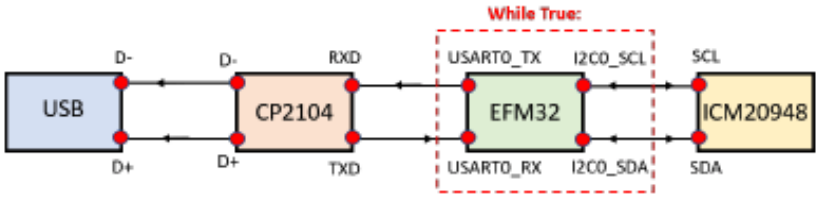

Figure 9.11: The communication flow of the components in the sensor card.

The sensor card uses two main communication protocols. The first one is I2C, which is an abbreviation for Inter-Integrated Circuit. There are three main functions [48] that uses I2C-communication between the microcontroller and IMU, which can be summarized by the following points

- **i2c_write_register**
  A write function that has chip-address, register-address and data to write as input. This function is used to select register banks and to configure the IMU on power-up.
- **i2c_read_register**
  A read function that has chip-address and register-address as input, and stores the output in a data-array. This function is used to read registers on the IMU.
- **i2c_read_registers**
  A read function that has chip-address, register address and the N number of registers that shall be read after the register address. This function is used to read multiple registers.

These functions let you read from an 8-bit register, write to an 8-bit register, or read from multiple 8-bit registers. The IMU stores the measurements in 16-bit series divided on two 8-bit registers. The combined bits from the two 8-bit registers then make up a 16-bit signed integer.

When the microcontroller communicates with the top side computer, the Universal Asynchronous Receiver/-Transmitter (UART) [49] is used. The communication protocol either uses "transmit" or "receive" serial data asynchronously. The protocol therefore uses a read bit to decide if it should read a data packet or not. All printed data from the microcontroller is therefore sent through UART to the topside computer serially.

The main program is from last year's team and is written in C++. The code is flashed onto the microcontroller, and automatically runs on power-up. The code consists of two main sections, where the first one is the setup-stage, and the second is the while-loop stage. The setup-stage has a set of functions that starts sequentially that sets up and configures the microcontroller and IMU. It also includes an optional calibration sequence for the IMU. The while-loop stage will run a number of functions that prints the read data from the sensor measurements, with an update frequency of approximately 60Hz. The different function declarations

[37] are shown below.

Setup()

- **CHIP-Init()** - init of EFM 32
- **gpioSetup()** - configure GPIO-pins on EFM32 using the header files generated by the MCU-configurator in Simplicity Studio
- **I2C-Init()** - init of I2C communication
- **i2c-read-register(ICM-address, WHO-AM-I)** - This function reads the WHO-AM-I-register of the ICM-20948 to confirm that there is a connection.
- **calibrateAccGyro()** - calibration function for accelerometer and gyroscope.
- **initICM20948()** - setting for ICM-20948 is written on to the chip
- **calibrateMagnetometer()** - calibration function for magnetometer

While(1)

- **readAccelData(accelCount)** - reads accelerometer data and stores the 3-dimensional vector it in an array called accelCount. This array is overwritten for every loop.
- **readGyroData(gyroCount)** - reads gyroscope data and stores the 3-dimensional vector in an array called gyroCount. This array is overwritten for every loop.
- **readMagData(magCount)** - reads magnetometer data and stores the 3-dimensional vector in an array called magCount. This array is overwritten for every loop.
- **print(...)** - all vector components are printed over serial for further analysis in Labview.
- **print("c", 0x04)** - a control-word is printed to stop the transmission.

9.3 Hydraulic System

When drilling, it is important to have sufficient fluid downhole to cool the drill bit. As this year focuses on using a PDM, high pressured fluid through the BHA is even more important. The hydraulic system is used primarily for these two objectives and is presented in Figure 9.12. The system has a solenoid valve on top of the fluid tank that is controlled by a solid-state relay to open or close the fluid input based on the readings from the pressure gauge at the bottom of the tank. The pump takes the fluid from the tank and uses a pump motor to pressurize the fluid based on the control feedback.

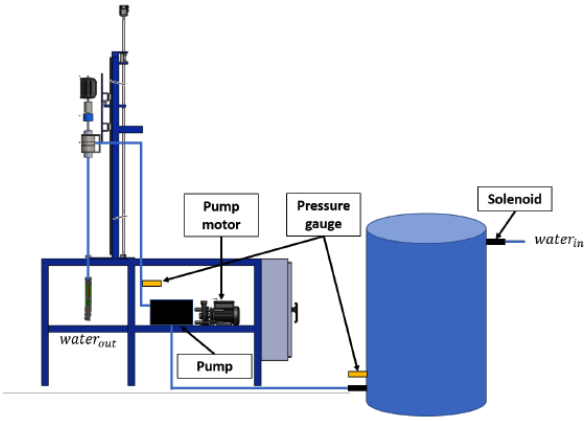

Figure 9.12: An overview of the hydraulic system.

9.3.1 Solenoid Valve

The solenoid valve used is the same as the previous year, 24V NC (normally closed) valve by RS Pro [50]. To control the valve, a solid-state relay P2RF-05-S [51] by Omron is used. This relay can be controlled by a 5V signal which translated to open or close the valve. Based on the readings from the pressure gauge at the bottom of the tank, the solenoid will automatically open or close. If the drilling fluid is chosen to be something other than water, there will be implemented closed-loop circulation of the fluid from the well to the tank. The solenoid valve and relay are shown in Figure 9.13.

Figure 9.13: The 24V NC solenoid [50] by RS Pro and P2RF-05-S solid-state relay [51] by Omron.

9.3.2 Pump Motor

The pump used to provide pressured water for the riser system and PDM is a 5CP6120, which there may be read more about in the datasheet given in [52].

9.3.3 Pump Pressure Gauge

Just like last year, the team will use pressure gauges to measure and control the pump pressure. As accurate directional drilling is even more important this year, it is important to have accurate control of the ROP. Since ROP is highly dependant on the pressure of the fluid, this must be controlled.

The gauge used to measure the pressure of the bottom of the tank, and the pressure of the pump outlet is a PCE-28 pressure transmitter [53] by Aplicens A-S, as last year. The gauge can measure 0-100 bar, which is converted to a current between $[4-20]mA$ or $[0-10]V$. As the previous team used the current model for the gauge, this team will do the same.

The tank pressure and pump outlet pressure can be calculated by the following equation

$$P = \frac{(I - I_1)(P_2 - P_1)}{I_2 - I_1} - P_{offset}, \tag{9.2}$$

where P [bar] is the tank or pump outlet pressure, I is the measured current [mA], I_2 and I_1 are the maximum and minimum current, respectively (4-20mA), and P_2 and P_1 is the maximum and minimum pressure, respectively (0-100 bar). P_{offset} is the pressure offset generated by calibrating the gauge. The PCE-28 can be seen in Figure 9.14.

Figure 9.14: The PCE-28 pressure gauge from Aplicens A.S. [53].

9.4 Power Distribution

The electrical power distribution can be seen in figure Figure 9.15.

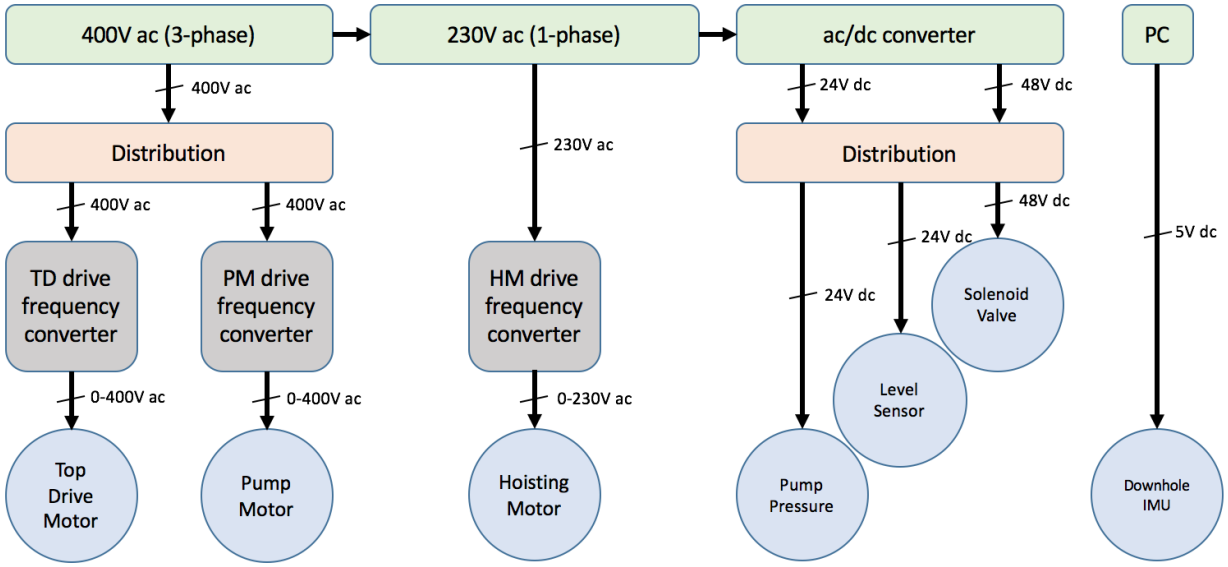

Figure 9.15: The electrical power distribution of the system.

9.5 Calibration of Sensors

Last year, there has been done calibration experiments on the IMU and the load cell. The calibration methods, as well as the results [37] will be presented here.

9.5.1 Accelerometer Calibration

During the tests from last year, it was found that the factory calibration for the accelerometer in the IMU is satisfactory, as it has an accuracy of 2 decimals. The team calibrated the sensor by measuring the gravitational acceleration for each axis by placing the sensor card in a 3D printed cube. Figure 9.16 shows how this was done. The method used to calibrate the accelerometer can be summarized by the following points.

- Level a table using a leveling bar
- Put sensor card in the 3D printed box as shown in Figure 9.16
- Measure the gravitational force for each side of the box with at least 1000 samples per side
- Calculate bias and needed scale to correct for bias

The results from doing the calibration are presented in Table 9.3.

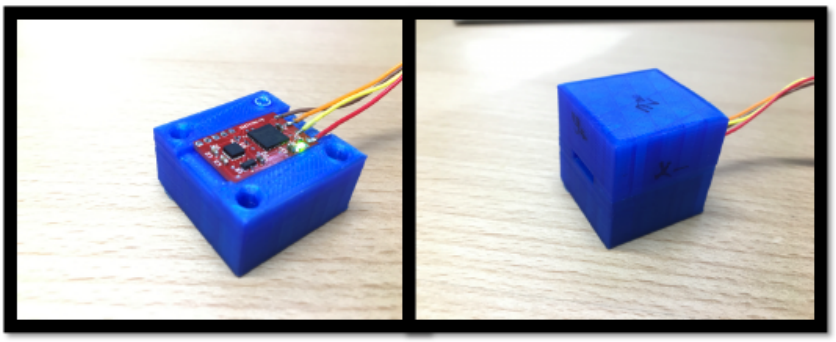

Figure 9.16: The sensor card placed in 3D printed cube for calibration [37].

Table 9.3: Found acceleration calibration scale constant from last years experimentation [37].

Axis	Max measure [g]	Min measure [g]	Bias [g]	Scale	Raw [g]	Calibration [g]
X	0.995953	-1.008914	-0.0129614	0.997572	1.002793	1.00033
Y	1.00235	-1.00567	-0.00332146	0.996008	1.003835	0.9995815
Z	0.992286	-1.01267	-0.0203821	0.997529	1.004273	1.001681
XYZ avg	0.996863	-1.009083	-0012221653	0.9970363	1.003634	1.000531

As seen in the table, the calibration gives an accuracy of three decimals compared to the factory calibration of two decimals. This should be accurate enough to control the drill bit along the reference path.

9.5.2 Gyroscope Calibration

Using a gyroscope for orientation is often not possible if high accuracy is needed. This happens because of drift in orientation [54], which is why gyroscopes are more often used for angular rate control. The last year's team has measured the drift of the gyroscope and tried to calibrate it. The result of the calibrated gyroscope is shown in Table 9.4.

Table 9.4: Last year's gyroscope calibration results [37].

Axis	Mean raw [deg]	Bias [deg]	Mean calibrated [deg]	Accumulated drift [deg/min]
X	0.54120	0.27060	0.00689	0.339863
Y	-0.48761	-0.23587	-0.243805	-0.913121
Z	-0.30714	-0.15357	-0.00054	0.0860555

As seen in the table, the drift is too high, even after calibration. The gyroscope may still be used with regards to measuring angular rate, but in the case for measuring orientation for position control, it will not be used.

9.5.3 Magnetometer Calibration

To estimate the orientation of the BHA, both the accelerometer and the magnetometer in the IMU will be used. A magnetometer will be very affected by soft- and hard iron distortion sources, and will therefore have to be calibrated after every new installment in the BHA. This has been done the previous year, and the results and methods will be presented here.

Calibration outside of the BHA

When calibrating the magnetometer outside of the BHA, the magnetometer is placed where there are very little external distortion sources. Then, the sensor card (with the IMU and therefore the magnetometer), is rotated around all the axis in an eight-figure motion. Then there is calculated a bias offset to the center that is around zero, which produces a linear scale correction. The calibration results from the previous year are shown in Figure 9.17.

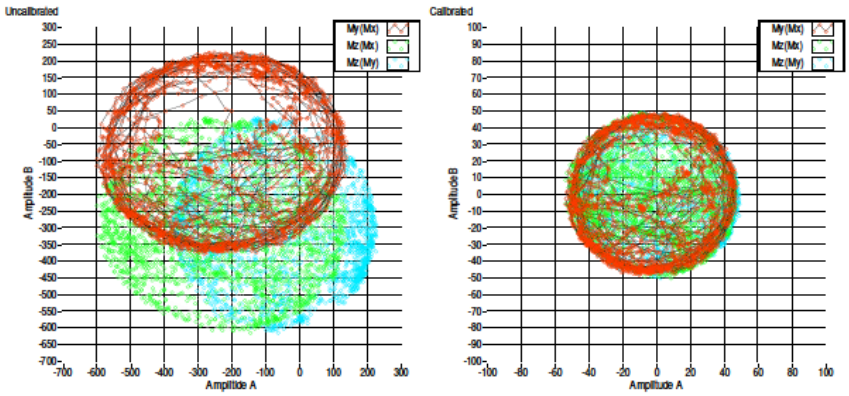

Figure 9.17: The outside calibration of the magnetometer [35].

As the figure shows, there is little soft-iron distortion since there is minimal stretching of the circles into ellipsoids. There is, however, hard-iron distortion, as there is a bias from the center around zero. After adding the bias, a linear scale factor is calculated to create perfect circles.

Calibration inside of the BHA

When the sensor card is placed inside the BHA, there are a lot of magnetic distortions coming from the different materials and components. The magnetometer must therefore be calibrated once it is inside the BHA. The same method is used as when the magnetometer is outside of the BHA. The results from the raw data, and after correcting for the found bias is shown in Figure 9.18.

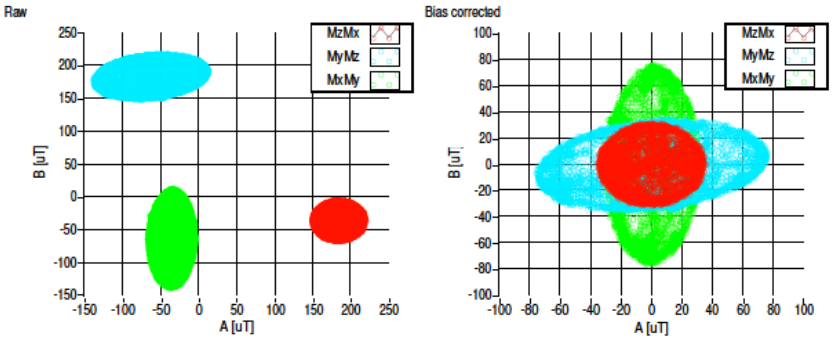

Figure 9.18: The raw magnitude plot and fixed bias plot [37].

As seen in the figure, the magnitude plot for the yz-plane has a small deviation from being aligned with the axis. Last year, it was found that the deviation was about 4 degrees, which is addressed by rotating the IMU body frame -4 degrees around the x-axis to compensate for this. The result from rotating the body frame is shown in Figure 9.19.

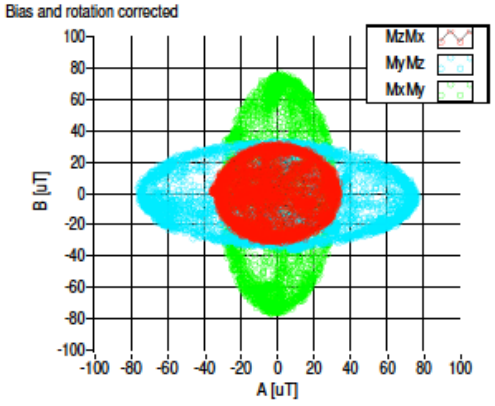

Figure 9.19: The result after adding calculated bias and rotation of yz-plane [37].

After rotation, it can still be seen that there is a lot of stretching in both the yz-plane and the xy-plane. The BHA is therefore rotated around all axis in an eight-figure motion as done earlier. The result is measured, and a linear scale factor is calculated. After finally adding this, the final result is shown in Figure 9.20.

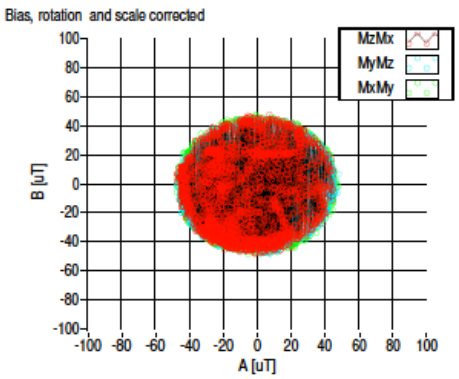

Figure 9.20: The result after adding the linear scale factor to create perfect circles.

As seen in the figure, the result is satisfactory for calibrating the magnetometer. However, this must be done every time the magnetic field changes around the sensor card.

10 System Description and Control Design

Since Drillbotics is an autonomous drilling rig competition, a control system must be in place to remove the manual need for control. In this section, an overall plan of controlling the rig to drill a path defined by the given x, y and z coordinates will be presented. Last year, the competition objective was to get as much horizontal displacement as possible, while the objective this year is to hit three coordinate points. The control system to achieve this new goal will be presented in this section.

10.1 System Description

To be able to control the system, the possible inputs and measurements will be presented in this section.

10.1.1 System Inputs

When autonomously controlling a drilling rig, the possible inputs are a key factor of the design considerations. The rig has three actuators that can affect the state of the system, namely

- **Hoisting motor**
  Controls Weight on Bit (WOB) by hoisting the rig either up or down when the drill bit is in contact with the stone. If not, the motor controls the z-position of the drill bit when the z^i-axis is given in the inertial frame.

- **Top drive servo motor**
  Controls both the drill string rotation position and RPM. It can only control one of the prior mentioned states at the same time.

- **Pump motor**
  The pump motor pumps fluid through the drill string into the Positive Displacement Motor (PDM), drill bit rotation. By controlling the pump motor, it is possible to control the drill bit RPM. The pump is also used to provide hole cleaning and bit cooling.

The three motors described are all controlled by an RPM input, with the top drive servo motor being an exception. This motor can be controlled both by giving it an RPM reference point, as well as a positional reference point. In Table 10.1, the summarized inputs of the system is given.

Table 10.1: Rig actuators and their respective variables, units and modes.

Motor	Named Variable	Unit	Mode
Hoisting motor	ω_{hm}	RPM	All configurations
TD motor	ω_{td}	RPM	TD-RPM mode
TD motor	ω_{td}	Steps	TD-Position mode
Pump motor	ω_{pm}	RPM	All configurations

10.1.2 System Measurements

To be able to generate input for the previously mentioned actuators, an estimation of the relevant states is needed. To get a good estimation, measurements will be used in a Kalman filter. It is therefore important to define the measurements from the sensors that are at the team's disposal, and these are shown in Table 10.2.

Table 10.2: Measurements from the different sensors.

Measurement Description	Named Variable	Unit
Hoisting motor RPM	ω_{hm}	RPM
Hoisting motor position	S_{hm}	steps
Hoisting motor torque	T_{hm}	Nm
TD motor RPM	ω_{td}	RPM
TD motor position	S_{td}	steps
TD motor torque	T_{td}	Nm
Pump motor RPM	w_{pm}	RPM
Pump motor pressure	P_{pm}	Bar
Pump motor torque	T_{pm}	Nm
Water Tank pressure	P_{wt}	Bar
WOB	P_{wob}	N
DH 3-axis IMU Magnetometer	$\vec{m} = [mx, my, mz]$	μT
DH 3-axis IMU Gyroscope	$\dot{\vec{g}} = [\dot{\phi}, \dot{\theta}, \dot{\psi}]$	deg/s
DH 3-axis IMU Accelerometer	$\vec{a} = [ax, ay, az]$	g
PDM RPM	ω_{pdm}	RPM

10.1.3 Control Objective

Now that the system inputs and measurements are defined, it is needed to define the control objective before defining the relevant states of the system. Comparing the current year's competition objective with the previous year's objective, the reference path for the drill bit may no longer be calculated prior to the competition. Instead, the path should be created during the competition with the given three x-, y- and z-points. These points may create a path that varies both in azimuth and inclination, which gives a more complex position control system, especially with regards to strain on the drill pipe.

10.2 State Machine

The drilling rig has many states that it can be in. Based on the states, there are several operations that must be done, and the rig must not move to a new state before the different requirements are met. Also, with unexpected events, the rig must be brought to a safe state from which it may continue.

The state machine is divided into two parts, where the first part concerns the initialization of the rig and drilling of the pilot hole, and the second part concerns the directional drilling part of the operation.

10.2.1 Vertical Drilling

As the competition guidelines state that the initial well must be a pilot hole of at least 4", the state machine will have its own separate part dedicated to this demand. The different normal states that the rig may be in, are shown in Figure 10.1.

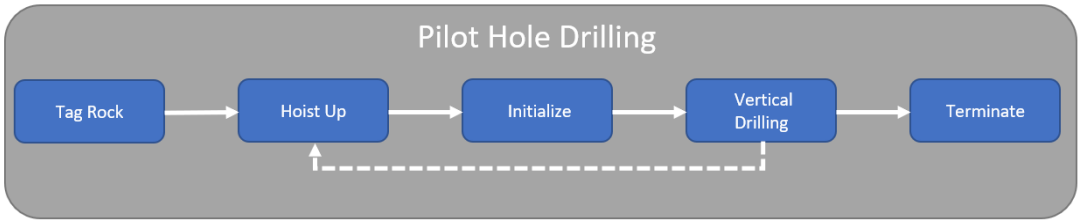

Figure 10.1: State machine for vertical drilling.

As seen, there are five normal states the rig can be in during vertical drilling. The active actuators, measurements and transition requirements in the different states can be summarized as follows:

1. **Tag Rock**
   The drill bit has not yet touched the rock, and therefore will not require any WOB. The hoisting motor pushes the rotary system down towards the rock while there is no other rotation. A figure of the state of the rig can be seen in Figure 10.2a. Once there is registered a WOB greater than a set threshold t_{tag}, i.e $P_{wob} > t_{tag}$, the state transitions to Hoist Up.

2. **Hoist Up**
   Hoist up is the next state after tag mode, but will also be used whenever vertical drilling needs to be reset due to factors as exceedingly high torque, pressure or WOB. When in hoist up mode, the main purpose is to hoist the rotary system up a height h, as shown in Figure 10.2b. When this is done, the state transitions to Initialize.

3. **Initialize**
   Initialize mode will always come after Hoist up mode. Hoist up mode hoisted the rotary system up a height h, so that it is possible to reach the desired RPM on the drill bit since there is no contact with the rock. The Top Drive (TD) and pump motor for the PDM starts, and when sufficient RPM is met, the rig transitions to the vertical drilling state.

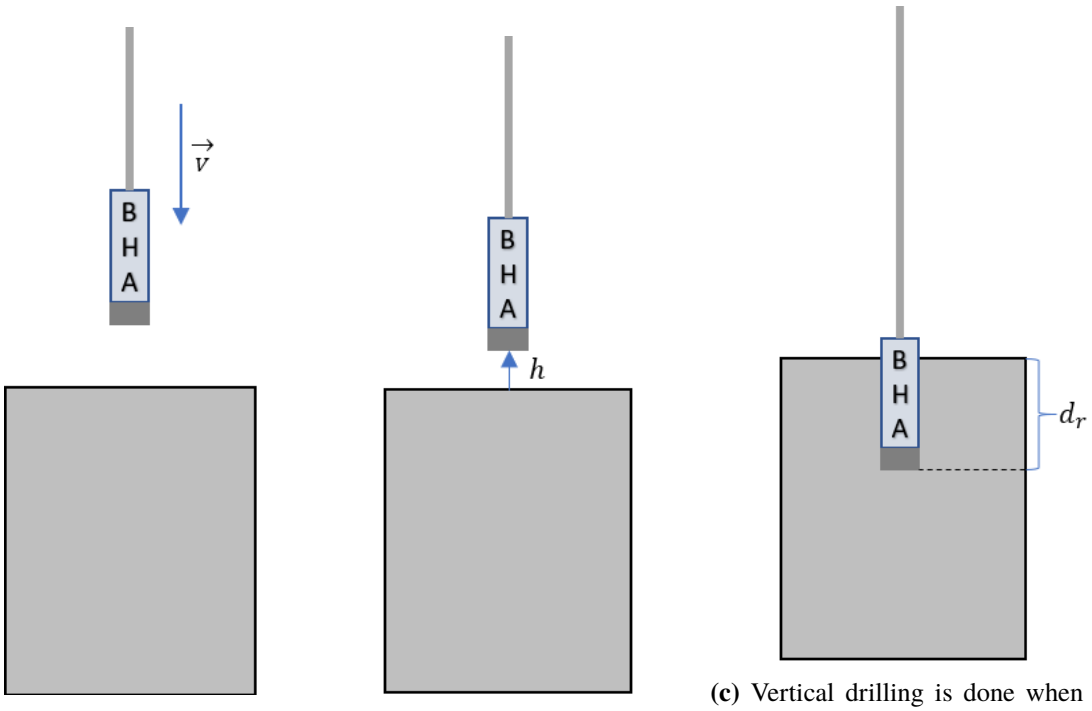

(a) The drill bit moves towards the rock when in tag rock state, and continues until it touches the rock.

(b) When the drill bit has touched the rock, the rotary system gets hoisted up until $z = -h$.

(c) Vertical drilling is done when the z-coordinate of the drill bit is greater than the requirements of the vertical well, i.e $z \geq d_r$.

Figure 10.2: Three of the possible states when in vertical drilling mode.

4. **Vertical Drilling**
   When in vertical drilling mode, one knows that the previous state was initialize, and that there is sufficient RPM on the TD and PDM. The hoisting motor will start to push the rotary system down, and drilling starts. The WOB, pump pressure and torque are measured continuously, and if they exceed defined thresholds, the state is immediately transitioned to hoist up. The z^I-coordinate of the drill bit is also monitored, and when $z \geq d_r$, where d_r is the desired depth of the pilot hole, vertical drilling stops, and the state transitions to the terminate state. This transitional state is shown in Figure 10.2c.

5. **Terminate**
   The termination state of the vertical hole drilling part is only reached when $z \geq d_r$. When this happens, the rotary system is hoisted up a height h_{vt}, before it transitions to the first state of directional drilling.

10.2.2 Directional Drilling

After the 4" pilot hole, the rig should drill a well path that follows a pre-calculated trajectory to hit multiple points given by their x, y, z-coordinates in the inertial frame. This is the directional drilling part of the autonomous rig, and its states can be seen in figure 10.3.

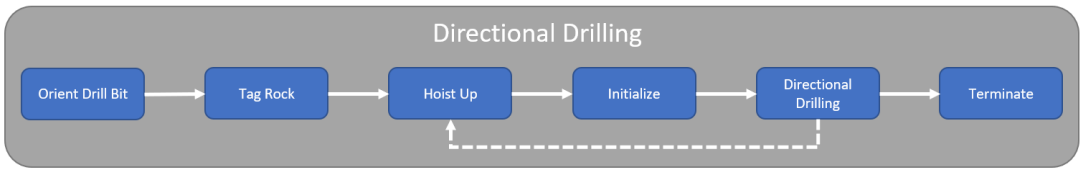

Figure 10.3: An overview of the different states when the system is in the directional drilling mode.

As seen, there are 6 states in the directional part compared to 5 in the vertical part. The extra state is the orient drill bit, as in this case it is needed to orient the drill bit as well before drilling. The active actuators, measurements and transition requirements in the different states can be summarized as follows:

1. **Orient Drill Bit**
   After terminating the vertical drilling part, the rotary system is hoisted up a height h_{vt} over the bottom of the 4" hole drilled by the vertical drilling part. The purpose is to let the control system orient the drill bit in the correct direction without touching the rock. The closest point in the reference path is calculated based on the z-coordinate of the drill bit, and a directional vector is calculated, which gives a TD reference position. This is better described in section 10.4.3. The TD is steered into this position, and then transitions to the Tag Rock state. An example of such a state can be seen in figure 10.4.

2. **Tag Rock**
   When the drill bit is oriented in the right direction, it will enter Tag Rock mode, which is the same as in the vertical drilling case. The rotary system is hoisted down until $P_{wob} > t_{tag}$, and then transitions to the Hoist Up state.

3. **Hoist Up**
   After the drill bit tags the rock, the state transitions to hoist up, which does the same as in the vertical drilling case. The rotary system is hoisted up a height h, and then transitions to the Initialize state.

4. **Initialize**
   When the drill bit has been hoisted up a height h, it is ready to gain RPM on the drill bit. The difference between the initialize state in directional versus vertical drilling mode, is that with directional drilling, only the pump motor is used to gain RPM on the PDM. That is, the TD is not used with directional drilling. When the desired RPM is reached, the state transitions to the directional drilling state.

5. **Directional Drilling**
   When in the Directional Drilling state, the RPM of the PDM is sufficient, since the previous state always is initialize. The rotary system is also hoisted up a height h from the hoist up state, so when the state transitions to directional drilling, it starts to hoist the rotary system down while monitoring the different states. The system then uses the position controller described in section 10.4, and the WOB controller described in section 10.3, to control the Rate of Penetration (ROP) and position of the drill bit.

The directional drilling state can transition to one of two states based on the state of the system. If the torque goes over a defined threshold, or the RPM falls under a certain threshold, it will transition to hoist up state, just as with the vertical drilling case. If the position of the drill bit has reached the last goal point, it will transition to the terminate state.

6. **Terminate**
   When terminate state is reached, the well path is done. The hoisting system will then stop all rotation of the PDM, and hoist the rotary system up.

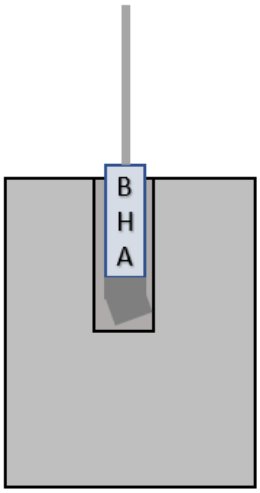

Figure 10.4: An example state when orient drill state transitions to new a state.

10.3 WOB Control

To control the speed of operation, the team has decided to control WOB in order to control ROP. This means that the team will control the ROP without controlling the RPM of the PDM. Instead, the RPM will be measured, and if it is under a certain threshold, the WOB will be controlled to 0 until the RPM of the PDM gets over that certain threshold. Using the desired ROP and the measured RPM of the PDM, the team will be able to calculate a reference WOB for the PI controller. A sketch of the planned WOB-controller can be seen in Figure 10.5.

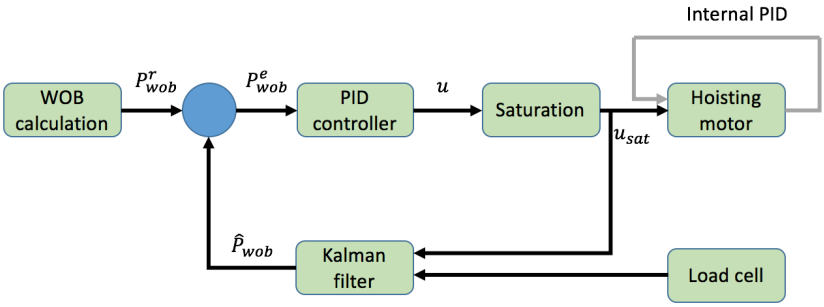

Figure 10.5: PID WOB control.

10.3.1 Design Considerations

As there are few changes that need to be done to the WOB controller, this year's design is inspired by the previous year's WOB design. When controlling the WOB, there are several considerations that must be done since too high WOB can, for instance, lead to twist-off or buckling. Also, too high WOB can lead to zero RPM for the PDM due to excessive torque generation. Summarized, the points that need considerations are

1. Drill pipe twist off limit [Nm]
2. Drill pipe buckling limit [Kg]
3. PDM torque limit [Nm]
4. Hoisting motor (HM) torque limit [Nm]
5. TD torque limit [Nm]
6. Competition time [hours]

Design Option 1 - Constant ROP The team has considered using a constant reference point for the ROP, such that the drilling operation will finish within a pre-calculated time. There are several reasons to why the team believes this will not be the best solution, especially when using a PDM. When controlling for a constant ROP, the HM would have to increase the WOB whenever ROP decreases. If the decrease of ROP is due to low RPM of the PDM, increasing WOB will decrease torque and in turn, ROP.

Design Option 2 - Torque
Another design option is to use torque as the control parameter. However, when using a PDM, it will be very hard to measure the torque at the drill bit. The control system would work by using HM RPM as input, and as long as the bit is rotating, this would change the WOB by a physical model. However, there have been done tests on a WOB control system based on controlling the torque, which gave a very low ROP. Also, this method would rely heavily on accurate knowledge of the RPM of the PDM, which will be hard to retrieve.

Design Option 3 - WOB

The final and chosen option is to control WOB directly by using the measurements from the load cell presented in section 9.1.2. This is also the method that there was found the most success with during the previous years. As WOB is a major factor in how much ROP the drilling operation has, it is possible to indirectly control ROP, given that the PDM has sufficient RPM. Because of this, this must be guaranteed and will be measured by vibrations in addition to excessive WOB measurements. Since WOB is directly responsible for buckling in the pipe, and indirectly affects torque, which affects possible pipe twist-off, these can both be avoided by controlling the WOB. Like the previous years, the 2020 team will also utilize a WOB controller to maintain and control the speed of operation.

10.3.2 Physical WOB Model

There will be two physical models to model the evolving WOB state. The first model is present in all the states in the state machine presented in section 10.2, up to a brief moment in the Initialize state in both vertical and directional drilling modes.

Physical WOB Model 1 - Before Rock Tag

The first model is when there are no normal forces due to the drill bit touching the rock. This model will therefore be used whenever this is the case, which is before the rock is tagged, and when the Bottom Hole Assembly (BHA) is hoisted up and on its way down to the rock. This is described more detailed in section 10.2. When this is the case, the linear velocity of the drill bit in the inertial frame can be modeled by

$$\dot{z}(t) = pk_{gr}k_c u(t), \tag{10.1}$$

where $\dot{z}$ is the linear velocity (which is parallel to the inertial z-axis), p is the ball screw pitch, k_{gr} is the gear ratio, k_c converts from RPM to m/s, and u is the HM RPM input. The z-position of the bit can therefore easily be modeled and controlled when the rock is un-tagged.

Physical Model 2 - After Rock Tag

When the rock is tagged, there are normal forces from the rock that points upwards into the drill string. These normal forces increase fast as the WOB increases, and it is therefore extremely important to control the WOB such that it does not exceed the buckling limit of the drill string. By experimentation, the team will find thresholds that satisfy the buckling limit constraints of the system.

10.4 Position Control

10.4.1 General Overview

In order for the drill bit to follow the reference points given by the calculated reference path, it is needed to implement a position controller. By using the reference path and the current position of the drill bit, the team will be able to calculate a reference orientation for the drill bit. This is further described in section 10.4.3.

When this reference orientation is calculated, it is compared to the current orientation of the drill bit gotten by the IMU, which is then fed into a PI controller. Since there is a twist off limit where, if we orient the drill bit extensively using the TD, there is a saturation to restrict the input to the TD to prevent pipe twist off.

The saturated input, as well as the readings from the IMU, is sent through a Kalman filter to estimate the current states. In some cases, the orientation of the drill bit can be directly found from looking at the position of the TD, but whenever there is twisting in the drill pipe, this will not be the case. Therefore, the Intertial Measurement Unit (IMU) measurements must be used. The position controller can be seen in Figure 10.6.

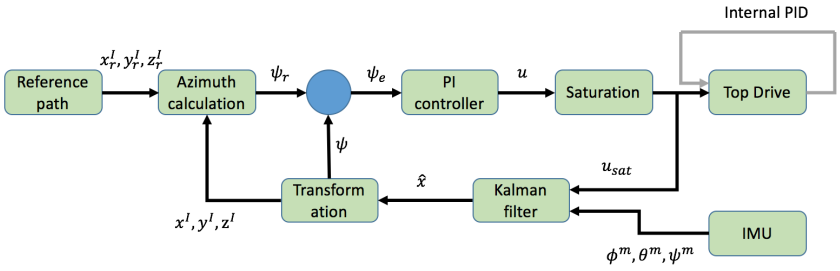

Figure 10.6: An overview over the PI positional control system.

The state space equations for the velocities and position is defined in the drill bit frame $\{db\}$. This is further described in section 10.5.1 and 10.5.2. The state dynamics can be expressed by the following equations

$$\dot{z}^{db} = ROP \tag{10.2}$$

$$\dot{\theta} = DLS \times ROP \tag{10.3}$$

$$\psi = u \tag{10.4}$$

The equations are based on the assumptions that the Dogleg Severity (DLS) and ROP are given in units from the metric system. The angular velocity of the drill bit building inclination angle is given by $\dot{\theta}^{db}$. The drill bit orientation angle is given by ψ. The azimuth build rate based on the input u has not been modeled completely yet, as this required a complex model that must be experimented with using a real stone block. A simplified solution that is used in the simulation shown in section 10.6, is to saturate the value of Δu to a reasonable value, such that the azimuth build angle $\psi = u$, but Δu is restricted to simulate pipe twisting.

10.4.2 Path Generation

The goal of the challenge is to hit a number of points provided on competition day. In order to be able to hit these points, the system must generate a reference path to be followed during the entire directional drilling phase. The basis for path generation is the given competition coordinates. The movement of the BHA is restricted by the mechanical design, hence generating a smooth path is important. The path is generated by using an interpolation function in MATLAB. The technique used is called cubic spline interpolation, and is described in section 5.4.7. An example path can be seen in Figure 10.7. According to [23], cubic spline

interpolation is a good way to avoid jumps in the reference angle ψ_r as would be experienced for example using a Dubins path. Jumps in the input is not a viable solution, as a big change in the TD position may end up in twist-off for the drill pipe.

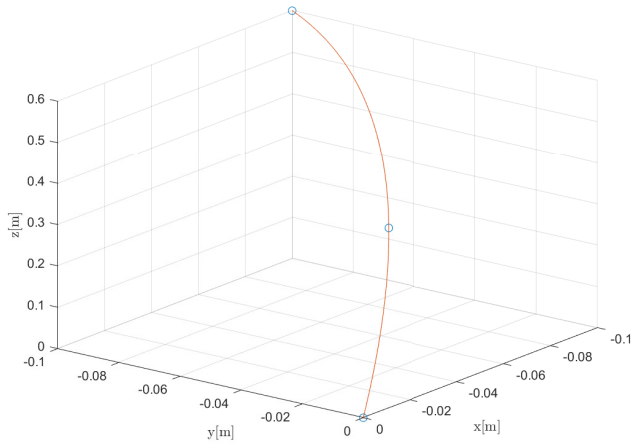

Figure 10.7: Example of reference path created using cubic spline interpolation. The blue dots are the three points provided.

10.4.3 Azimuth Calculation

Since the orientation of the IMU is known based on the measurements, the team will be able to check whether the drill bit frame is oriented correctly with regards to the reference path. An example is given in Figure 10.8, where the drill bit and reference point is given in the x-y-plane. First, the system calculates an estimated z-position of the drill bit using the measurements. Then this z-position gets mapped to the reference path to find the corresponding x-y-coordinates of the closest point in the path. By using the estimated x-y-coordinates of the drill bit and the x-y-coordinates of the reference point, it is possible to calculate a directional vector to use as a reference for drill bit orientation as shown in Figure 10.8.

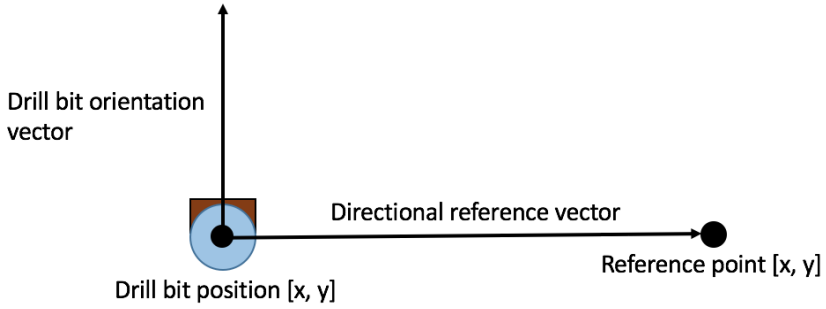

Figure 10.8: Drill bit orientation and reference vector in the X-Y-plane.

The objective for the position controller is to minimize the the cross-track error which is described in Equation 10.7. This is done by rotating the z^b-axis. In other words, to get the drill bit to point in the

desired direction, the reference angle ψ_r will be calculated. When the inclination angle is relatively small, the drilling direction in the xy^I-plane, is the same as the orientation of the drill bit, ψ.

$$e_x = x_r - x \tag{10.5}$$

$$e_y = y_r - y \tag{10.6}$$

$$e_{ct} = \sqrt{e_x^2 + e_y^2} \tag{10.7}$$

To calculate the desired drill bit angle, it is necessary to know in which quadrant the orientation angle belongs to in the unit circle. If the reference is the center of the unit circle, and the actual position of the dril lbit is given by $x > x_r$ and $y > y_r$, the actual position is located in the first quadrant. The angle between the line parallel to the x^I-axis and passing through the reference point, and the actual position is given by Equation 10.8.

$$\psi_e = \arctan \frac{e_y}{e_x} \tag{10.8}$$

The desired angle of the drill bit is computed based on the error angle ψ_e, and the signs of the error components e_y and e_x. E.g. if both the signs are negative, the angle between the line that is parallel with the x^I-axis and passing through the reference point, and the real position, is given by ψ_e. The drill bit should be oriented in the other direction to get closer to the reference point, hence the desired orientation of the drill bit is $\psi_r + \pi$, as shown in Figure 10.9.

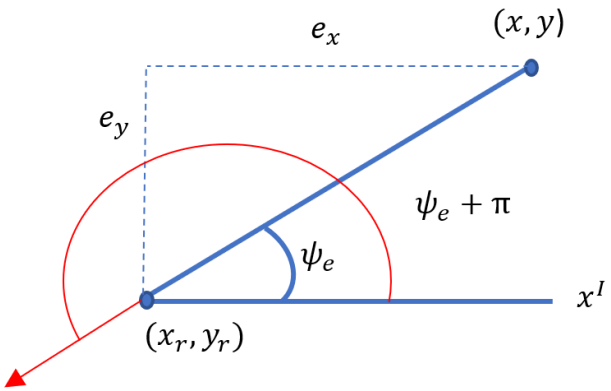

Figure 10.9: This figure describes the desired orientation based on the error angle ψ_e and the signs of the error components e_y and e_x.

The calculation of the orientation angle is dependent on the quadrant. When the actual position is in the third quadrant relatively to the reference point, the calculation of ψ_e gives the desired bit angle directly because $\arctan$ gives an angle between $[\frac{\pi}{2}, -\frac{\pi}{2}]$, as shown in Figure 10.10.

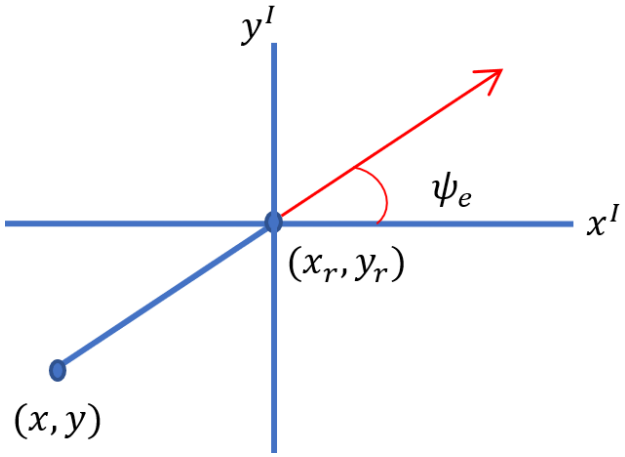

Figure 10.10: The error angle ψ_e describes the desired bit orientation around the z^b-axis, when the real position is in the third quadrant.

The general rule for calculating the desired bit rotation can be expressed as

1. quadrant: $\psi_r = \psi_e + \pi$
2. quadrant: $\psi_r = \psi_e$
3. quadrant: $\psi_r = \psi_e$
4. quadrant: $\psi_r = \psi_e + \pi$

To make the drill bit converge to the reference path as fast as possible, as well as minimizing stress on the drill pipe, the reference angle ψ_r is calculated according to Equation 10.9 and Equation 10.10. An example is if $\psi = \frac{\pi}{6}$, the reference angle should be $\psi_r = -\frac{\pi}{6}$ not $\psi_r = \frac{11\pi}{6}$.

$$n = \arg\min_{n \in \mathbb{Z}} \{|\psi - (\psi_r + 2\pi n)|\} \tag{10.9}$$

$$\psi_r = \psi_r + 2\pi n \tag{10.10}$$

10.5 Coordinate Frames

The system consists of three coordinate frames; the inertial frame, body frame and drill bit frame. The inertial frame $\{I\}$ is located with its origin at the point where the drill bit tags the rock. The x^I-axis of $\{I\}$ is pointing towards north while the z^I-axis is pointing down.
The body frame is centered at the IMU, and is representing the position and the orientation of the BHA. The z^b-axis is parallel with the BHA pointing downwards. The x_b-axis is pointing straight into the BHA. Initially, when drilling starts, the coordinate frame $\{b\}$ has the same position and orientation as the inertial frame I.

The drill bit is placed with a constant linear offset to where the IMU is placed. This frame is located at the center of the drill bit and has a z^{db}-axis that points in the same direction as the drill bit, and x^{db}-axis that points in the same direction as x^b.

10.5.1 Derivation of Position

When calculating the position of the drill bit, it is important to note that all of the position change is contained in the ROP. Since ROP also travels through the z-axis of the drill bit coordinate frame, it is possible to transform this vector into its inertial frame to find position equations for x, y and z. We get

$$\dot{\mathbf{p}}^{\mathbf{I}} = \mathbf{R}_b^I \mathbf{R}_{db}^b \dot{\mathbf{p}}^{db}, \tag{10.11}$$

where $\mathbf{R}_{db}^b$ is the rotation matrix from the drill bit to the IMU body, and $\mathbf{R}_b^I$ is the rotation matrix from the IMU body to inertial frame. As shown in section 10.5.2, the rotation from the drill bit to the IMU is given by

$$\mathbf{R}_{db}^b = \begin{bmatrix} \cos\alpha_{db}\cos\theta_{db} & -\sin\theta_{db} & \cos\theta_{db}\sin\alpha_{db} \\ \cos\alpha_{db}\sin\theta_{db} & \cos\theta_{db} & \sin\alpha_{db}\sin\theta_{db} \\ -\sin\alpha_{db} & 0 & \cos\alpha_{db} \end{bmatrix}, \tag{10.12}$$

while rotation from the IMU to inertial frame is just a simple ROLL-PITCH-YAW rotation given by the matrices introduced in section 5.4.2. When multiplying these ROLL-PITCH-YAW matrices together, it can be shown that

$$\mathbf{R}_b^I = \begin{bmatrix} \cos\psi\cos\theta & -\sin\phi\cos\psi + \cos\phi\sin\theta\sin\psi & \sin\phi\sin\psi + \cos\phi\sin\theta\cos\psi \\ \sin\phi\cos\theta & \cos\phi\cos\psi + \sin\phi\sin\theta\sin\psi & -\cos\phi\sin\psi + \sin\phi\sin\theta\cos\psi \\ -\sin\theta & \cos\theta\sin\psi & \cos\theta\cos\psi \end{bmatrix}, \tag{10.13}$$

where ϕ is roll, θ is pitch, and ψ is yaw. Calculating $\mathbf{R}_b^I \mathbf{R}_{db}^b$ gives a very big matrix. An important note here is that the ROP only moves in the z-axis of the drill bit coordinate frame. That means that

$$\dot{\mathbf{P}}^{db} = \begin{bmatrix} 0 \\ 0 \\ \dot{z}_{db} \end{bmatrix}, \tag{10.14}$$

which gives that the two first columns of the calculated matrix $\mathbf{R}_{db}^{I} = \mathbf{R}_{b}^{I}\mathbf{R}_{db}^{b}$ does not matter, as they get multiplied by zero. The ROP orientation in inertial frame is given by Equation 10.15.

$$ROP^{I} = \dot{z}^{db} \begin{bmatrix} \sin(\psi)^2 + \cos(\psi)^2 \sin(\theta) \\ \frac{1}{2}\sin(2\psi)(\sin(\theta) - 1) \\ \cos(psi)\cos(\theta) \end{bmatrix} \tag{10.15}$$

The angles ϕ, θ and ψ, are calculated as explained in section 5.4.3.

10.5.2 Drill Bit Location

Since the BHA is a rigid body during the entire drilling operation, it is easy to transform the position of the IMU to the position of the drill bit. The bent sub has a fixed angle α_{db} with respect to the vertical center line. When the bent sub is installed, it will also point in a random direction in the xy_b-plane, depending on how much torque is used. The angle which the bent sub is pointing with respect to the body frame is denoted θ_{db}. The position of the bit with respect to the body frame $\{b\}$ is denoted as $\mathbf{p}_{b,bit}^{b}$. This position is given by the matrix

$$\mathbf{T}_{b,bit}^{b} = \mathbf{T}_{1}^{b}\mathbf{T}_{2}^{1}\mathbf{T}_{3}^{2}\mathbf{T}_{4}^{3}\mathbf{T}_{db}^{4} \tag{10.16}$$

$$= \begin{bmatrix} 1 & 0 & 0 & s_1 \\ 0 & 1 & 0 & 0 \\ 0 & 0 & 1 & 0 \\ 0 & 0 & 0 & 1 \end{bmatrix} \begin{bmatrix} 1 & 0 & 0 & 0 \\ 0 & 1 & 0 & 0 \\ 0 & 0 & 1 & s_2 \\ 0 & 0 & 0 & 1 \end{bmatrix} \begin{bmatrix} \cos\theta_{db} & -\sin\theta_{db} & 0 & 0 \\ \sin\theta_{db} & \cos\theta_{db} & 0 & 0 \\ 0 & 0 & 1 & 0 \\ 0 & 0 & 0 & 1 \end{bmatrix}$$
$$\begin{bmatrix} \cos\alpha_{db} & 0 & \sin\alpha_{db} & 0 \\ 0 & 1 & 0 & 0 \\ -\sin\alpha_{db} & 0 & \cos\alpha_{db} & 0 \\ 0 & 0 & 0 & 1 \end{bmatrix} \begin{bmatrix} 1 & 0 & 0 & 0 \\ 0 & 1 & 0 & 0 \\ 0 & 0 & 1 & s_3 \\ 0 & 0 & 0 & 1 \end{bmatrix} \tag{10.17}$$

$$= \begin{bmatrix} \cos\alpha_{db}\cos\theta_{db} & -\sin\theta_{db} & \sin\alpha_{db}\cos\theta_{db} & s_1 + s_3\sin\alpha_{db}\cos\theta_{db} \\ \cos\alpha_{db}\sin\theta_{db} & \cos\theta_{db} & \sin\alpha_{db}\sin\theta_{db} & s_3\sin\alpha_{db}\sin\theta_{db} \\ -\sin\alpha_{db} & 0 & \cos\alpha_{db} & s_2 + s_3\cos\alpha_{db} \\ 0 & 0 & 0 & 1 \end{bmatrix} \tag{10.18}$$

where s_1 is the distance from the IMU to the center line along the x_b-axis, and s_2 is the distance from the IMU to the bent sub along the translated z_b-axis. s_3 is the distance from the bent sub to the drill bit along the translated and rotated z_b-axis. The position and orientation relations between the IMU and the drill bit can be seen in Figure 10.11.

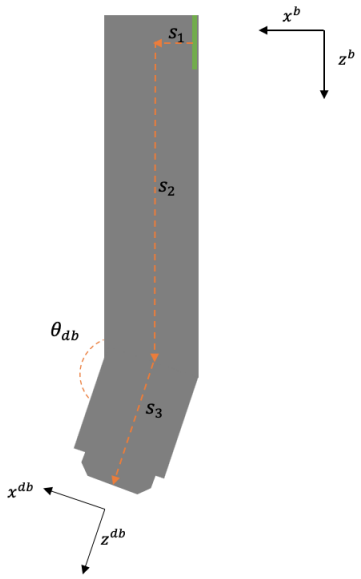

Figure 10.11: The relation between IMU and the drill bit. The center of the coordinate frames are located at the center of the IMU and the center of the tip of the drill bit.

Since only the orientation of the drill bit is needed, it is enough to use the upper left 3×3-matrix of the matrix shown in equation (10.18). It is assumed that $\theta_{db} = 0$, so the expected result of the relation in orientation would be a simple rotation

$$\mathbf{R}_{db}^{b} = \begin{bmatrix} \cos\alpha_{db} & 0 & \sin\alpha_{db} \\ 0 & 1 & 0 \\ -\sin\theta_{db} & 0 & \cos\theta_{db} \end{bmatrix} \tag{10.19}$$

10.5.3 Position and Orientation Estimation

After deriving the relation between the orientation of the drill bit given in the different frames, the position can be estimated using Euler's method. The position can be calculated as seen in Equation 10.20.

$$\mathbf{p}_k^I = \mathbf{p}_{k-1}^I + h\mathbf{R}_b^I\mathbf{R}_{db}^b\dot{\mathbf{p}}^{db} \tag{10.20}$$

The orientation of the drill bit can also be estimated. By aligning the x-axis of the body frame with the orientation of the drill bit, the angular velocities of the body frame can be expressed by the effect of the DLS

and the rotation of the drill bit. The angular velocity around the y^b-axis can be estimated by Equation 10.21, and the rotations around the z^b-axis can be estimated by differentiating the rotation of the top drive.

$$\omega_{y^b} = -\text{DLS} \cdot \text{ROP} \tag{10.21}$$

In Equation 10.21, DLS is given in rad/m and ROP is given in m/s. There will never be rotations around x^b-axis. The rotations in the inertial frame is given by Equation 10.22.

$$\omega_{Ib}^I = \omega_z(\dot{\psi}) + \mathbf{R}_z(\theta)\omega_y(\dot{\theta}) \tag{10.22}$$

The angles are given by

$$\mathbf{\Theta}_{Ib(k)}^I = \mathbf{\Theta}_{Ib(k-1)}^I + h\omega_{Ib}^I. \tag{10.23}$$

Since the different angles are defined in the different frames, it is important that the angles get integrated in the right frame. An example is the angle θ, which is the angle after rotating the inertial frame around z^I.

10.6 Simulation of Directional Control System

To be able to cope with the new Drillbotics 2020 challenge, a more sophisticated directional drilling controller is needed. For last year's challenge, the previous team relied heavily on the design of the rig to be able to drill along a path, provided before the competition. For the challenge in 2020, the path to be followed is generated by points given on the competition day. Compared to the last year's challenge, the path created by the provided points can have an azimuth change up to $\pm 15^\circ$.

In the simulation that has been done, it is assumed that the rotation of the TD is the same as the rotation of the BHA, and that the change in angle of the TD is saturated between every time step. To create a better model, further investigation is necessary. Currently, the rig is not running, so this will be done as soon as possible in phase two. The angle of the BHA will be calculated by using the measurements from the IMU as seen in section 5.4.3, and the estimated angles as explained in section 10.5.3. In the simulation script created in MATLAB, the focus has only been on directional control. This means that it is assumed constant torque and a constant WOB. The result of this is a constant ROP along the z^{db}-axis. The position and orientation is calculated as described in section 10.5.3.

The purpose of the simulation is to confirm the calculations on the relations between position and orientation in the different frames and to confirm that the control system works as expected. A simulation when the path is created using cubic spline interpolation and using the control system is explained earlier in this chapter and can be seen in Figure 10.12.

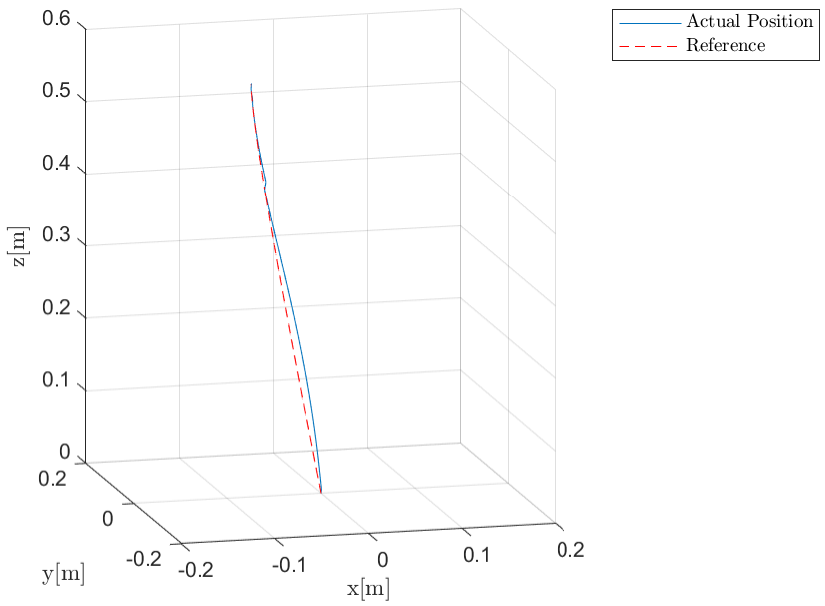

Figure 10.12: Simulation of directional drilling phase.

10.7 Last Years' Implementation of Control System - LabView

As the objective of the competition this year has been changed from having no azimuth change to having to control the azimuth, the position controller will be drastically changed. In addition, the WOB might be utilized for further directional control with regards to more inclination in the bent sub with higher WOB. The last year's control system will be presented, and possible changes that will have to be done.

10.7.1 Kalman Filter

To implement the Kalman filter in LabView, a built-in discrete Kalman filter has been used. The filter can be found in the control and simulation package in LabView. The built-in Kalman filter works as the presented theory in section 5.4.4. Instead of creating a Kalman filter from scratch, the built-in version has the advantage of being made for real-time operations. This means that it may run faster than creating a new Kalman filter. To use the filter, the state-space model, noise model, prior estimate, initial estimate, system output and input is fed into the block. It is possible to only filter noise with the Kalman filter if the physical model can not be translated into a state-space model. In this case, the input u is set to zero, and the estimated state $\hat{x}$ is based only on the measurements. The estimated state will then be used in both the WOB and the positional controller.

10.7.2 WOB PID Controller

By using the estimated states that are outputted from the Kalman filter, the team is now able to use this as feedback for WOB control. The previous year used a self-made PID controller with inspiration from the 2018 WOB controller. By creating an own PID controller, there is added more user-customizability, as for

example integral effect reset when there is WOB build up in soft rock formations. The last year's outer WOB controller is shown in Figure 10.13. As seen, it takes in the estimated WOB state, and compares it to the designated WOB set point, and feeds it to the inner PID controller, which is described in section 10.7.4. It is also added that the estimated state is set to zero if the set point is set to zero to avoid control around the zero level. The inner PID controller outputs a reference for the hoisting motor, but will first go through saturation such that the reference does not exceed the limits of the hoisting motor.

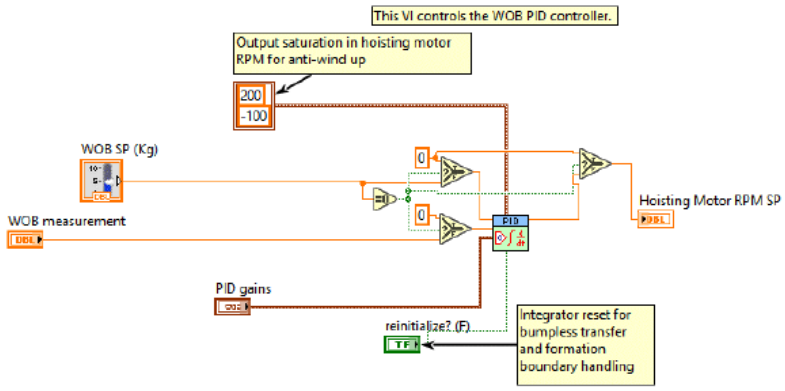

Figure 10.13: The outer WOB controller [37].

10.7.3 Position PI Controller

As mentioned in section 10.4.3, the team will calculate a reference top drive set point in order to drill a pre-calculated well path that goes through the points given in the competition. These set points will be compared to the state estimates of the IMU, which will produce a toolface orientation error, which then is fed into the inner PID controller. The saturations added to the output of the PID controller are used to make sure the set point of the top drive never exceeds its limits, although this will not be necessary unless the system fails due to the maximum azimuth change given in the competition. The outer position controller can be seen in Figure 10.14.

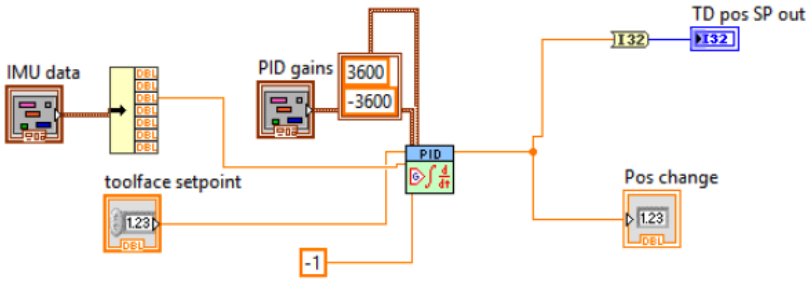

Figure 10.14: The outer position controller [37]

10.7.4 Inner PID Controller

The inner PID controller can be seen in Figure 10.15, and works by the same principles and equations that are presented in section 5.4.1

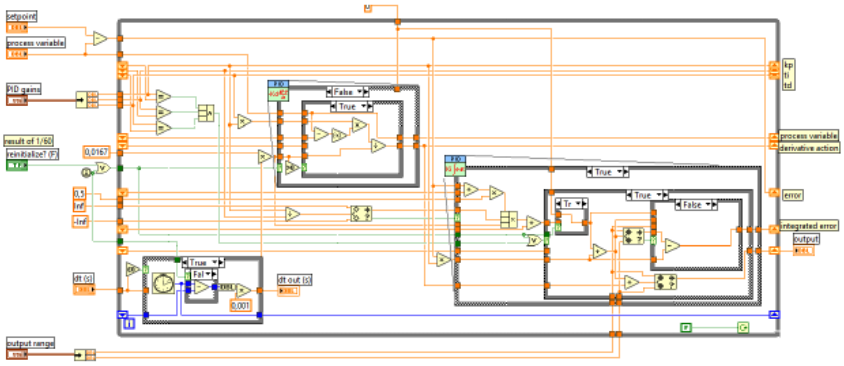

Figure 10.15: The outer position controller [37].

10.7.5 Safety Implementation

The safety implementation from the previous year consists of two parts, one being a medium safety layer and the other one being a critical safety layer. The medium safety layer is used to get the rig in a safe state, such that drilling may continue. An example of such a situation is if something goes wrong while in directional drilling mode. This might be exceedingly high WOB, in which the rotary system will be hoisted up and then continue the directional drilling after high enough RPM in the PDM is reached. If the system reaches any critical exceptions or exceeds a higher threshold than set in the medium safety later, the critical safety layer will initiate, immediately ending the drilling operation. The purpose of these two systems is so that the medium safety layer can catch the system moving to a bad state before it becomes critical, and then fix it. If this is not possible, termination will be handled by the critical safety layer. The two systems are presented in Figure 10.16.

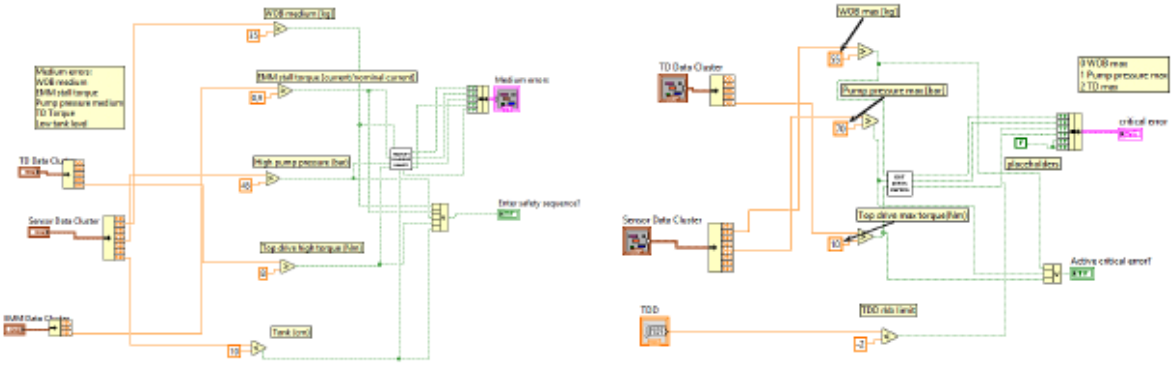

Figure 10.16: The medium safety layer and critical safety layer [37].

The thresholds used to enter the two different safety layers last year are presented in Table 10.3.

Table 10.3: Thresholds for medium and critical safety layer [37].

Medium Safety Layer		**Critical Safety Layer**	
Threshold	Unit	Threshold	Unit
$P_{wob} > 35$	[kg]	$P_{wob} > 55$	[kg]
$P_p > 45$	[bar]	$P_p > 70$	[bar]
$T_{TD} > 8$	[Nm]	$T_{TD} > 10$	[Nm]
$h_{tank} < 10$	[cm]	$h_{tank} < 5$	[cm]

where P_{wob} is the measured WOB, P_p is the measured pump pressure, T_{TD} is the TD torque, and h_{tank} is the height in the water tank.

11 Risk Analysis

Risk analysis is an important part of the project, and it should be discussed early to avoid unexpected obstacles and risks along the way. This process entails identifying and analyzing potential issues, considering their negative impact and the risk can be avoided or mitigated. Possible risks to identify are associated with Health, Safety and Environment (HSE), financial and time management. A risk analysis will be performed on the probable risks identified with the project to make the team members aware of these and if possible implement mitigating measures.

11.1 Protection Glass

The acrylic safety glass protects personnel around the rig during operation. During rig up/down it is lifted up and locked in place, this gives easy access to the components above Rotary Kelly Bushing (RKB). To lock it in place there is manually inserted one bolt on each side of the rail, and as shown in Figure 11.1 this is done in great height and the probability of unsuccessful placement is present.

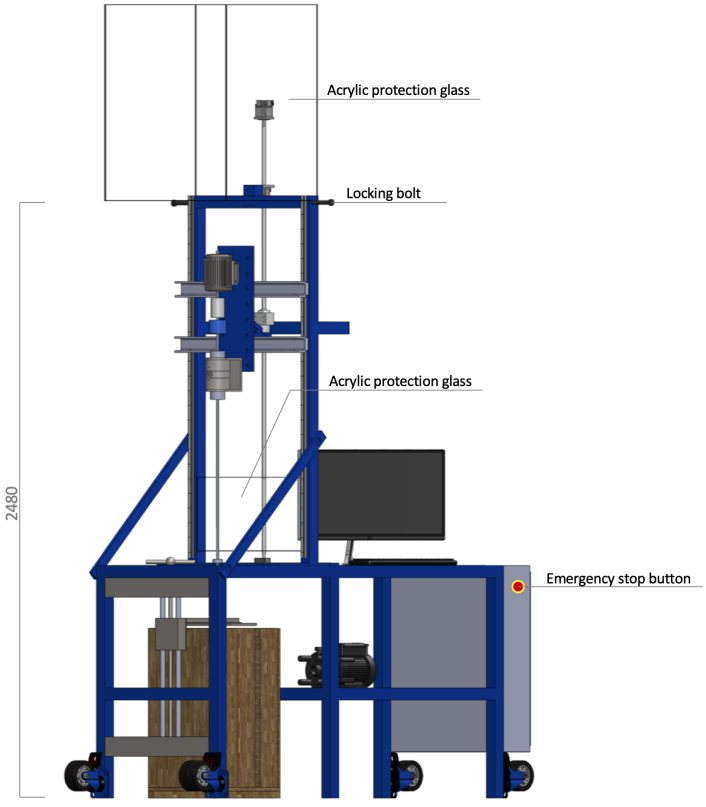

Figure 11.1: Rig in maintenance mode

Misplacement of the bolts may result in a downwards free fall of the protection glass. If any object is located beneath the moving glass and then hit, this may lead to severe damage especially for personnel.

After a thorough review of the operations the probability of unsuccessful bolt placement is very unlikely, but the consequence is rated as moderate. By using Table 3.1 the risk of free-falling protection glass is rated as Low medium, and therefore there is a need for risk-reducing measures.

11.2 Time Management

Throughout this project, it is important for the team to manage their time effectively. Therefore the team has implemented thorough time management, leading to improved efficiency and productivity. Specifically, this includes:

- **Setting goals.** They should be measurable and achievable. The team used the SMART method to set appropriate goals; **S**pecific, **M**easurable, **A**ttainable, **R**elevant, and **T**imely [55].
- **Prioritize wisely.** Tasks should be completed based on their importance and urgency.
- **Planer.** A planer is established with continuous deadlines, helping the team stay focused and be efficient. Also, the planer makes the team plan ahead, granting each engineering challenge a decent amount of time.
- **Structure.** It is important to maintain structure long-term in regards to the final deadlines from the Drillbotics© committee. Also, the team must be well structured in regards to logistics.

Even though the team manages their time effectively, there are risks related to the manufacturer in terms of production time and delivery. The team must plan accordingly and order necessary parts in a timely manner, to avoid challenges related to delays.

12 Finance

The 2019 Drillbotics© Guidelines states, as previous years, that all costs related to the rig and materials shall not exceed 10,000 USD [3]. As an engineer in a project team, there are not only technical parts of projects they have to excel at, managing project expenses and maintain control of the budget is an essential part of it all. With this competition, each student will learn and develop in many different segments of the upcoming work-life that this project offers. One of those is the ability to utilize and make the best out of the limited resources you have - which in this case is 10,000 USD. This budget is excluded from the tools and equipment the team already is in possession of from the last year's competition and will be used for progression, new equipment and improvements being done on this year's rig.

12.1 Budget

This budget is to be used on rock samples for test drilling, computer equipment, pieces for the rig and tools. In Table 12.1, all expected costs related to the project are listed, with their expected prices i NOK (Norwegian Kroner). These costs will be converted to USD with the currency exchange rate as of December, 16th, which currently is: USD 1 = 8.99 NOK. The VAT in Norway is 25%, in addition to add a rough shipping cost estimate of 10%. So given the cost estimate is a total of USD 3518, the total price of the expenses, including VAT will be 1.25 times the total price, which ends up being USD 4398.

Table 12.1: Estimated cost of items to be acquired for the drilling rig

Item describtion	Price per item (NOK)	No. of items	Total Cost (NOK)
Computer Screen	5000	1	5000
Computer	10000	1	10000
Drill pipes	80	0	0
Plastic for 3D-printer	200	2	400
EMM and Gear	8000	1	8000
Sensor Card	100	1	100
O-rings and packers	890	1	8130
Total Cost (NOK)			**31630**
Total Cost (USD)			**3518**

12.2 Funding

The rules state that the project is limited to 10,000 USD, but the guidelines also state that it is allowed to contact external resources and ask them about sponsorship and support in the form of "gifts" and/or knowledge and guidance sharing.

Through contacts, this year's team has been so privileged to cover the full budget of 10,000 USD by the collaboration between Norwegian University of Science and Technology (NTNU) and BRU21.

Through a sponsorship between the Department of Geoscience and Petroleum (IGP) and an oil and gas company, the team has also received a 3D-printer that will be utilized for the design and production of the Positive Displacement Motor (PDM) used in the competition.

As mentioned in section 7.3.5, the team plans to design their own drill bit. Last year's team was able to establish a partnership with Lyng Drilling where they got assistance from experts regarding the design of the bit. The plan this year is to accomplish the same, as the drilling rig needs a new bit corresponding to the updated guidelines of increased diameter.

12.3 Transport Expenses

The competition will most likely be held in Germany, which means the team along with the rig, in addition to some of the professors.

The drilling rig itself needs to get transported all the way from Norway to Germany, in addition to getting it through the customs. This has been estimated to cost around 30 000 NOK.

The team consisting of five members along with four professors will be accounted for that will travel to Germany and are in need of ticket coverage. This will be set to cost around 1500 NOK per person.

The sum for covering the travel expenses ends up at a total of **43 500 NOK**.

13 Conclusion

With this year's Drillbotics© competition continuing its focus on improving the development of drilling automation, the Norwegian University of Science and Technology (NTNU) team's main focus has been to develop a sustainable mechanical design capable of directional drilling. After careful consideration, Positive Displacement Motor (PDM) was chosen as the primary solution, with the intention of adjusting and optimizing last year's design. To manufacture and test the PDM-design, a 3D printer is available for the team to use. With the increase in bit size, the team seeks to utilize the extra space acquiring enough torque and Revolutions per Minute (RPM) to drill through the rock sample. The team has decided to have a back-up solution as circumstances allow for it to quickly be implemented, this solution is Electrical Miniature Motor (EMM).

Building direction shall be done using an adjustable sub, as it is more sustainable in regards to uncertainties associated with the dog-leg severity required to hit the targets given by the committee. The team seeks to design their own drilling bit, in collaboration with Lyng Drilling. As for the mechanical design of the rig, only minor modifications to improve safety will be done. Besides that, the rig has been proven to be well designed and sustainable for the wanted operations.

In order for the drilling operation to be executed autonomously the team will use sensors to gather real-time data that will be used in a closed-loop feedback control system. The main parts needed to be controlled is Weight on Bit (WOB) and drill bit position to achieve a well path that goes through the competition points. Wired communication is used to achieve feedback from the sensors downhole to the topside computer. Different phases of the control system is defined as states in a state machine, which are used during different parts of the operation. The states are primarily separated into a vertical and directional drilling phase. To ensure safe operation, the system will transition into a safety layer in the event of any measurements exceeding the defined safety thresholds.

14 Future Work

As Phase I comes to an end, the focus switches over to Phase II and planning towards the international competition in May/June of next year. The same time management, as described in section 11.2, will be practiced by the team to reach the finish line. Prioritizing will be important, starting with identifying tasks that other work is dependent on; these should be tackled first. Rig adjustments are therefore of highest priority, thus most other tasks depend on it and processes including third-parties will be handled early on as the team expects delays. Rock samples to test drill must be ordered early in the semester, the same goes for designing the drill bit in collaboration with Lyng Drilling. Fortunately, though the team already had aluminum Drill pipe (DP) available as well as the 3D printer to be used for creating the Positive Displacement Motor (PDM).

For the primary solution that is a PDM a new improved design, based on last year's findings, will be made using Solidworks and 3D printed. As for stabilizers and sensor sub, the design will be adjusted and the parts will be ordered. Designing of the adjustable housing should be done early in the semester so it can be manufactured and used for testing drilling.

Parts for the Electrical Miniature Motor (EMM) will be ordered consecutively and the team plan on test drill early in the semester, as presented in Table 14.1.

Table 14.1: Tentative schedule for Phase II

	January	**February**	**March**	**April**	**May**
Obtaining necessary equipment					
Finalize improvements on rig					
Implement Control System					
Finalize improvements on EMM and test drilling					
Design and manufacturing PDM					
Test drill with PDM and make adjustments					
Drill with finalized PDM design					
Drillbotics© Competition					

References

Literature

[1] United States Department of Labor. *Safety Hazards Associated with Oil and Gas Extraction Activities*. URL: https://www.osha.gov/SLTC/oilgaswelldrilling/safetyhazards.html.

[2] M. Arnø et al. *Design and Implementation of a Miniature Autonomous Drilling Rig for Drillbotics 2018*. Society of Petroleum Engineers, 2019. DOI: https://doi.org/10.2118/194226-MS.

[3] Society of Petroleum Engineers (SPE) and Drilling Systems Automation Technical Section (DSATS), eds. *Drillbotics™ Guidelines*. Sept. 20, 2019. URL: https://drillbotics.com/download/guidelines/2020-Drillbotics-Guidelines.pdf.

[4] B. Brechan et al. *Drilling, Completion, Intervention and P&A - design and operations*. Department of Geosciense and Petroleum, 2017.

[5] PetroWiki, ed. *Directional Deviation Tools*. Nov. 12, 2019. URL: https://petrowiki.org/Directional_deviation_tools.

[6] G. R. Samuel and S. Miska. *Analytical Study of the Performance of Positive Displacement Motor (PDM): Modelling for Incompressible Fluid*. Society of Petroleum Engineers, 1997. DOI: https://doi.org/10.2118/39026-MS.

[7] H. R. Motahhari, G. Hareland, J. A. James, et al. "Improved drilling efficiency technique using integrated PDM and PDC bit parameters". In: *Journal of Canadian Petroleum Technology* 49.10 (2010), pp. 45–52. DOI: https://doi.org/10.2118/141651-PA.

[9] K. T. Lowe. *Selection and Integration of Positive Displacement Motors into Directional Drilling Systems*. University of Tennessee Honors Thesis Project, 2004.

[10] Schlumberger, ed. *PowerPak - Steerable Motor Handbook*. Dec. 4, 2019. URL: https://www.slb.com/-/media/files/drilling/brochure/powerpak-handbook-br.ashx.

[11] J. J. Azar and G. Robello Samuel. *Drilling Engineering*. PennWell Books, 2007.

[12] B. Brechan, S. Hovda, and P. Skalle. *Introduction to Drilling Engineering*. Department of Geoscience and Petroleum, Jan. 30, 2017.

[13] MechaniCalc, ed. *Column Buckling*. Nov. 1, 2019. URL: https://mechanicalc.com/reference/column-buckling.

[14] A. J. Adams et al. *The Barlow Equation for Tubular Burst: A Muddled History*. Society of Petroleum Engineers, Mar. 6, 2018. DOI: https://doi.org/10.2118/189681-MS.

[15] A. T. Bourgoyne Jr et al. *Applied Drilling Engineering*. 2nd ed. Society of Petroleum Engineers, 1991.

[16] Fridtjov Irgens. *Fasthetslære*. 7th ed. Tapir Akademisk Forlag, 2006.

[17] A. Austin and J.H. Swannell. “Stresses in a pipe bend of oval cross-section and varying wall thickness loaded by internal pressure”. In: *International Journal of Pressure Vessels and Piping* 7.3 (1979), pp. 167–182. ISSN: 0308-0161. DOI: https://doi.org/10.1016/0308-0161(79)90016-4. URL: http://www.sciencedirect.com/science/article/pii/0308016179900164.

[18] J.G. Balchen, T. Andresen, and B.A Foss. *Reguleringsteknikk*. Department of Engineering Cybernetics, 2016.

[21] R.W. Beard and T.W. McLain. *Small Unmanned Aircraft. Theory and Practice*. Princeton University Press, 2012.

[22] O Egeland and J.T. Gravdahl. *Modeling and Simulation for Automatic Control*. Marine Cybernetics, 2003.

[23] T.I. Fossen. *Handbook of Marine Craft Hydrodynamics and Motion Control*. John Wiley & Sons, 2011.

[25] MathWorks, ed. *Understanding Kalman Filters*. Nov. 12, 2019. URL: https://www.mathworks.com/videos/series/understanding-kalman-filters.html.

[27] Jacques F. Smuts. *Ziegler-Nichols versus Cohen-Coon for PID tuning*. URL: https://blog.opticontrols.com/archives/383.

[29] A.M. Kvarving. *Natural cubic splines*. Ed. by Department of Mathematical Sciences Norwegian University of Science and Technology. URL: https://www.math.ntnu.no/emner/TMA4215/2008h/cubicsplines.pdf.

[30] Y. A. Çengel and J. M. Cimbala. *Fluid Mechanics: Fundamentals and Applications*. 3rd ed. McGraw-Hill, 2014.

[31] EngineeringToolBox, ed. *Reynolds Number*. Nov. 18, 2019. URL: https://www.engineeringtoolbox.com/reynolds-number-d_237.html.

[32] B. S. Aadnøy. *Modern Well Design*. 2nd ed. CRC Press, 2011.

[33] Kruge, ed. *Elastisitetsmodul og flytegrense R_e for stål (Temperaturavhengig)*. Nov. 19, 2019. URL: https://www.kruge.no/mediabank/store/2/2586/Elastisitetsmodul-og-flytegrense-Re-for-stAxl-Temperaturavhengig.pdf.

[34] ASM - Aerospace Specifications Metals Inc., ed. *ASM Material Data Sheet*. Nov. 26, 2019. URL: http://asm.matweb.com/search/SpecificMaterial.asp?bassnum=MA6061T6.

[35] H. E. Helle, M. U. Azam, and J. M. Montoza. “Design and Implementation of an Autonomous Miniature Drilling Rig for Directional Drilling”. Thesis. Department of Geoscience and Petroleum, 2019.

[36] Cat Pumps, ed. *Data Sheet - 5CP Plunger Pumps*. Dec. 5, 2019. URL: http://www.catpumps.com/products/pdfs/5CP6120_E.pdf.

[37] M. B. Nåmdal. “Design and Implementation of an Autonomous Miniature Drilling Rig for Directional Drilling”. Thesis. Department of Engineering Cybernetics, 2019.

[38] Lenze. *Lenze AC Motor*. URL: https://www.lenze.com/en-no/products/motors/ac-motors-inverter-operation/ie3-m550-p-ac-motors/.

[39] Lenze. *Lenze Motor and Gearbox*. URL: https://www.lenze.com/fileadmin/lenze/documents/en/catalogue/CAT_GST_GFL_MF_15593808_en_GB.pdf.

[40] Lenze. *Lenze Frequency Inverter*. URL: https://www.lenze.com/en-no/products/inverters/control-cabinet-installation/8400-topline-frequency-inverters/.

[41] AEP Transducers. *TC4-AMP AEP Transducer*. URL: http://www.aeptransducers.com/force-transducers/104-tc4-amp.html.

[42] Schneider Electric. *Top Drive Servo Motor BCH2MM1523CA6C*. URL: https://docs-emea.rs-online.com/webdocs/14d7/0900766b814d71da.pdf.

[43] Schneider Electric. *Top Drive Servo Drive LXM28AU15M3X*. URL: https://www.se.com/ww/en/product/LXM28AU15M3X/motion-servo-drive---lexium-28---single-and-three-phase-200...230-v---1.5-kw/.

[44] Senring, ed. *Electrical Swivel SNG012-12 by Senring*. Dec. 9, 2019. URL: https://www.senring.com/high-speed-slip-ring/g012-12.html.

[45] Omnetics, ed. *Nano 360 Plastic connectors*. Dec. 9, 2019. URL: https://www.omnetics.com/products/micro-and-nano-circulars/nano-360-circulars-plastic#1803-tab2.

[46] InvenSense, ed. *ICM-20948 IMU from TDK InvenSense*. Dec. 9, 2019. URL: https://www.invensense.com/wp-content/uploads/2016/06/DS-000189-ICM-20948-v1.3.pdf.

[47] Silicon Labs, ed. *EFM32 Gecko microcontroller*. Dec. 9, 2019. URL: https://www.silabs.com/documents/public/data-sheets/efm32g-datasheet.pdf.

[48] Wikipedia, ed. *I2C communication*. Dec. 9, 2019. URL: https://en.wikipedia.org/wiki/I%C2%B2C.

[49] Circuit Basics, ed. *UART Communication*. Dec. 9, 2019. URL: http://www.circuitbasics.com/basics-uart-communication/.

[50] RS Pro, ed. *24V NC solenoid valve by RS Pro*. Dec. 9, 2019. URL: https://uk.rs-online.com/web/p/solenoid-valves/1440801/.

[51] Omron, ed. *P2RF.05.S solid state relay by Omron*. Dec. 9, 2019. URL: https://no.rs-online.com/web/p/products/7948230/?grossPrice=Y&cm_mmc=NO-PPC-DS3A-_-google-_-3_NO_NO_Relay+Sockets_Omron_Exact-_-Omron+-+Relay+Sockets+-+7948230-_-p2rf05s&matchtype=e&kwd-306523915131&gclid=CjwKCAjw0ZfoBRB4EiwASUMdYWnB0LVI-fC-hJOhafG4ENo2YJhZ_CqipyiAqMOV-FimtZQGwMWxKxoCC5EQAvD_BwE&gclsrc=aw.ds.

[52] Cat Pumps, ed. *5CP6120 pump by Cat Pumps*. Dec. 9, 2019. URL: http://www.catpumps.com//products/pdfs/5CP6120_B.pdf.

[53] Aplisens A.S., ed. *PCE-28 pressure gauge by Aplisens*. Dec. 9, 2019. URL: https://www.aplisens.com/pc-28.html.

[54] Analog Dialogue Ian Beavers, ed. *Gyroscope drift*. Dec. 9, 2019. URL: https://www.analog.com/en/analog-dialogue/raqs/raq-issue-139.html#.

[55] CFI™, ed. *Time Management*. Dec. 5, 2019. URL: https://corporatefinanceinstitute.com/resources/careers/soft-skills/time-management-list-tips/.

[56] T. C. Nguyen, E. Al-Safran, and V. Nguyen. *Theoretical modeling of Positive Displacement Motors performance*. Volume 166. 2018.

[57] PetroWiki, ed. *Directional Drilling*. Nov. 12, 2019. URL: https://petrowiki.org/PEH:Directional_Drilling.

[58] PetroWiki, ed. *Cuttings transport*. Nov. 18, 2019. URL: https://petrowiki.org/Cuttings_transport.

[59] PetroWiki, ed. *Drillpipe failures*. Dec. 3, 2019. URL: https://petrowiki.org/Drillpipe_failures.

Figures

[8] Micon Downhole Tools, ed. *Positive Displacement Motors (PDM)*. Dec. 3, 2019. URL: https://micon-drilling.de/Download/Catalog_PDM_EN.pdf.

[19] Wikipedia, ed. *PID Controller figure*. Dec. 6, 2019. URL: https://en.wikipedia.org/wiki/PID_controller#/media/File:PID_en.svg.

[20] National Instruments, ed. *PID Response*. Dec. 6, 2019. URL: https://www.ni.com/en-no/innovations/white-papers/06/pid-theory-explained.html.

[24] MathWorks, ed. *Understanding Kalman Filters*. Nov. 19, 2019. URL: https://www.mathworks.com/videos/series/understanding-kalman-filters.html.

[26] S3 Data Science, ed. *Euler Stability*. Dec. 6, 2019. URL: http://www.s3datascience.com/z-s3-data/educating-the-user/a-brief-history-of-calculation.

[28] Control Engineering, ed. *Cohen Coon Process Gain*. Dec. 6, 2019. URL: https://www.controleng.com/articles/tuning-pid-control-loops-for-fast-response/.

Appendix

A Summary of Equation

Table A.2: Summary of equations

Calculating	Equation	Result	Reference
Dogleg Severity	$DLS = \frac{\phi}{CL}$	$43.4°/m$	Equation 5.1
Cource Length	$CL = \frac{RC\pi(I_2 - I_1)}{180}$	$52.1cm$	Equation 5.2
Dogleg Severity based on BHA	$DLS = \frac{2\,\theta}{L_1 + L_2}$	$\theta = 5.1°$	Equation 5.4
Ideal PDM RPM	$RPM = \frac{q}{q_0}$	Figure 7.24b	Equation 5.6
Ideal PDM Torque	$T = 1.256 \cdot 3.066 q_o \Delta P_{pdm}$	Figure 7.24a	Equation 5.7
Maximum Allowable WOB	$F_{max\ WOB} = \sigma_{cr} A$	Table 6.2	Equation 5.14
Barlow's burst equation	$P_{burst} = 2\frac{0.875\sigma_{yield}t}{dSF}$	$210 \cdot 10^5 Pa$	Equation 5.15
Twist-off Torque	$T_{max} = \tau_{max}\frac{\pi}{16}(OD^2 - ID^2)(OD + ID)$	Table 6.3	Equation 5.16
Axial Stress from Pressure	$\sigma_z^p = \frac{(\frac{ID}{OD})^2}{1-(\frac{ID}{OD})^2} p$	Figure 6.2	Equation 5.20
Axial Stress from WOB	$\sigma_z^{WOB} = \frac{WOB}{A_{cs}}$	Figure 6.2	Equation 5.21
Axial Stress from Pipe Bending	$\sigma_z^b = \frac{E}{RC} y$	Figure 6.3	Equation 5.22
Laminar Slip Velocity	$v_{sl} = \frac{d_s^2 g(\rho_s - \rho_f)}{18\mu_f}$	Table 6.5	Equation 5.68
Slip Velocity	$v_{sl} = \sqrt{\frac{4(\rho_s - \rho_f) g d_s^2}{3 f \rho_f}}$	Table 6.5	Equation 5.69
Flow Rate	$q = A_{cs}\frac{v_{sl}}{1 - R_t}$	Table 6.5	Equation 5.70
Pipe Pressure Losses	$\Delta P_i = f_i \frac{L_i}{d_{h,i}} \frac{\rho_f v_i^2}{2}$	Table 6.6	Equation 5.71
Bit Nozzle Pressure Loss	$\Delta P_{nozzle} = \frac{\rho_f q^2}{2 A_n^2 C_d^2}$	Table 6.6	Equation 5.75

B Cuttings Transportation Derivation

In order to get efficient removal of cuttings from the wellbore, the slip velocity and gravitational force acting of the cutting particle has to be overcome by the buoyant force and viscous drag force caused by the drilling fluid.

$$W = -\rho_s \frac{\pi}{6} d_s^3 g \tag{B.1}$$

$$F_b = \rho_f \frac{\pi}{6} d_s^3 g \tag{B.2}$$

The slip velocity of the cutting particle is caused by it's weight given by Equation B.1 where $W[N]$ is the weight force, $\rho_s[kg/m^3]$ is the solid particle density and d_s is the solid particles diameter. Equation B.2 calculates the buoyant force acting on the particle, where $F_b[N]$ is the buoyant force and $\rho_f[kg/m^3]$ is the fluid density.

The viscous drag force is given as [58]:

$$F_d = 3\pi\mu_f d_s v_{sl} \tag{B.3}$$

where $\mu[Pas]$ is the fluid viscosity and $v_{sl}[m/s]$ is the slip velocity. Newton's first law of motion gives:

$$\sum F = 0 = W + F_b + F_d \tag{B.4}$$

Solving Equation B.4 gives the slip velocity of cutting particles:

$$v_{sl} = \frac{d_s^2 g(\rho_s - \rho_f)}{18\mu_f} \tag{B.5}$$

Equation 5.68 is also known as "Stokes' law" and is only valid for Newtonian fluids in a laminar flow regime, acceptable for Reynolds number below 0.1 [15]. Flow regime with $Re > 0.1$ has the shear drag force given as [4]:

$$F_d = f \frac{\pi}{8} d_s \rho_f v_{sl}^2 \tag{B.6}$$

f is an empirical friction factor, in Figure B.1 expressed as a function of Reynolds number and sphericity, $\Psi = 1$ will be used as we assume spherical cuttings. The Reynolds number can be estimated by using Equation B.7, using the estimated slip velocity from Equation B.5.

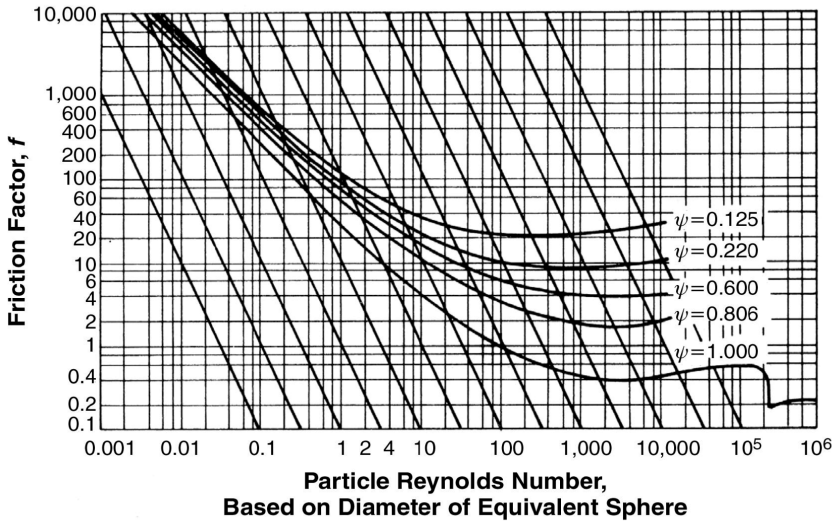

Figure B.1: Relationship between f and Re for settling particles in Newtonian fluids [15]

$$Re = \frac{\rho_f v_{sl} d_h}{\mu_f} \tag{B.7}$$

where d_h is the hydraulic diameter, for flow in annulus area given as:

$$d_h = OD_{hole} - OD_{DP/BHA} \tag{B.8}$$

and for flow inside pipe:

$$d_h = ID_{DP/BHA} \tag{B.9}$$

Using Equation B.4 but using Equation B.6 as F_d, the slip velocity of a particle in all flow regimes can be estimated as:

$$v_{sl} = \sqrt{\frac{4(\rho_s - \rho_f) g d_s^2}{3 f \rho_f}} \tag{B.10}$$

C MATLAB scripts

C.1 Wellpath

```
figure(1)
run cube
set(findall(gca, 'Type', 'Line'),'LineWidth',1.25);
set(gca,'FontSize',12)
X = [0 0];
Y = [0 0];
Z = [0 4];
```

```
n = 4000;
phi=linspace( pi*15/180,pi*15/180,n);
z = linspace(4,24,n);
tm = 30*pi/180;
xmax = sqrt((1 cos(tm))/((1+cos(tm))))*(z(end) z(1));
RC = ((z(end) z(1))^2+xmax^2)/(2*xmax);
r = RC*(1 sqrt(1 ((z z(1))/RC).^2));
plot3(X,Y,Z,'b')
set(gca,'Zdir','reverse')
hold on
for i = 1:n
    x=r(i)*cos(phi);
    y=r(i)*sin(phi);
    plot3(x,y,zeros(1,numel(x))+z(i),'r')
end
xlim([ 12 12])
ylim([ 6 6])
zlim([0 24])
set(findall(gca, 'Type', 'Line'),'LineWidth',1.25);
view(40,40)
xticks([ 12 0 xmax 12])
xticklabels({' 12','0',num2str(max(x),3),'12'})
yticks([ 6 0 max(y) 6])
yticklabels({' 6','0',num2str(max(y),3),'6'})
zticks([0 4 24])
title('Wellpath')
disp(xmax)
disp(RC*.0254)
disp(tm*180/pi)
teta = linspace(0,26.97*pi/180,n);
x = RC * cos(teta)   RC;
z = RC * sin(teta) + 4;
plot3( x,x*0,z,'r')
```

C.2 Buckling

```
function [] = Buckling(E, ys)
%% Parameters
n = 990;
```

```
Conv = 0.0254;                          % Converting in to meter
t = 0.049 * Conv;                       % [m]
OD = 3/8 * Conv;                        % [m]
ID = 3/8 * Conv    2 * t;               % [m]
L = linspace(0.01,1,n);                 % [m]       Length DP, Length
    rock sample, Length Curvature, Remaining length
K = [0.5, 1/sqrt(2), 0.9];              % Effective length factor, K



%% Calculations
I = pi/64 * (OD^4    ID^4);             % [m2]      Second Moment of
    Area, I
A = pi/4 * (OD^2  ID^2);                % [m2]      Cross Sectional
    Area, A
rg = sqrt(I/A);                         % [m]       Radius of gyration,
     rg

% Slenderness Ratio
SR = zeros(1,n);
for j = 1:n
    SR(j) = L(j)/rg;
end

% Critical Slenderness Ratio
SR_cr = zeros(1,length(K));
for j = 1:length(K)
     SR_cr(j) = sqrt((2*pi^2*E)/(K(j)^2*ys));
end

% Johnsons formula, sigma_cr
S_cr = zeros(n,length(K));
for j = 1:length(K)
     for k = 1:n
          S_cr (k,j) = ys    ((ys * K(j) * L(k))/(2 * pi * rg))^2 * 1/E;
     end

end

```

```
39
40 SE_cr = zeros(n,length(K));
41 for j = 1: length(K)
42     for k = 1:n
43         SE_cr(k,j) = pi^2*E/((K(j)*L(k)/rg))^2;
44     end
45 end
46
47 % Max WOB with different K values
48 WOB_max = zeros(n,length(K));
49 for j = 1:length(K)
50     for k = 1:n
51         if SR(k) <= SR_cr(j)
52             WOB_max(k,j) = S_cr(k,j)*A/1000;
53         else
54             WOB_max(k,j) = SE_cr(k,j)*A/1000;
55         end
56     end
57 end
58
59 %% Plot
60 plot(L, WOB_max(:,1), L, WOB_max(:,2), L, WOB_max(:,3));
61 set(gca,'FontSize',12);
62 xlabel('Unsupported length of pipe [m]', 'fontsize', 14)
63 ylabel('Maximum WOB [kN]', 'fontsize', 14)
64 title('Maximum allowable WOB vs Length', 'fontsize', 14)
65 legend('K=0.5', 'K=0.9', 'K=1/sqrt(2)')
66 ylim([0 10])
67
68 grid on
69
70 end
```

C.3 Bending Stress

```
1 n    = 100;
2 sy   = 196e6;                    %Yield strength[Pa]
3 E    = 200e9;                    %Youngs modulus[Pa]
4 %                  Calculations
```

```
OD  = 3/8*.0254;                    %[m]
t   = 0.049*.0254;                  %[m]
ID  = OD   (2*t);                   %[m]
RC  = linspace(0,5,n);              %m
WOB = linspace(0,500,n);            %N
p   = linspace(0,100,n);            %bar
A   = pi/4*(OD^2 ID^2);
y   = OD/2;
I   = pi/64*(OD^4 ID^4);
M   = E*I./RC;
szb = M*y/I;
szw = WOB/A;
szp = ((ID/OD)^2)/(1 (ID/OD)^2)*p*10^5;
%                   Plots
figure(1)
a=axes('units','normalized','position',[.1 .35 .8 .6],'xlim',[0 5],'
    color','red','xtick',0:0.5:5);
plot(RC,szb,'k ')
hold on
plot(p/20,szp,'b ')
plot(WOB/100,szw,'r ')
ylim([1e5 1e10])
set(gca,'FontSize',12,'YScale', 'log')
set(findall(gca, 'Type', 'Line'),'LineWidth',1.25);
legend('\sigma_z^b','\sigma_z^p','\sigma_z^{WOB}','fontsize'...
     ,12,'location','southeast')
ylabel('Stress [Pa]','fontsize',14)
grid on
set(gca,'xcolor','k')
xlabel(a,'Radius of Curvature[m]','Color','k','fontsize',14)
b=axes('units','normalized','position',[.1 .21 .8 0.000001],'xlim',[0
    50],'color','b', 'xtick',0:10:100);
set(gca,'xcolor','b')
xlabel(b,'Pressure[bar]','Color','b','fontsize',14);
c=axes('units','normalized','position',[.1 .10 .8 0.000001],'xlim',[0
    500],'color','r', 'xtick',0:50:500);
set(gca,'xcolor','r')
xlabel(c,'WOB','Color','r','fontsize',14);
figure(2)
```

```
plot(RC,szb,'r ',RC,szb*0+sy,'k ')
xlabel('Radius of Curvature[m]','fontsize',14)
ylabel('Stress [Pa]','fontsize',14)
title('Bending stress vs. Radius of Curvature','fontsize',14)
legend('\sigma_z^b','\sigma_{ys}','fontsize',12,'location','northeast')
set(gca,'FontSize',12)
set(findall(gca, 'Type', 'Line'),'LineWidth',1.25);
grid on
ylim([0 10e8])
```

C.4 Simulation Script

```

close all
clear all

% Sample point
a = [0, 0.05, 0.1];
b = [0, 0.03, 0.1];
c = [0,0.3,0.6];
t = [1,1.7,3]; % Assumed time stamp
% Apply interpolation for each x,y and z
tt = linspace(t(1),t(end),501);
xx = interp1(t,a,tt,'spline');
yy = interp1(t,b,tt,'spline');
zz = interp1(t,c,tt,'spline');
plot3(a,b,c,"o");
hold on
grid on
plot3(xx,yy,zz);
xlabel("x[m]","interpreter","latex")
ylabel("y[m]","interpreter","latex")
zlabel("z[m]","interpreter","latex")
%% constants
s1 = 1; s2 = 1; s3 = 1; alpha_db = pi/36; theta_db = 0; phi = 0; theta
    = 0; psi = 0; DLS = 10.87/0.3048*pi/180;phi_dot = 0; %rad/meter
theta_dot = 0; phi_2 = 0;
kp = 10;
ROP = [
```

```
27      0;
28      0;
29      0.1;
30      ];
31
32  h = 0.05;
33  T = 50;
34  t = linspace(0,T,T/h);
35
36  X_s = zeros(3,T/h);
37  p0 = [
38      0;
39      0;
40      0
41      ];
42
43  thetas = zeros(T/h);
44  psis = zeros(T/h);
45  phis = zeros(T/h);
46  %% Rotation drillbit to IMU
47  db1 = [
48      1 0 0 s1;
49      0 1 0 0;
50      0 0 1 0;
51      0 0 0 1;
52      ];
53  db2  = [
54      1 0 0 0;
55      0 1 0 0;
56      0 0 1 s2;
57      0 0 0 1
58      ];
59  db3 = [
60      cos(theta_db)  sin(theta_db) 0 0;
61      sin(theta_db) cos(theta_db) 0 0;
62      0 0 1 0;
63      0 0 0 1
64      ];
65  db4 = [
```

```
    cos(alpha_db) 0 sin(alpha_db) 0;
    0 1 0 0;
     sin(alpha_db) 0 cos(alpha_db) 0;
    0 0 0 1
    ];
db5 = [
    1 0 0 0;
    0 1 0 0;
    0 0 1 s3;
    0 0 0 1
    ];


T_b_db = db1*db2*db3*db4*db5;
R_b_db = T_b_db(1:3,1:3);
%% Referance path
X_r = [xx; yy; zz];
%% Simulation using eulers method

X_s(:,1) = p0;
ref = zeros(T/h);
lookAhead = 0;
saturation = 1000;

for i = 1:T/h

    [d, ix ] = min( abs(X_r(3,:)    X_s(3,i)));
    x_r = X_r(1,ix);
    y_r = X_r(2,ix);
    x_s = X_s(1,i);
    y_s = X_s(2,i);
    dx = x_r    x_s;
    dy = y_r    y_s;

    if dx  == 0 && dy == 0
        [d, ix ] = min( abs(X_r(3,:)    X_s(3,i)));
        ix = ix + 5;
        x_r = X_r(1,ix);
        y_r = X_r(2,ix);
```

```
105             x_s = X_s(1,i);
106             y_s = X_s(2,i);
107             dx = x_r   x_s;
108             dy = y_r   y_s;
109         end
110         if dy < 0 && dx < 0
111             psi_r = atan((dy)/(dx)) + pi;
112         elseif  dy < 0 && dx > 0
113             psi_r = atan((dy)/(dx));
114 
115         elseif  dy > 0 && dx > 0
116             psi_r = atan((dy)/(dx));
117 
118         elseif  dy > 0 && dx < 0
119             psi_r = atan((dy)/(dx)) + pi;
120         else
121             psi_r = psi;
122 
123         end
124         ref_shift = [psi_r 4*pi,psi_r 2*pi, psi_r, psi_r + 2*pi, psi_r + 4*
               pi];
125         [d, ix] = min(abs(ref_shift   psi));
126         psi_r = ref_shift(ix);
127 
128         ref(i) = psi_r;
129 
130         thetas(i) = theta;
131         psis(i) = psi;
132         phis(i) = phi;
133 
134 %       figure(1)
135 %       plot3(X_r(1,:), X_r(2,:), X_r(3,:),"r  ");
136 %       grid on
137 %       hold on
138 %       plot3(X_s(1,1:i), X_s(2,1:i), X_s(3,1:i));
139 %       axis([ 2  2  2  2  0  3])
140 
141         u  = min(saturation,max((psi_r   psi), 1*saturation));
142         psis_dot = diff(psis);
```

```
143
144     w = ang_vel(0, theta, psi, 0, theta_dot, psis_dot(i));
145     x_dot = R_Ib(0,theta,psi)*R_b_db * ROP;
146
147
148
149
150     theta_dot =  DLS  * ROP(3);
151     psi = psi + u;
152
153     theta = theta + h*w(2);
154     phi = phi + h*w(1);
155     X_s(:,i+1) = X_s(:,i) + h .* x_dot;
156 end
157 %run("cube_si.m")
158 figure(2)
159 plot3(X_s(1,:), X_s(2,:), X_s(3,:));
160 xlabel("x[m]","interpreter","latex")
161 ylabel("y[m]","interpreter","latex")
162 zlabel("z[m]","interpreter","latex")
163 hold on
164 grid on
165 plot3(X_r(1,:), X_r(2,:), X_r(3,:),"r  ");
166 legend("Actual Position", "Reference" ,"interpreter","latex")
167 axis([ 0.2  0.2  0.2  0.2  0  0.6]);
168
169
170
171 [d, ix ] = min( abs(X_r(3,:)   0.6));
172 figure(69420);
173 plot(X_s(1,1:64),X_s(2,1:64))
174 grid on
175 hold on
176 plot(X_r(1,:),X_r(2,:),"r  ")
177 xlabel("x[m]", "interpreter", "latex")
178 ylabel("y[m]", "interpreter", "latex")
179
180
181
```

```
182
183 figure(3)
184 plot(t,ref)
185
186
187 figure(4)
188 subplot(3,1,1)
189 plot(phis)
190 subplot(3,1,2)
191 plot(thetas)
192 title("theta")
193 subplot(3,1,3)
194 plot(psis)
195 title("Psis")
```

D Power consumption

D.1 Top Drive Motor

The power consumpion of the Top Drive (TD) motor given that the motor can provide a maximum of 2000 RPM and 8.34 Nm of torque, the power consumption can be estimated with Equation D.11

$$P = \frac{T\omega}{\eta}, \tag{D.11}$$

where P is power consumption, T is torque, ω is angular velocity of the motor, and η is the motor efficiency. The RPM set for the TD must therefore be converted to the angular velocity ω. This is done as shown in Equation D.12

$$\omega = \frac{2\pi N}{60}, \tag{D.12}$$

where N is the RPM. Given a motor efficiency of $\eta = 90\%$, Table D.3 shows an estimation of the power consumption P for the TD.

Table D.3: Estimated power consumption for the top drive motor

	Top Drive motor torque T [N]			
	2	4	6	8
Rotary speed N [RPM]	**Power Consumption P [W]**			
200	46.7	93.3	140	187
500	115.6	231.1	346.7	462.2
1000	233.3	466.7	700	933.3
1500	348.9	697.8	1046.7	1395.8
2000	464.4	928.9	1393.3	1857.8

D.2 Hoisting motor

The rotational motion of the hoisting motor gets translated to vertical motion of the rotary system. This is done through the connected ball screw. The torque provided by the hoisting motor can be calculated with Equation D.13

$$T = \frac{F \cdot l}{2\pi\epsilon}, \tag{D.13}$$

where T [Nm] torque, F [N] is the force provided by the weight of the rotary system, l is the lead of the ball screw, and ϵ is the ball screw and hoisting motor efficiency. The weight of the rotary system is estimated to be around 490 N, and the lead of the ball screw is 5 mm. Given an efficiency factor $\epsilon = 90\%$, Equation D.11 and Equation D.12 with a constant torque T of

$$T = \frac{F \cdot l}{2\pi\epsilon} = \frac{490 \cdot 0.005}{2 \cdot \pi \cdot 0.9} = 0.433 \tag{D.14}$$

can be used to estimate the power consumption of the hoisting motor given different RPMs. Table D.4 shows the estimated power consumption for the hoisting motor.

Table D.4: Estimated power consumption for the hoisting motor

Rotary Speed N [RPM]	**Power Consumption P [RPM]**
100	5.67
300	17
600	34
1200	68
2000	113
3000	170

E EMM Specifications

DCX 26 L Graphite Brushes
DC motor ∅26 mm

Key Data: 40/74 W, 59.8 mNm, 14 400 rpm

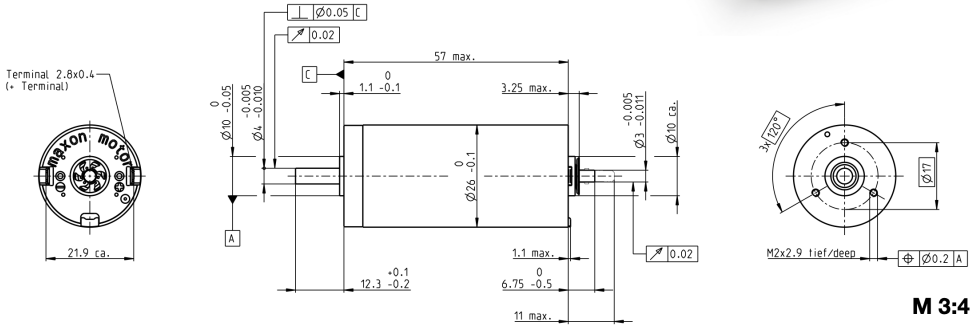

	Motor Data							
1_	Nominal voltage	V	12	18	24	36	48	60
2_	No load speed	rpm	10600	11100	10700	11100	10700	10900
3_	No load current	mA	131	93	65.7	46.5	32.9	27.3
4_	Nominal speed	rpm	9460	10000	9690	10000	9730	10000
5_	Nominal torque (max. continuous torque)	mNm	46.9	54.3	57.8	54	59.1	59.8
6_	Nominal current (max. continuous current)	A	4.5	3.59	2.76	1.79	1.41	1.17
7_	Stall torque	mNm	532	653	695	639	697	750
8_	Stall current	A	49.7	42.2	32.4	20.6	16.2	14.3
9_	Max. efficiency	%	88	90	91	90	91	91
10_	Terminal resistance	Ω	0.242	0.427	0.74	1.75	2.95	4.19
11_	Terminal inductance	mH	0.032	0.067	0.129	0.268	0.514	0.768
12_	Torque constant	mNm/A	10.7	15.5	21.4	31	42.9	52.4
13_	Speed constant	rpm/V	890	616	445	308	223	182
14_	Speed/torque gradient	rpm/mNm	20.1	17	15.4	17.4	15.3	14.6
15_	Mechanical time constant	ms	4.5	3.79	3.45	3.53	3.4	3.16
16_	Rotor inertia	gcm²	21.4	21.3	21.4	19.4	21.2	20.7

	Thermal data		
17_	Thermal resistance housing-ambient	K/W	10.2
18_	Thermal resistance winding-housing	K/W	3.01
19_	Thermal time constant winding	s	24
20_	Thermal time constant motor	s	620
21_	Ambient temperature ball bearings	°C	-40…+100
	Ambient temperature sleeve bearings	°C	-30…+100
22_	Max. winding temperature	°C	155
	Mechanical data ball bearings		
23_	Max. speed	rpm	14400
24_	Axial play	mm	0...0.1
	Preload	N	5.5
25_	Radial play	mm	0.02
26_	Max. axial load (dynamic)	N	5.5
27_	Max. force for press fits (static)	N	40
	(static, shaft supported)	N	500
28_	Max. radial load [mm from flange]	N	20.5 [5]
	Mechanical data sleeve bearings		
23_	Max. speed	rpm	8600
24_	Axial play	mm	0...0.2
	Preload	N	0
25_	Radial play	mm	0.02
26_	Max. axial load (dynamic)	N	0.1
27_	Max. force for press fits (static)	N	80
	(static, shaft supported)	N	500
28_	Max. radial load [mm from flange]	N	5.5 [5]
	Other specifications		
29_	Number of pole pairs		1
30_	Number of commutator segments		11
31_	Weight of motor	g	170
32_	Typical noise level	dBA	44

Motor specifications may vary for version with sintered bearing (max. winding temperature 125°C).

Operating Range

n [rpm] Winding 18 V

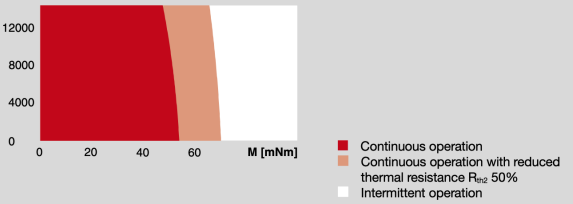

maxon Modular System Details on catalog page 30

maxon gear	Stages [opt.]	maxon sensor	maxon motor control
311_GPX 26 A/C	1–2 [3]	398_ENX 10 EASY	454_ESCON 36/2 DC
312_GPX 26 LN/LZ	1–2 [3]	398_ENX 10 QUAD	455_ESCON Module 50/5
313_GPX 26 HP	2–3 [4]	399_ENX 10 EASY XT	457_ESCON 50/5
314_GPX 32 A/C	3	401_ENX 16 EASY	463_EPOS4 50/5
315_GPX 32 LN/LZ	3	402_ENX 16 EASY XT	463_EPOS4 Module/Comp. 50/5
316_GPX 32 HP	4	403_ENX 16 EASY Abs.	470_EPOS2 P 24/5
		404_ENX 16 EASY Abs. XT	473_MAXPOS 50/5
		410_ENX 16 RIO	
		439_ENC AEDL 5810	
		440_ENC 30 HEDS 5540	
		446_ENC 30 HEDL 5540	

Configuration

Bearing: Ball bearings preloaded/sleeve bearings
Commutation: Precious metal brushes with CLL/graphite brushes
Flange front/back: Standard flange/configurable flange/no flange
Shaft front/back: Length/diameter/flat face
Electric connection: Terminals or cable/alignment of connection/cable length/connector type

xdrives.maxonmotor.com

Figure E.2: EMM Specifications